Maritime Tsunami Hazard Assessment for southwest Washington

Technical Report

December, 2023

Alex Dolcimascolo
Washington Geological Survey
Washington State Department of Natural Resources

Contents

1. Introduction

This Tsunami Hazard Assessment (THA) tests a tsunami scenario from a single earthquake source: the Cascadia subduction zone (CSZ) for southwest, Washington. The modeled tsunami results from this source are useful for estimating potential tsunami current speeds, inundation depths, and wave arrival times to aid with community planning. Due to the large area that makes up the intended southwest Washington study area, the tsunami modeling for this project was broken up into four distinct model regions, known as fgmax regions (Figure 1). An fgmax region is a fixed grid (fg) that saves the maximum (max) values of model variables attained during the duration of the simulation. These variables include water depth (h) and water speed (s) derived from the velocity components (s = √ u2 + v2), as well as other quantities of interest derived from the depth (h) and horizontal momenta (hu and hv; the quantities modeled in the shallow water equations). A single earthquake source model corresponds to its own set of fgmax results. Therefore, one earthquake source model (CSZ) and four fgmax regions yield 4 netCDF files that store the quantities of interest on a set of points with 1/3 arc-second (1/3") spacing in both longitude and latitude. See Appendix A for further discussion of the data format. All digital elevation models (DEMs) and project data utilize World Geodetic System 1984 (WGS84, ESPG:4326) as the standard coordinate system for this study.

The tsunami modeling for this study was done using GeoClaw, version 5.9.0 (Clawpack Development Team, 2023). GeoClaw open source software is available at http://www.clawpack.org/geoclaw. The exact version of the code used in the simulations reported here is also available by request from the Washington Geological Survey (WGS) at the Washington State Department of Natural Resources (WADNR). GeoClaw simulates tsunami generation, propagation, and inundation. This model, which solves the nonlinear shallow water equations and uses Adaptive Mesh Refinement (AMR) to focus fine computational grids around the defined fgmax regions, has undergone extensive verification and validation (Berger and others, 2011; LeVeque and others, 2011). GeoClaw has been accepted as a validated model by the U.S. National Tsunami Hazard Mitigation Program (NTHMP) after conducting multiple benchmark tests as part of an NTHMP benchmarking workshop (González and others, 2011). The following THA generally follows the format of reports developed by the University of Washington Tsunami Modeling Group (UWTMG; http://depts.washington.edu/ptha/projects/index.html). Some of the text in this report describes modeling methods developed by the UWTMG, and is also used in those earlier reports.

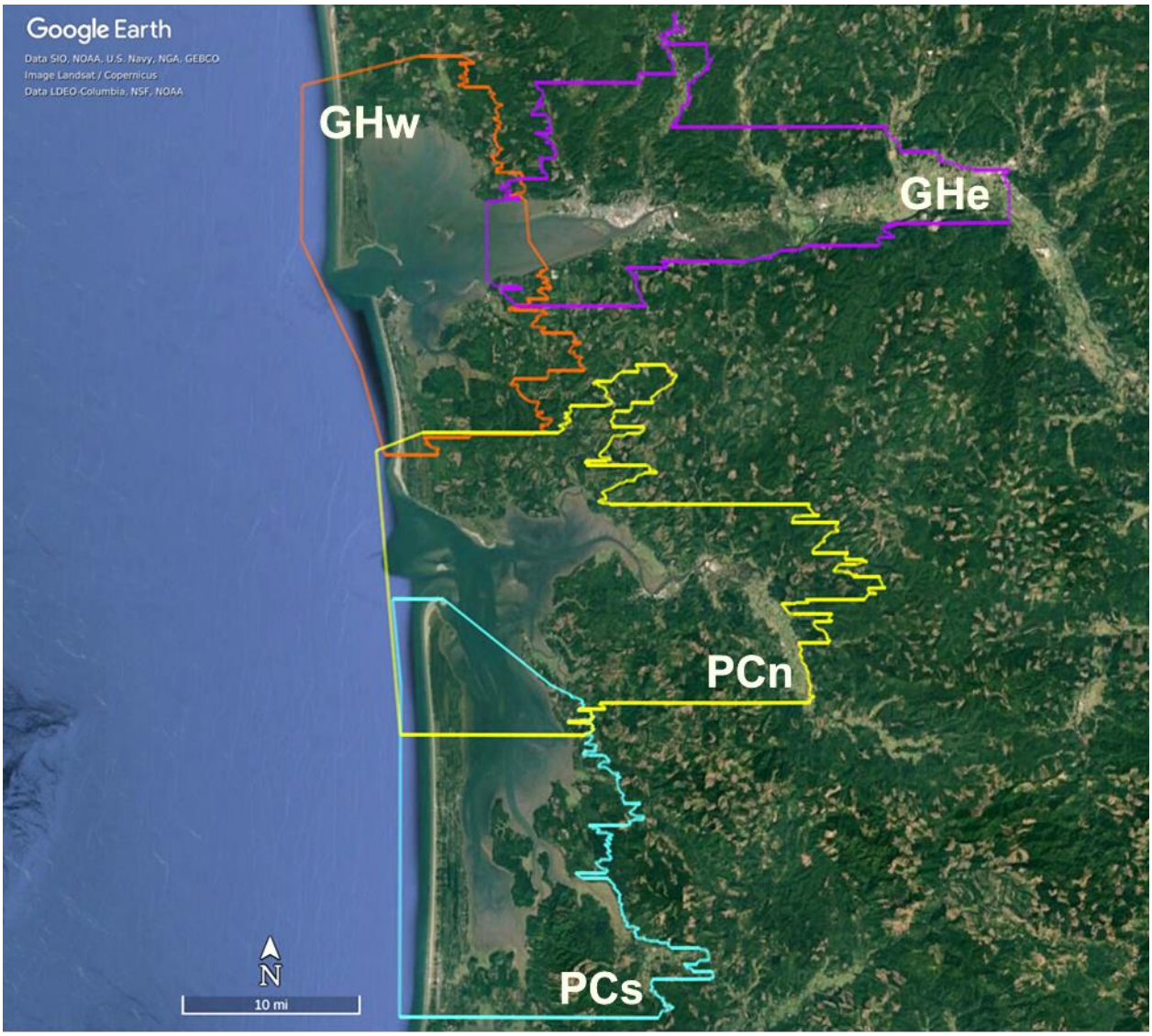

Figure 1. Southwest Washington study area, divided into four distinct fgmax regions: Grays Harbor west (GHw; orange), Grays Harbor east (GHe; purple), Pacific County north (PCn; yellow), and Pacific County south (PCs; teal). We modeled all regions at the 1/3rd arc-second (1/3") resolution.

1.1 Earlier southwest Washington tsunami modeling

This THA for southwest Washington uses the CSZ L1 earthquake source to generate the modeled tsunami (refer to section 2). WADNR previously published tsunami inundation and current speed maps for southwest Washington (Eungard and others, 2018c) using the same earthquake source and digital elevation model (DEM) used in project. Technical details of this earlier modeling project were included in PMEL's project report, Tsunami Inundation Modeling of Ocean Shores and Long Beach, Washington due to a Cascadia Subduction Zone Earthquake (Gica and others, 2014). However, due to earlier data limitations at the time of that previous project, the tsunami modeling did not propagate into some major river valleys as they were outside the available DEM domain. This led to the upriver stretches of

the Chehalis, Hoquiam, Willapa, and Wishkah Rivers (and the communities along these stretches) being omitted in the THA. The main intent of this new THA presented here was to provide an updated THA for southwest Washington that includes a comprehensive tsunami assessment of these upriver areas from the CSZ L1 source. This was done by modifying the original DEM with newer available data that was previously absent (refer to section 3.1 for this summary).

2. Earthquake source

This study assesses a hypothetical tsunami generated by a megathrust event of the Cascadia Subduction Zone (CSZ). The CSZ spans from Northern California to British Columbia and has been seismically quiet since the year 1700 (Jacoby and others, 1997; Satake and others, 2003; Yamaguchi and others, 1997; Atwater and others, 2005). However, geologic evidence of submerged coastal areas and tsunami deposits (Atwater and Hemphill-Haley, 1997; Atwater and others, 2004), in addition to offshore sedimentary evidence (Goldfinger and others, 2012; Goldfinger and others, 2017), reveals that Cascadia has had at least 23 approximate magnitude 9 earthquakes in the last 10,000 years. In addition, global positioning data show that Cascadia is currently building seismic stress, portending a future great earthquake (Burgette and others, 2009; Yousefi and others, 2020). The USGS estimates that there is a 10-14% chance of a magnitude 9 earthquake, and a 30% chance of a magnitude 8 on the CSZ within the next 50 years (Petersen and others, 2002).

The CSZ fault model used for this study is the L1 scenario, which represents an earthquake with a moment magnitude (M_w) of 9.0 (Witter and others, 2011; 2013). This scenario is one of 15 seismic scenarios used in a hazard assessment study of Bandon, Oregon based on an analysis of offshore data spanning 10,000 years (Witter and others, 2011). The rupture geometry of the L1 model also includes a surface-rupturing splay fault structure that amplifies tsunami waves. Figure 2 displays the crustal and seafloor deformation produced by the L1 model; which is significant in the southwest Washington study area (~1.5-3 meters). Washington State has adopted this L1 scenario and its derivative (the Extended L1) as the “maximum considered case" for many of its inundation modeling studies and evacuation maps. The L-category source models have an estimated mean recurrence interval of ~3,333 years (Witter and others, 2013). This is a close and conservative approximation to design requirements for critical facilities in the international building code for seismic hazards that build to the engineering standard of a 2,500-year event (International Code Council, 2015).

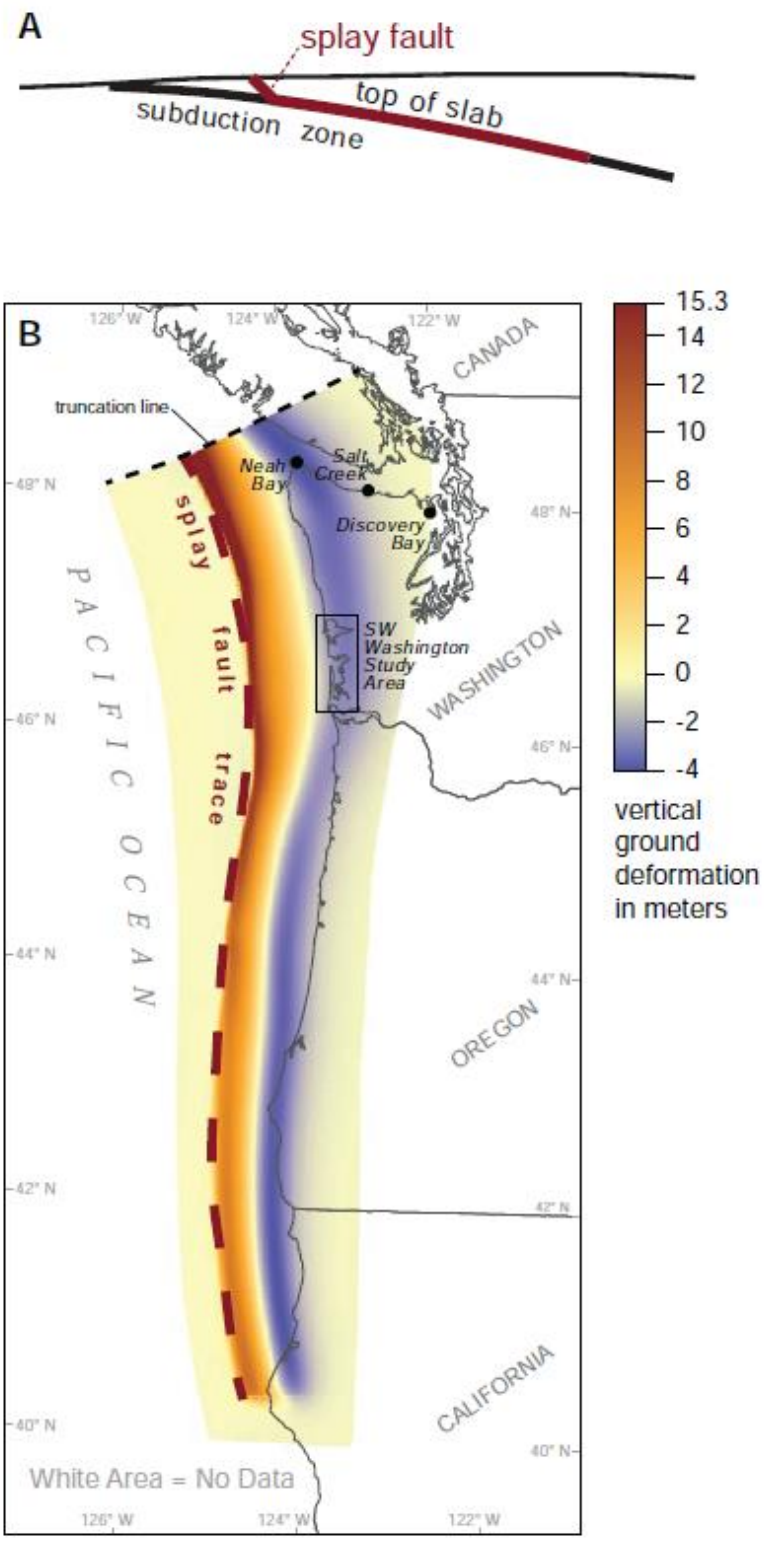

Figure 2. L1 splay fault model diagram (A) and map of vertical ground deformation (B) during a great Cascadia earthquake in the L1 scenario of Witter and others (2011). The northern part of the scenario is truncated south of where the Juan de Fuca plate is beginning to break up into microplates.

3. Topography and bathymetry

Digital Elevation Models (DEMs) are needed by the GeoClaw modeling software to effectively track the movement of tsunami waves from the source to the study area. The footprints of the DEMs used in this study were developed/hosted by the NOAA National Centers for Environmental Information (NCEI) and are listed in Table 1. All DEMs used in this study are vertically referenced to mean high water (MHW), so that the "0" elevation reference point for model outputs is MHW. All of the DEMs used in this study are projected in the World Geodetic System 1984 (WGS84, ESPG:4326) coordinate system. Note that published DEMs may have errors, or the landscape may have changed since the DEM was initially developed.

Table 1. DEMs used in this tsunami modeling study.

Name	Resolution	Source
ETOPO1 Global Relief Model	1 arc-minute	Amante and Eakins, 2009
Astoria	1/3 arc-second	NOAA NGDC, 2012

3.1 Study DEMs

The highest resolution model outputs for this study were run on the 2012 Astoria DEM with 1/3" grid points (NOAA NGDC, 2012). The WGS incorporated the latest available lidar data (USGS, 2019; hosted by the WGS) to increase the coverage of this DEM to encompass the upland areas of the Chehalis, Hoquiam, Willapa, and Wishkah Rivers. This allows for the delineation of the overall L1 tsunami inundation zone for the waters connected to Grays Harbor and Willapa Bay that was previously undetermined (Eungard and others, 2018c). Additionally, due to the nature of these DEMs generally having hydro flattened river channels that lack water depth, the WGS extracted available river depths measured by soundings published in NOAA hydrographic surveys and nautical charts to better characterize each river channel (Office of Coast Survey, 2023). These sounding depths were converted from Mean Lower Low Water (MLLW) to Mean High Water (MHW) using NOAA's VDatum and then merged into the updated DEM to complete tsunami modeling; river channel elevations were linearly interpolated along the river channel between the sounding points. However, the upstream stretches where no soundings were available (unnavigable parts of the river) were still hydro flattened to the elevation of the river without an associated depth. This led to upstream sections, where river elevations were greater than MHW, to initialize dry prior to the earthquake deformation (such as the Chehalis River section east of Montesano [-123.6° longitude]; see Figure 7). Tsunami inundation upstream of these areas may be underestimated due to the lack of water initializing in the river (a data limitation). This modified Astoria DEM is available upon request by the WGS.

The modified Astoria MHW DEM captures the entirety of the southwest Washington study area and was the only high-resolution dataset needed for this project due to its direct connection to the Pacific Ocean and closeness of the CSZ (Figure 3). However, the tsunami simulations also used the ETOPO1 1-minute topography (Amante and Eakins, 2009). This ETOPO1 dataset was needed to cover the entire modeling domain and the CSZ earthquake source, which initiates in the Pacific Ocean and is located beyond the boundaries of the Astoria DEM.

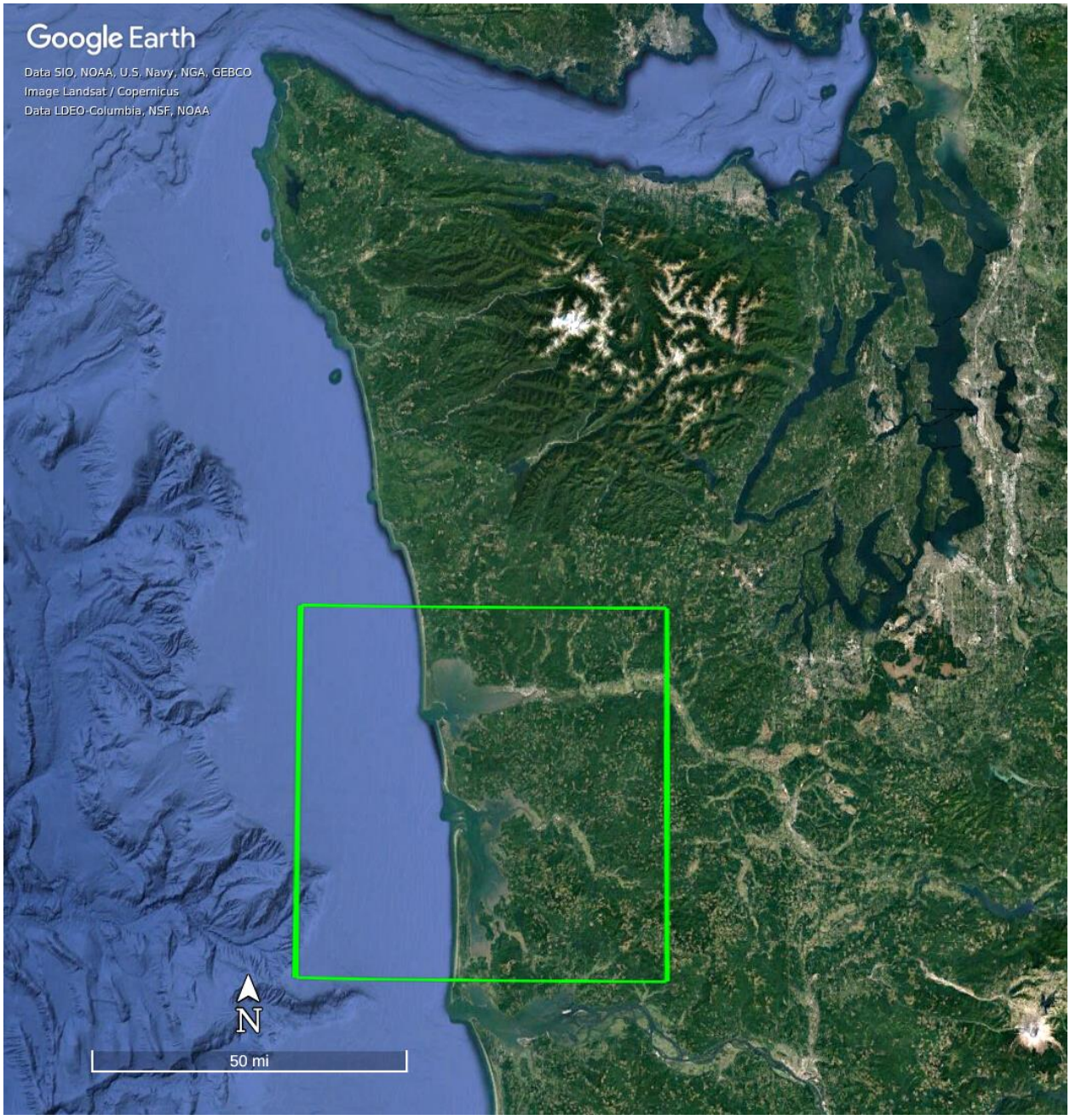

Figure 3. The modified Astoria DEM, outlined in green, used in this study. All simulations also used the ETOPO1 1-minute resolution DEM for the Pacific Ocean and initiation of the CSZ-induced tsunami (not shown; Amante and Eakins, 2009).

4. Study area

The four fgmax regions modeled in this project are denoted as Grays Harbor west (GHw), Grays Harbor east (GHe), Pacific County north (PCn), and Pacific County south (PCs; Figure 1; Figure 4). All fgmax regions use a fixed set of points (independent of adaptive mesh refinement [AMR]) on which the maximum of each quantity of interest is monitored during the course of the simulation. The quantities monitored are the flow depth, flow speed, and momentum flux. These fgmax regions also monitors the

time of the maximum values and the first wave arrival at each grid point. All fgmax points lie on a grid with spacing 1/3" by 1/3" and align with the DEM grids.

Each fgmax region has a set of fgmax points to monitor maxima values. Table 2 gives an overview of the number of points included in each fgmax region. Although maxima values were only monitored and saved in the defined fgmax regions, all of Grays Harbor and the immediate offshore Pacific Coast (as far west as -124.2944 and -124.2947 offshore Grays Harbor and Long Beach, respectively) were refined to 1/3" to match the previous high-resolution modeled area from Gica and others (2014; Figure 4). This setup was also preferred in Grays Harbor due to the complicated shoreline westward of the GHe boundary, which helped mitigate any "edge of model" problems between the overlapping fgmax regions. This did not pose an issue for the PCs job run (and this region does not contain the main upriver areas of interest [Chehalis, Hoquiam, Willapa, or Wishkah]). It has been standard in previous tsunami modeling with multiple fgmax regions to have only one region refined to 1/3" resolution at a time with the other adjacent regions to refine to at least 2" resolution. This was the setup in the case of the PCs job run (where the neighboring PCn region was refined to 2").

Table 2: The fgmax regions used in this tsunami hazard assessment. The fgmax points align with the polygon regions specified in Figures 1 and 4, with 1/3" spacing in longitude and 1/3" in latitude. These fgmax areas only contains grid points for which the topography elevation is less than 30 m above MHW in the specified region boundaries. The column labeled "Count" gives the number of fgmax points in the region. See Section 6 for plots of the fgmax points and of sample results for each region.

Fgmax region	Count	Results section
Grays Harbor west (GHw)	7,233,307	6.1
Grays Harbor east (GHe)	4,318,998	6.2
Pacific County north (PCn)	7,230,703	6.3
Pacific County south (PCs)	7,345,185	6.4

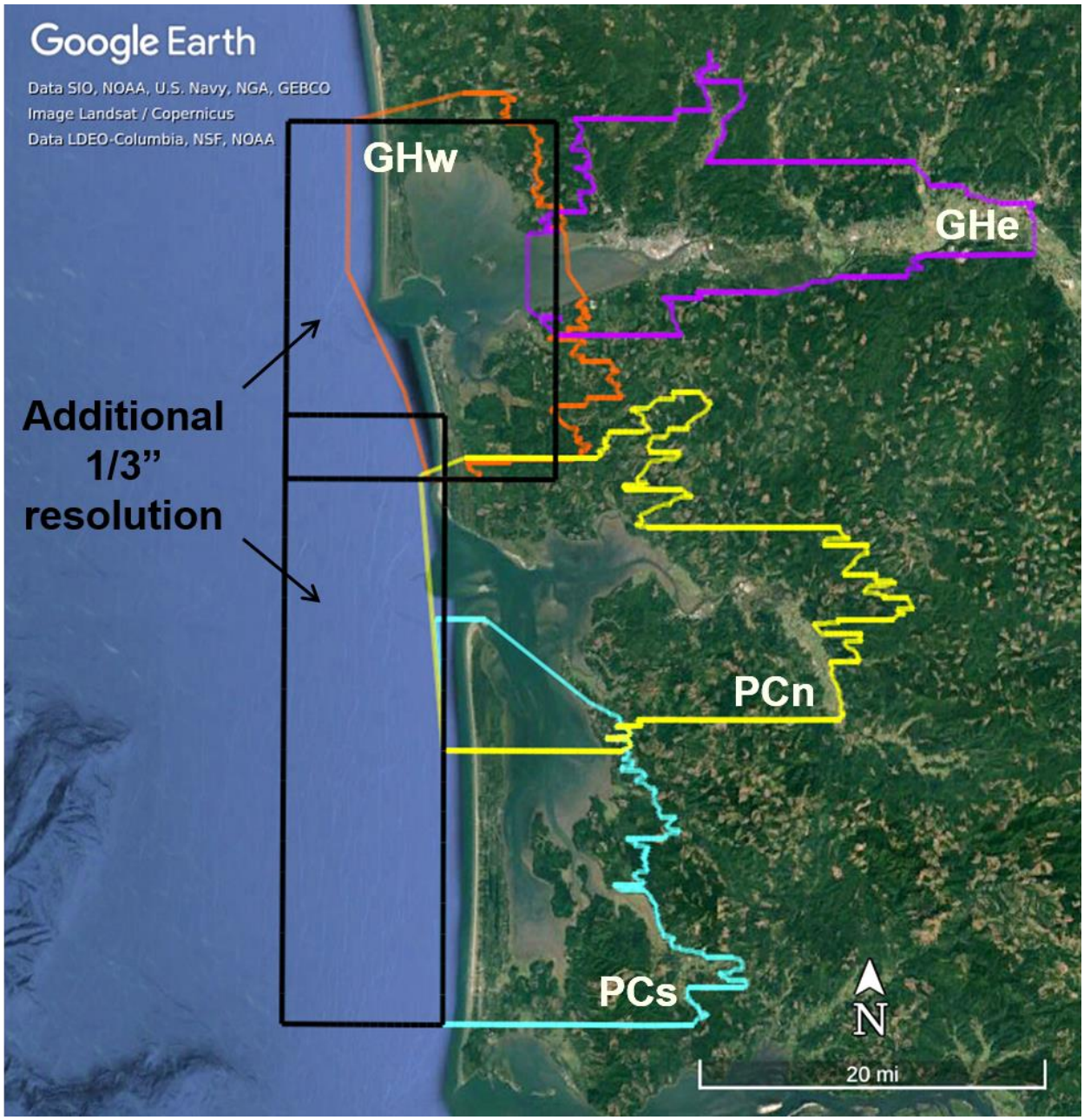

Figure 4. The four 1/3" fgmax regions, each modeled separately in this study: Grays Harbor west (GHw; orange), Grays Harbor east (GHe; purple), Pacific County north (PCn; yellow), and Pacific County south (PCs; teal). Black rectangles indicate DEM points refined to 1/3"in addition to the points within the fgmax regions in each modeled job run, though were not saved. These extended regions of the 1/3" grid points match the high resolution area previously modeled in the area (Gica and others, 2014).

4.1 Fgmax selection improvements and limitations

All fgmax regions within this project were specified as polygons, or "Ruled Rectangles". The UWTMG developed this capability in an effort to greatly reduce the number of selected fgmax points (LeVeque and others, 2019). Prior to this capability, the previous approach of specifying fixed rectangles

to select fgmax points did not carry over well given the complicated geometry Washington's coastline. For example, if fixed rectangles covered the desired study area instead of polygons, they would include many more and possibly irrelevant fgmax points in locations of discernable "high ground" due to the nature of 'filling' the rectangle. This became inefficient when working with large study areas as it led to needing more fgmax regions to cover the same area; model computations would break down if the number of fgmax points was too high (maximum points allowed is seemingly ~8,000,000; determined through personal testing). The maximum number of fgmax points is a current limitation in the GeoClaw code, though this number will likely increase in future versions of the software.

However, to minimize the number of fgmax points selected in a specified region, the UWTMG also developed the improvement to only select grid points that return topography elevations below a specified limit, Zmax. For the current project, Zmax was set to 30 meters. Additionally, if only onshore inundation and nearshore currents need to be modeled, there is also the capability to set a maximum depth threshold (e.g. -60 m or -40 meters). This would then only select fgmax points within the polygon where the bathymetry elevation is both above the specified value and less than Zmax. Note that this project includes all water points in each fgmax polygon to model currents farther from shore and did not include a maximum depth threshold. To run the code with many fgmax points efficiently, the UWTMG also improved the way the GeoClaw code internally handled the fgmax points. This resulted in a substantial computational speedup, while still monitoring values in the same manner as in previous versions of GeoClaw. Refer to LeVeque and others (2019) for a more complete summary of all improvements developed when selecting fgmax points and increasing computation efficiency.

4.2 Dry land below Mean High Water

Few locations in each fgmax region represent dry land with elevations below MHW, though protected from inundation under normal conditions. The standard GeoClaw software would initialize these points with water up to the level of MHW at the start of the simulation. Inadvertently, GeoClaw would flood these locations even if no tsunami arrived, which can be a misleading result. Moreover, for locations where the tsunami does reach land below MHW, there would be very different wave dynamics if the tsunami moved over an initially flooded artificial lake rather than moving over dry land. In these scenarios, the maximum depths recorded would be very different, with the former being incorrect. For example, water entering an artificial lake will spread out rapidly and eventually raise the level everywhere by a small amount. On the other hand, the same quantity of water overtopping a dike or levee and moving across dry land will quickly decelerate due to high bottom friction, giving higher maximum depth near the dike and little or no flooding farther inland. To deal with this problem, the UWTMG first developed a capability used in their project that modeled Whatcom County (Adams and others, 2019) and then improved upon it in the Island and Skagit County project (LeVeque and others, 2019) that forces these areas dry prior to tsunami wave arrival. Documentation of this "force dry" capability has been built into the GeoClaw code since v5.7.0 and is used in this current project. The locations that were subject to this problem in each region were effectively forced dry and were saved as a variable in the input netCDF file needed to run the tsunami simulation (see Figure 5, 7, 9; Appendix A). This file is available upon request from the WGS.

5. Model uncertainties and limitations

The inputs to the GeoClaw model include the earthquake source, the DEMs used, and the Fgmax areas (discussed in sections 2-4). In addition, other geophysical parameters are designated. Some physical processes are not included in these simulations, which use the two-dimensional shallow water equations. See below for the discussion of these parameters and their potential effect on the modeling results.

5.1 Tide stage and sea level rise

The simulations for this study were run at using the Mean High Water (MHW) tidal datum. The MHW datum is conservative for tsunami inundation depths as the deeper tidal stage amplifies flooding over land. However, the MLW datum is often conservative for tsunami currents, in that current speeds tend to increase at lower water levels in shallow areas, and also are conservative for minimum water depths, which can be used to infer maximum drawdown values. Running simulations at only the MHW tidal stages will not capture the range of variability of expected conditions in the study area during a tsunami event. Additionally, while consideration of future sea level rise is important for planning, this study does not account for potential sea level rise projections.

5.2 The built environment

The topographic DEMs used in this study are “bare earth” and are created by stripping the land surface of built structures, buildings, and vegetation. The presence of structures and vegetation can alter tsunami flow patterns and generally impede inland flow. To some extent, the lack of structures in the model makes the model results more conservative, because structures can reduce inland penetration of the tsunami wave. Actual tsunami flows are likely to interact with structures that may impede flow and cause water to pile up in some areas. Bare earth DEMs may lead to simulations with higher flow velocities because there is nothing to slow the flows. Actual tsunami flows may be slowed by structures, or conversely may speed up in areas where the flow is channelized, such as between buildings. Structures also contribute to debris that interacts with tsunami flows. In some cases, structures may be necessary to best model an area.

5.3 Bottom friction

Each simulation uses the value 0.025 for Manning’s Roughness Coefficient. This is a standard value used in tsunami modeling and corresponds to a gravelly earth surface material. Using 0.025 is conservative in some sense, because the presence of trees, structures, and vegetation would justify the use of a larger value, which might tend to reduce the inland flow. On the other hand, larger friction values can lead to deeper flow in some areas, since the water may pile up more as it advances more slowly across the topography. There has not been a sensitivity study using other friction values at this time.

5.4 Tsunami modification of bathymetry and topography

Scour, erosion, and deposition all occur in a tsunami. These topographic and bathymetric changes will inherently alter flow patterns of the tsunami wave. The erosion of natural berms or ridges along the coastline (or manufactured levies, dikes, or breakwaters) by the tsunami could increase more extensive flooding. On the other hand, the movement of material in a tsunami also requires an expenditure of tsunami energy, which could reduce the inland extent of inundation. These complex changes to the land

are largely uncertain in a tsunami, and GeoClaw does not currently account for erosional or bathymetric/topographic change during simulations. Because there is no active modification to the topography and bathymetry in these results, the modeling dynamics of flow presented here may not entirely predict future tsunami behavior in the study area.

5.5 River flow

Water levels over the entire study area, including upriver stretches, were initialized to MHW at the start of the tsunami simulation. Therefore, all tsunami simulations did not include any natural river flow within the model setup. River discharges often vary over the course of the year and can be impacted by many environmental factors. Incorporating possible rates of discharge to each river and completing a sensitivity study of various rates of flow for the purpose of simulating tsunami propagation along a river valley is an area of future research. Additionally, because many of the rivers included in this study are tidally influenced, incorporating dynamic tides is also worth exploring. For example, if the difference in the tidal range is large enough and greater than the tsunami wave height, it is possible for a falling tide to 'mask' the tsunami arrival (or amplify inundation in the reverse scenario). This was recorded in Anchorage, Alaska in 1964 when the tsunami generated from the 9.2 earthquake along the Alaskan-Aleutian subduction zone (AASZ) arrived at low tide when the tide level was negative-16 feet; because this water level was far below normal high tide at the time of the tsunami arrival, there was no disturbance observed. (https://storymaps.arcgis.com/stories/c146aa74a3694059b4c0e5db33559a49).

6. Fgmax (highest resolution) results

This section contains figures of maximum modeling results from a tsunami generated by the CSZ L1 earthquake scenario for each fgmax region. The plots included show the specified fgmax polygon in reference to the southwest Washington study area, the fgmax points selected within the polygon, the maximum tsunami speeds, and the maximum flow depths for all four fgmax regions simulated at the MHW tidal stage. The maximum flow depth and speed plots show the maximum values recorded during the computation over the full 12 hour simulation time. In the flow depth plots, the points colored green represent locations that remain dry throughout the entire simulation. White regions are where there was initially water, or where there were no fgmax points. In the speed plots, both the water and points that were initially dry that become wet represent the maximum speed. White regions are where there were no fgmax points.

The intent of this technical report is not to display high quality graphics of the results, but to outline the model setup and provide plots that give an indication of the flooding and flow speeds observed in simulation. These plots are also available as a future reference if the simulations are re-run. The WGS have developed the same model results into high-quality graphics for official publication (Dolcimascolo and others, 2023). However, in addition to the plots shown in this technical report, there are also high-resolution png files of the input data and results embedded into kml files that are available for viewing in Google Earth. The low-resolution figures in this report cannot possibly show all the details, whereas with the kml files, the user can zoom in to explore the results in more detail. These downloadable kml files, the Python code that produced them, in addition to the raw results in netCDF format are available upon request from the WGS. The netCDF files will plot with sophisticated GIS tools. The user can apply different color maps and other modifications as necessary.

6.1 Region Grays Harbor west

Figure 5 displays the location of the Grays Harbor west (GHw) fgmax region in the context of the full study region in addition to the fgmax points selected within this region. Points are colored by elevation relative to MHW. Figure 6 provides the maximum current speed and flow depth results for this region.

Noteworthy in this region:

- This study region covers the entrance into Grays Harbor, in addition to North Bay and South Bay. Some of the communities within this region include Ocean Shores, Westport, Bay City, Ocosta, and Markham. This study region does not include Hoquiam or the communities farther east of the Bowerman Airport.
- The deformation of the CSZ L1 earthquake scenario generates ~1.5-3 meters (~5-10 feet) of coseismic subsidence in this region (increasing eastward). This may cause significant land loss to the daily tide range within the low-lying areas of Westport and Ocean Shores, among other areas in the region. It may take decades to centuries for the subsided land surface elevation to rebound back to pre-earthquake conditions.
- The first impacts of the simulated tsunami generated by the CSZ L1 earthquake scenario appear at the entrance the Grays Harbor in ~5 minutes following the subsidence produced by the earthquake initiation. This is a rising wave (leading trough is seemingly masked out by subsidence and proximity to the L1 deformation area). A 0.3-meter (1-foot) and ~1-meter (3-foot) high wave arrives approximately 10 and 15 minutes after the earthquake, respectively. This first wave also reaches a maximum height of ~8 meters (~26 feet) approximately 30-35 minutes after the earthquake (refer to Section 7.1, Gauge 1; and Appendix B.1, Gauge 1).
- The first simulated tsunami wave appears to be the largest (most drastic Δh; Section 7.1, Gauge 1) and represents the largest change in water height over the course of the tsunami simulation.
- Onshore coastal inundation is significant, especially near the Pacific Coast as the tsunami overwashes the Ocean Shores and Westport Peninsulas. Current speeds are dangerously fast in this region, exceeding 6 meters/second (~12 knots) entering into Grays Harbor.
- High resolution maps covering this study region are available in Eungard and others (2018c).

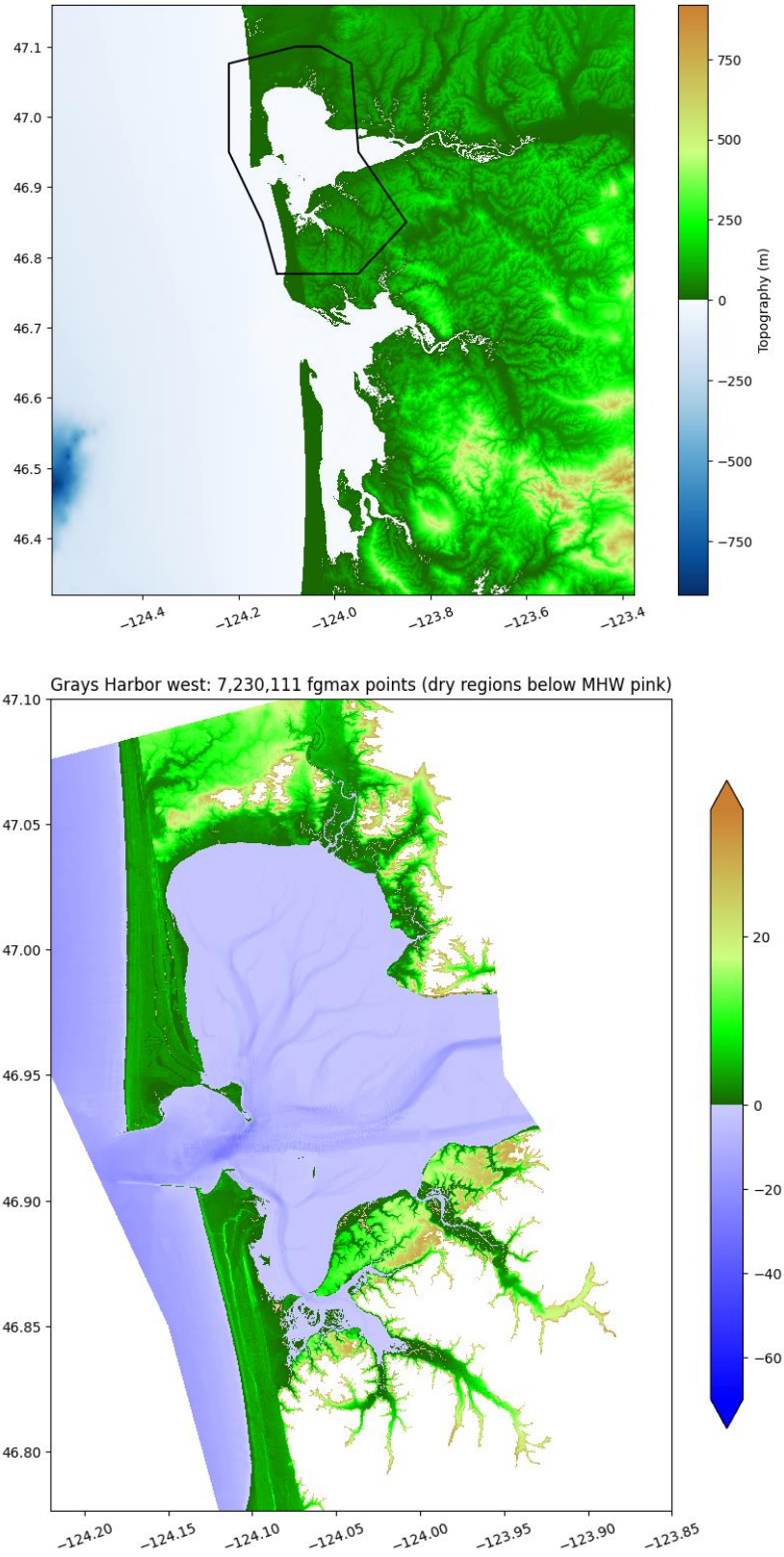

Figure 5: Polygon used to select fgmax points for the Region: Grays Harbor west (GHw; top). 7,233,307 points selected in the fgmax region (bottom).

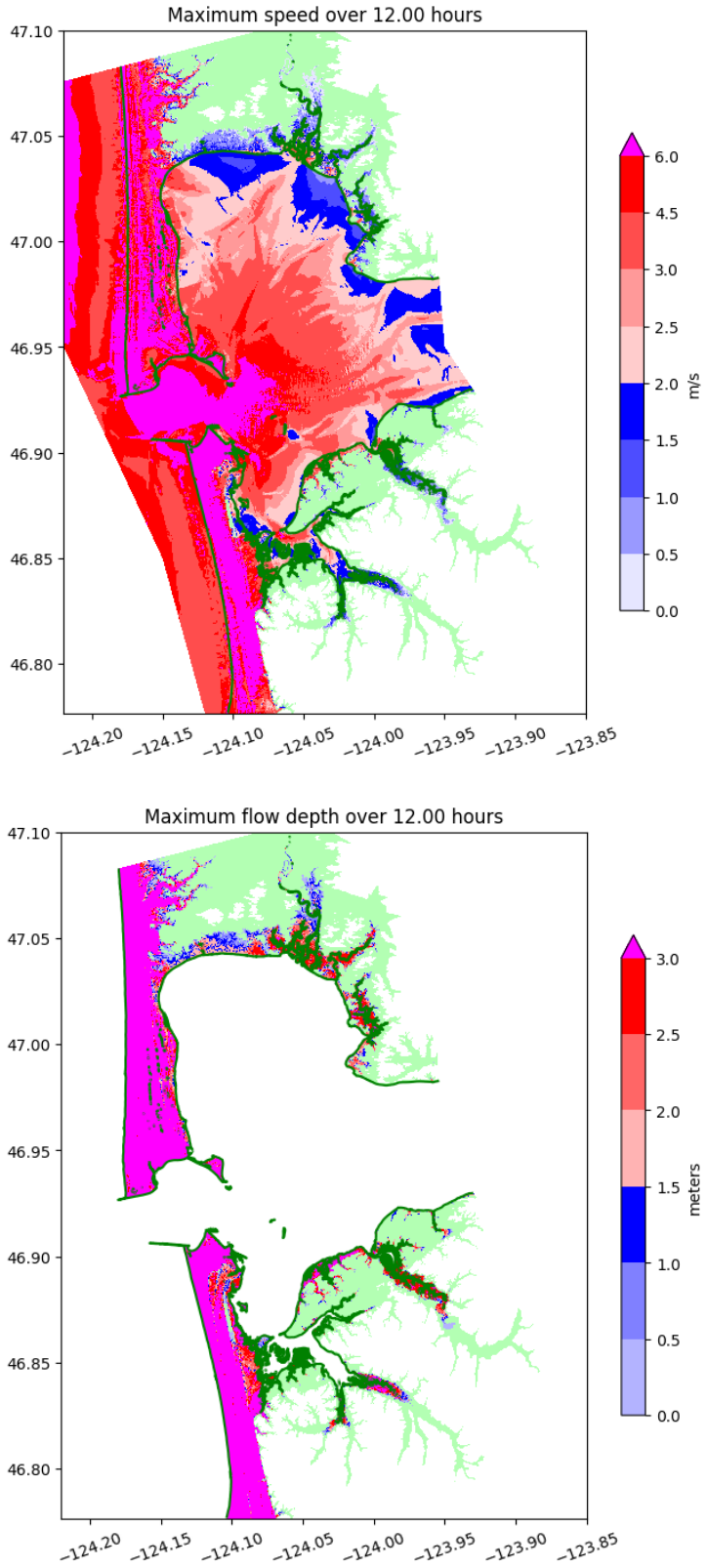

Figure 6: Sample results of maximum speeds (top) and flow depths (bottom) in the Region: Grays Harbor west (GHw).

6.2 Region Grays Harbor east

Figure 7 displays the location of the Grays Harbor east (GHe) fgmax region in the context of the full study region in addition to the fgmax points selected within this region. Points are colored by elevation relative to MHW. Figure 8 provides the maximum current speed and flow depth results for this region.

Noteworthy in this region:

- This study region covers Grays Harbor east of Grays Harbor City and includes the upriver extents of the Chehalis, Hoquiam, and Wishkah Rivers.
- The deformation of the CSZ L1 earthquake scenario generates ~1.5-3 meters (~5-10 feet) of coseismic subsidence in this region (decreasing eastward). The subsided sea surface level appears to recover back to pre-earthquake conditions ~4-5 hours after the earthquake in the eastern portion of Grays Harbor. The land surface does not and it may take decades to centuries for the land surface elevation to rebound back to pre-earthquake conditions. This may cause significant land loss to the daily tide range within low-lying areas in Aberdeen, Hoquiam, and Cosmopolis.
- Due to the combination of subsidence and proximity of this region to the CSZ L1 source, the initial trough phase of the simulated tsunami does not appear to be discernable in Grays Harbor locations east of Grays Harbor City. However, the trough phase of the tsunami may be noticeable at the mouth of the Wishkah River and areas further uprivers as these locations are farther away from the CSZ L1 earthquake rupture area (see 7.1, Gauge 28; Appendix B.2).
- The first rising wave of the tsunami arrives in ~15 minutes after the earthquake southwest of Rennie Island (see Section 7.1, gauge 22; Appendix B). This wave increases to a ~0.3-meter (1-foot) wave height in ~30-35 minutes, and then a ~1-meter (3-foot) wave height in 50-55 minutes, posing significant onshore flooding to the low-lying areas within Hoquiam and Aberdeen.
- The first simulated tsunami wave appears to be the largest (most drastic Δh; Section 7.1, Gauge 22). However, the first wave does not represent the largest change in water heights, which occurs at ~4.5-5 hours after the earthquake; this value includes both tsunami inundation from the earthquake-generated wave and the amount of sea-surface recovery following subsidence, which adds an additional ~3 meters (~9-10 feet) of flooding above the subsided seafloor over the course of the tsunami simulation.
- The simulated tsunami travels approximately 13 kilometers (8 miles) up both the Hoquiam (west and east forks) and Wishkah Rivers, and approximately 21 kilometers (13 miles) up the Chehalis River (river miles). Upland flooding over roadways within the Hoqiuam and Wishkah River flood plains could potentially isolate upriver communities.
- Tsunami current speeds are generally less than 2 meters/second (4 knots) within the Chehalis, Hoquiam, and Wishkah River valleys.
- High resolution maps covering this study region, with the exception to the upstream stretches of the Chehalis, Hoquiam, and Wishkah Rivers, are available in Eungard and others (2018c). High resolution maps covering the extent of tsunami flooding along the Chehalis, Hoquiam, and Wishkah Rivers are available in Dolcimascolo and others (2023).

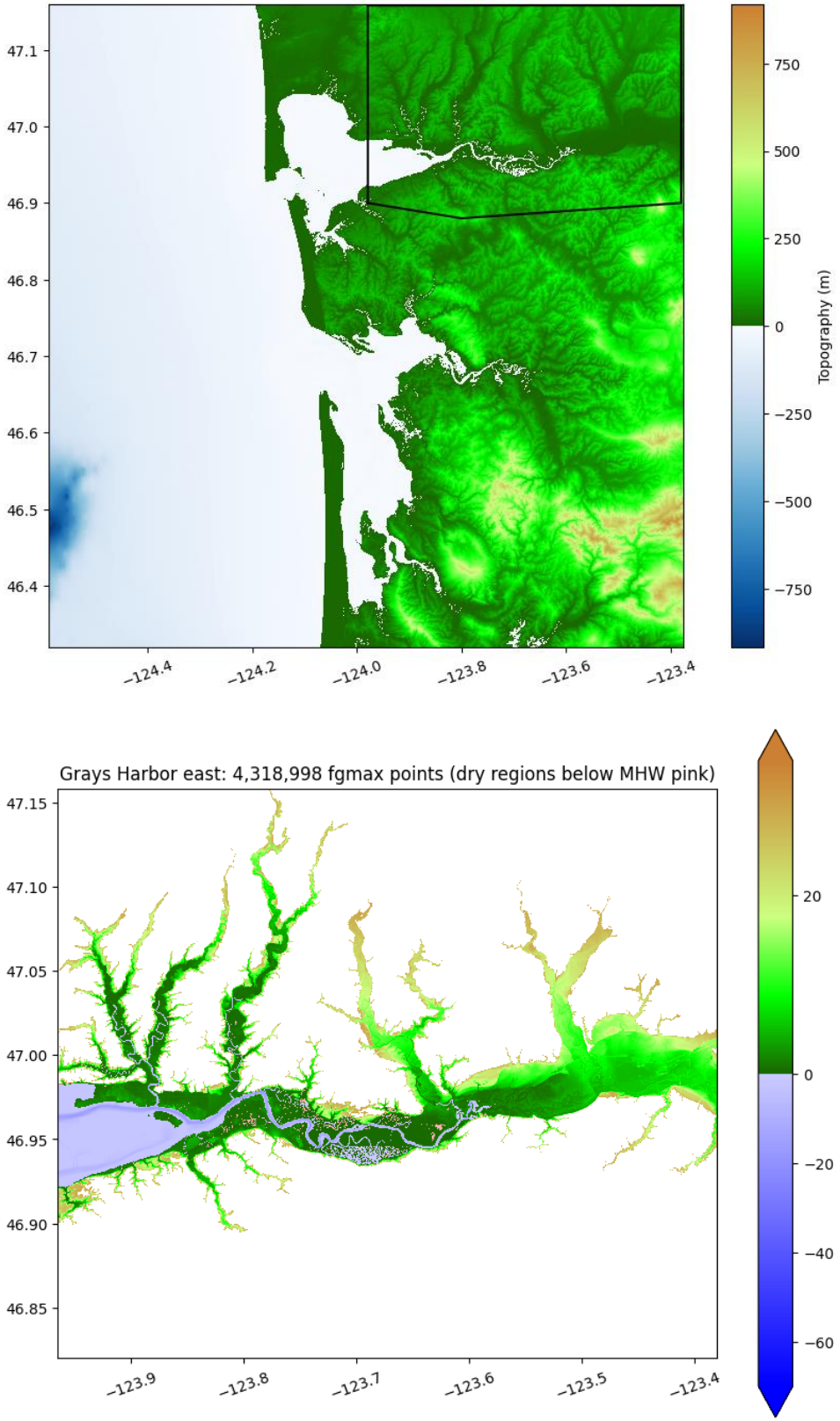

Figure 7: Polygon used to select fgmax points for the Region: Grays Harbor east (GHe; top). 7,233,307 points selected in the fgmax region (bottom).

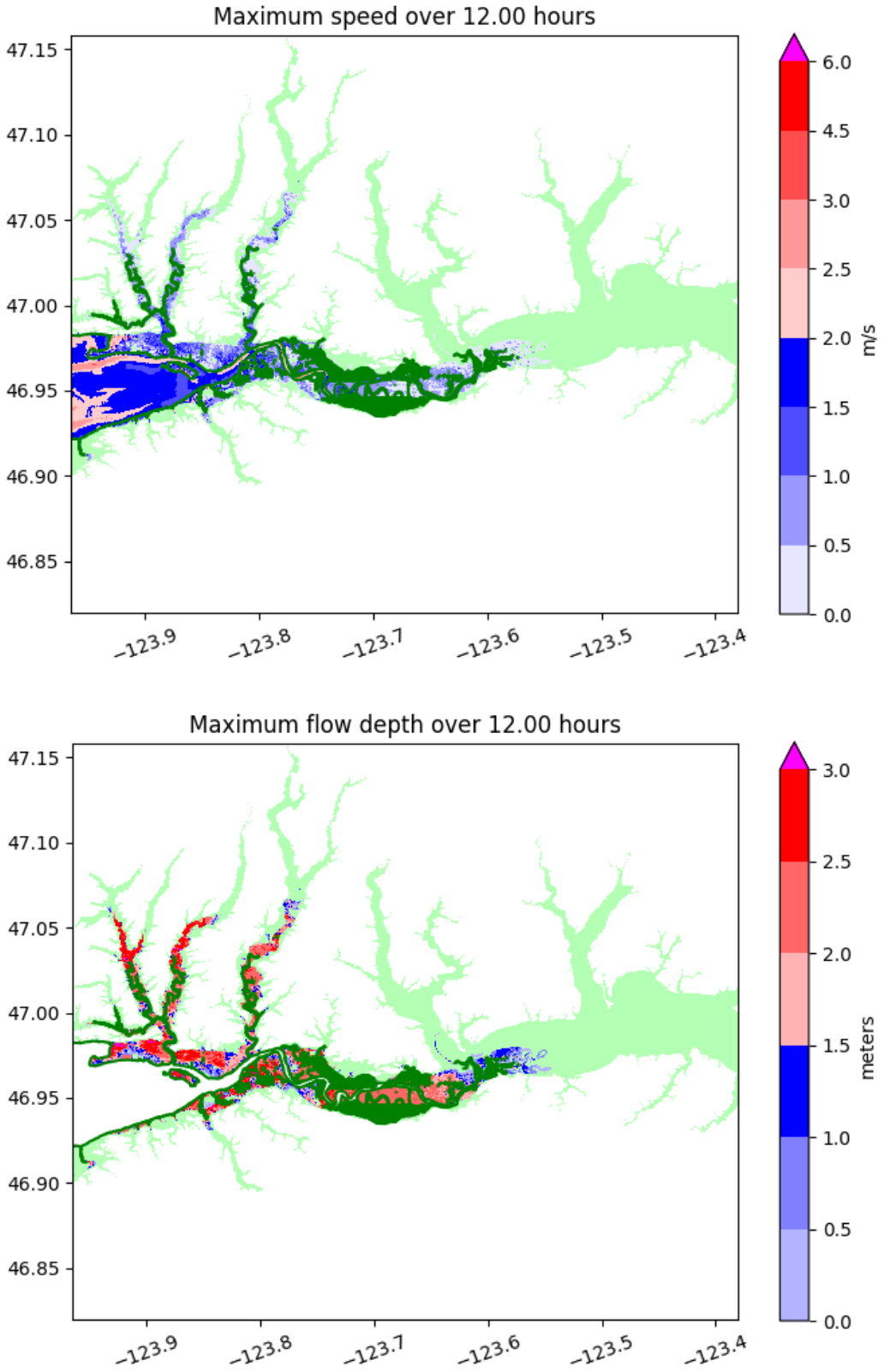

Figure 8: Sample results of maximum speeds (top) and flow depths (bottom) in the Region: Grays Harbor east (GHe).

6.3 Region Pacific county north

Figure 9 displays the location of the Pacific County north (PCn) fgmax region in the context of the full study region in addition to the fgmax points selected within this region. Points are colored by elevation relative to MHW. Figure 10 provides the maximum current speed and flow depth results for this region.

Noteworthy in this region:

- This study region covers the entrance into Willapa Bay, in addition to the Tokeland Peninsula, Leadbetter Point State Park on the Long Beach Peninsula, South Bend, Raymond, and the Willapa River Valley through Willapa, Washington (CDP).
- The deformation of the CSZ L1 earthquake scenario generates ~1.8-3 meters (~6-10 feet) of coseismic subsidence in this region (decreasing eastward and westward from the Bone River Natural Preserved Area). This may cause significant land loss to the daily tide range within the Tokeland Peninsula, Leadbetter Point State Park, and South Bend. It may take decades to centuries for the land surface elevation to rebound back to pre-earthquake conditions.
- Similarly to the locations with Grays Harbor, the initial trough phase of the simulated tsunami does not appear to be noticeable in Willapa Bay locations of this region.
- The first modeled tsunami wave is seemingly the largest (most drastic Δh; see Section 7.1, Gauge 56). It arrives at the mouth of the Willapa River in just ~13 minutes. This wave height exceeds a 0.3-meters (~1-foot) at ~30 minutes and increases to 1+ meters (~3 feet) after ~45-50 minutes of simulated time following the earthquake shaking. However, this first wave does not represent the largest change in water heights, which occurs at ~5 hours after the earthquake; this value includes both tsunami inundation from the earthquake-generated wave and the amount of sea-surface recovery following subsidence, which adds an additional ~3 meters (~9-10 feet) of flooding above the subsided seafloor over the course of the tsunami simulation.
- (Appendix B.3, Gauge 56).
- Modeled onshore coastal inundation is significant in this region, especially near the Pacific Coast as the tsunami overwashed the Tokeland Peninsula and the majority of the Long Beach Peninsula, leaving few pockets of high ground along bayside sand ridges.
- Modeled current speeds are also dangerously fast entering Willapa Bay, exceeding 6 meters/second (~12 knots). Modeled tsunami current speeds were generally less than 1.5 meters/second (~3 knots) along the Willapa River east of Raymond.
- The simulated tsunami travels approximately 20 kilometers (~12 miles) up the Willapa River (river miles). Much of the city of Raymond lies within the modeled tsunami zone and could expect ~1.5-2.5 meters (~5-8 feet) of flooding, with the exception to the “island community” at the eastern limit of the city that modeling designates as high ground.
- High resolution maps covering this study region, with the exception to the upstream stretch of the Willapa River, are available in Eungard and others (2018c). High resolution maps covering the extent of tsunami flooding along the Willapa River are available in Dolcimascolo and others (2023).

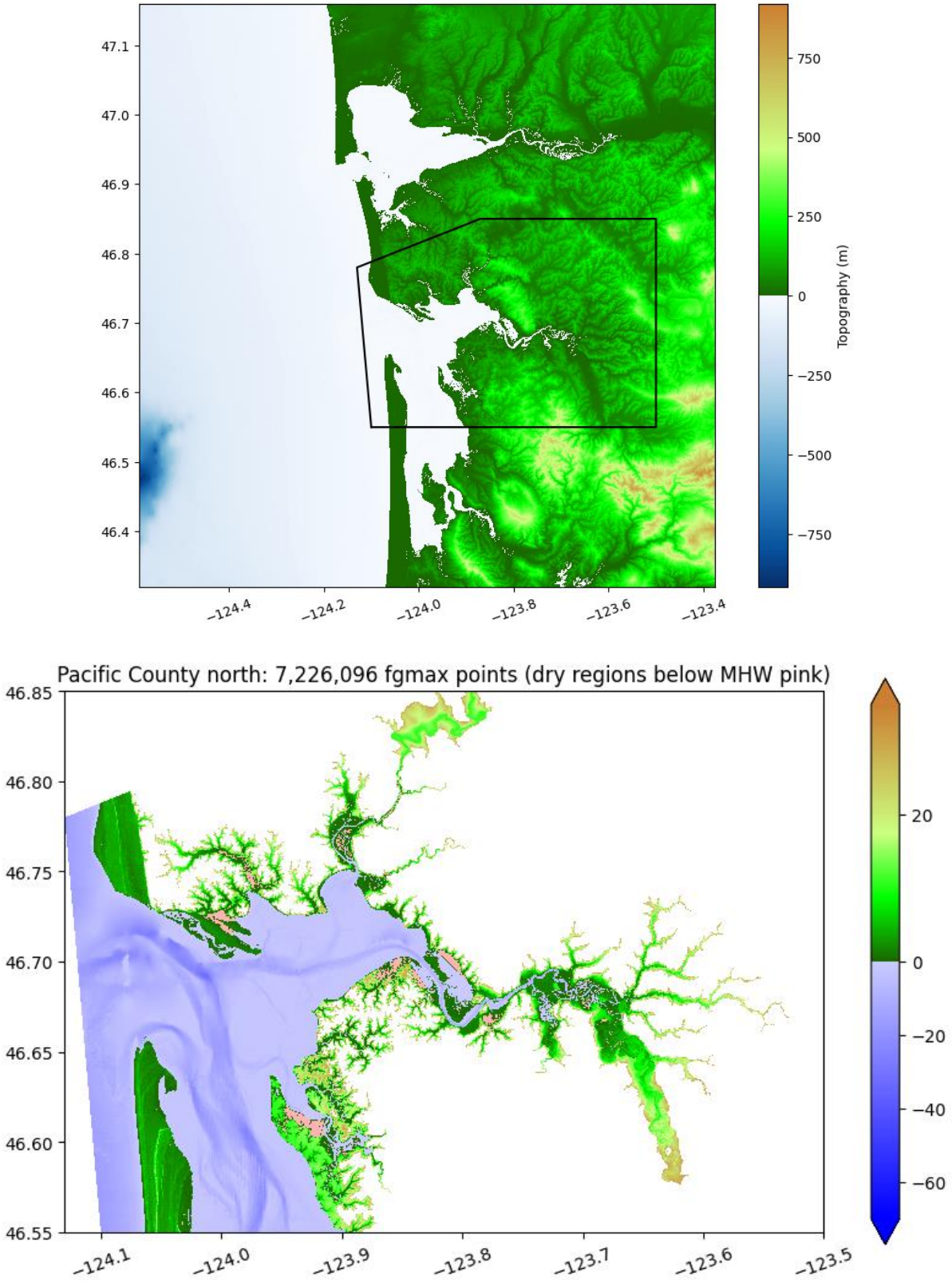

Figure 9: Polygon used to select fgmax points for the Region: Pacific County north (PCn; top). 7,233,307 points selected in the fgmax region (bottom).

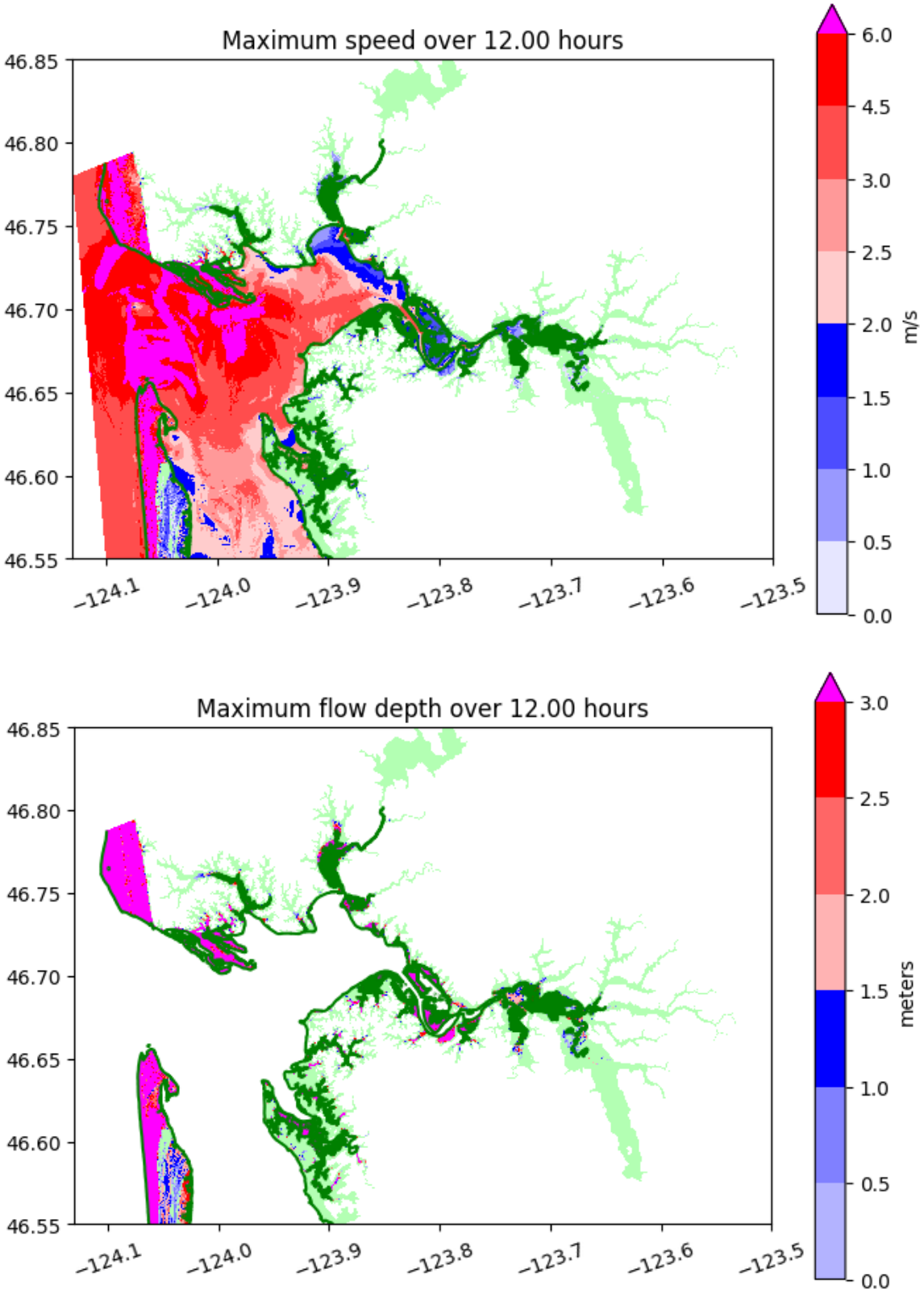

Figure 10: Sample results of maximum speeds (top) and flow depths (bottom) in the Region: Pacific County north (PCn).

6.4 Region Pacific county south

Figure 11 displays the location of the Pacific County south (PCs) fgmax region in the context of the full study region in addition to the fgmax points selected within this region. Points are colored by elevation relative to MHW. Figure 12 provides the maximum current speed and flow depth results for this region.

Noteworthy in this region:

- This study region covers the entirety of the Long Beach Peninsula and Willapa Bay south of Bay Center.
- The deformation of the CSZ L1 earthquake scenario generates ~1.5-2.7 meters (~5-9 feet) of coseismic subsidence in this region (increasing eastward until Naselle). This may cause significant land loss to the daily tide range on the Long Beach Peninsula, especially near the Willapa National Wildlife Refuge, on Long Island, and near Nemah. It may take decades to centuries for the land surface elevation to rebound back to pre-earthquake conditions.
- Modeled onshore coastal inundation is significant in this region, especially near the Pacific Coast as the tsunami overwashed the majority of the Long Beach Peninsula, leaving few pockets of high ground along bayside sand ridges. Modeled current speeds are also dangerously fast in the northern reaches of Willapa Bay, ranging from 2-5 meters/second (4-10 knots), but tend to slow in the southern reaches of Willapa Bay, falling below 2 meters/second (~4 knots).
- High resolution maps covering this study region are available in Eungard and others (2018c).

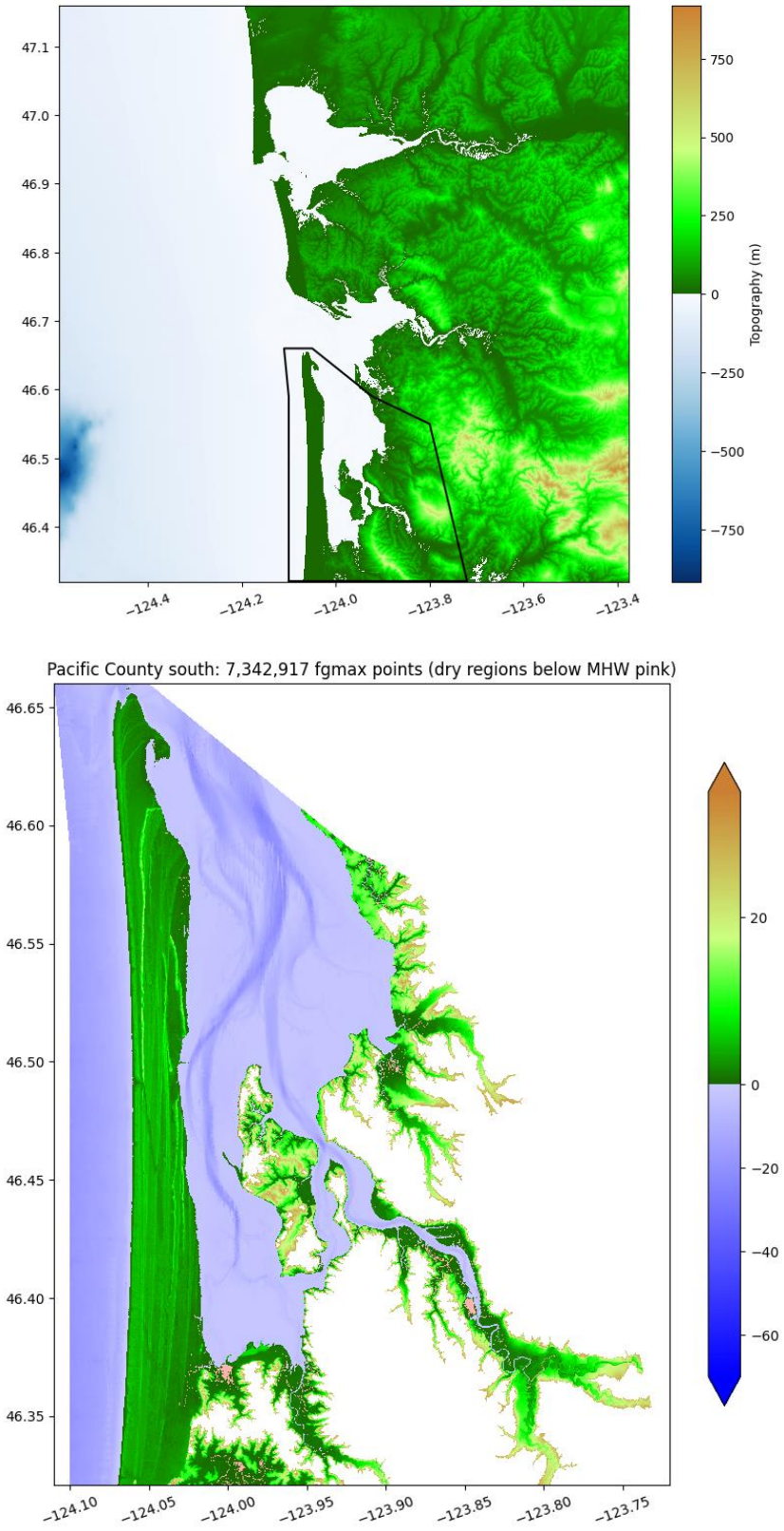

Figure 11: Polygon used to select fgmax points for the Region: Pacific County south (PCs; top). 7,233,307 points selected in the fgmax region (bottom).

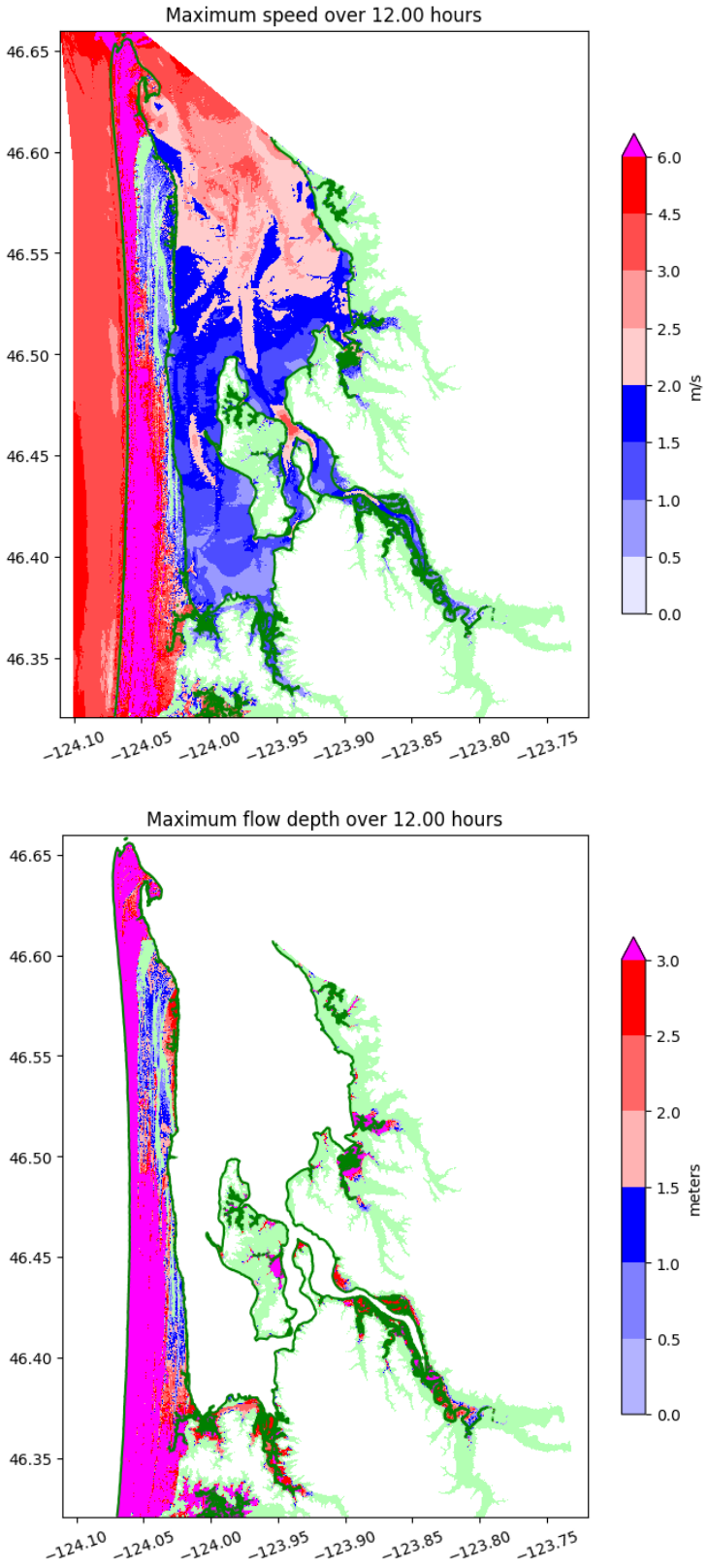

Figure 12: Sample results of maximum speeds (top) and flow depths (bottom) in the Region: Pacific County south (PCs).

7. Synthetic tide gauge locations

Figure 13 provides a map visual for 75 synthetic tide gauges used to capture time series of the water surface elevation, bathymetry depth, current speed, and u-v velocity plane at specified locations for tsunami simulation generated by the L1 earthquake scenario. Not all 75 gauges were used in each fgmax region simulation: Figure 14 shows the locations of the gauges modeled within the GHw region; Figure 15 shows the locations of the gauges modeled within the GHe region; Figure 16 shows the locations of the gauges modeled within the PCn region; and Figure 17 shows the locations of the gauges modeled within the PCs region. All synthetic gauges were placed in the water and modeled at 1/3" resolution. Timestep 0 in each tide gauge also recorded the amount of coseismic subsidence generated by the L1 earthquake scenario (Appendix B, dzi). Table 3 summarizes all tide gauge locations and which fgmax region it was simulated in.

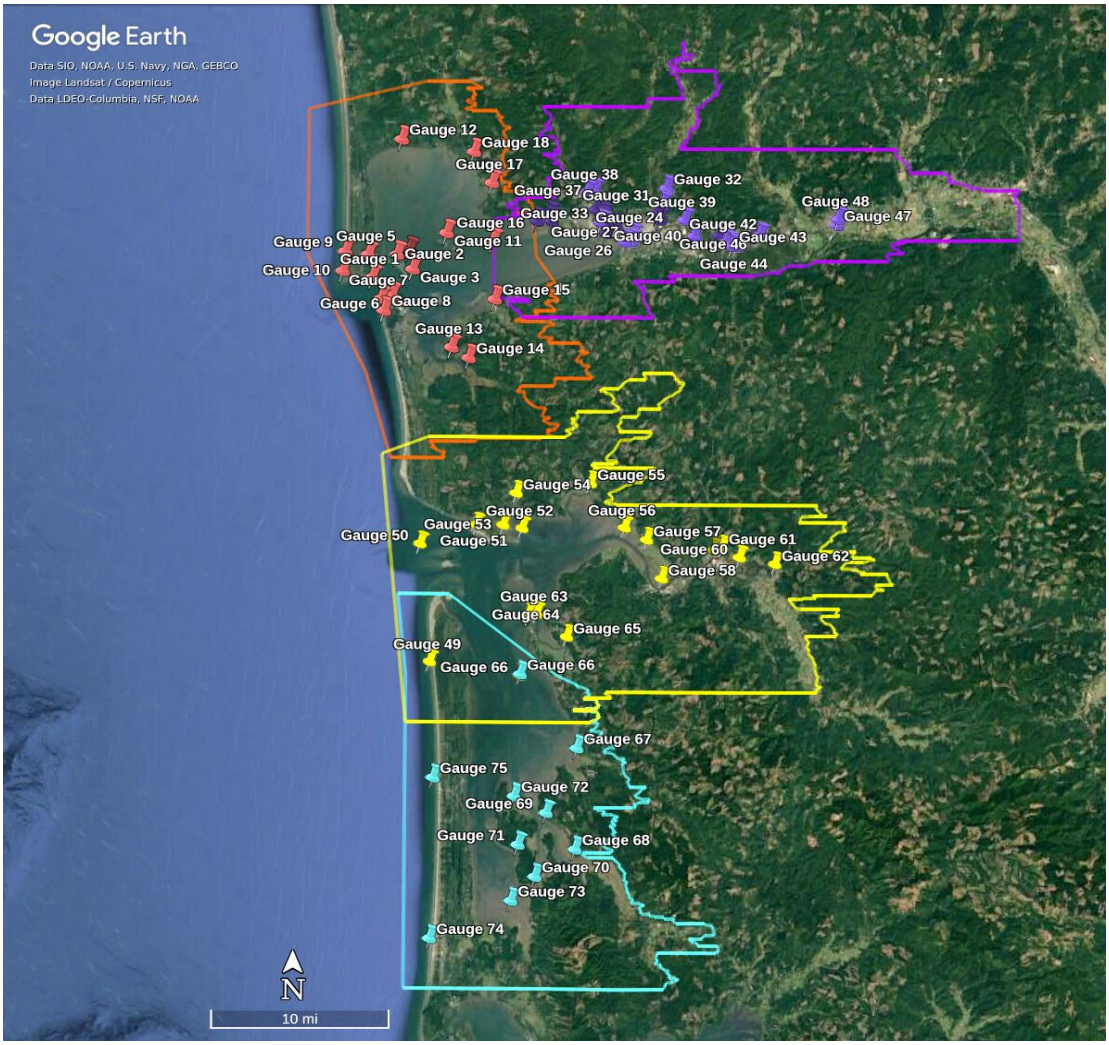

Figure 13. All 75 synthetic gauge locations used for this study. Gauges are color coded to the fgmax region they were simulated on: Grays Harbor west (orange), Grays Harbor east (purple), Pacific County north (yellow), and Pacific County south (teal). Gauge 66 was simulated in both the Pacific County north and south runs and yielded near-identical results. All time series were recorded with 1/3rd arc-second (1/3") resolution.

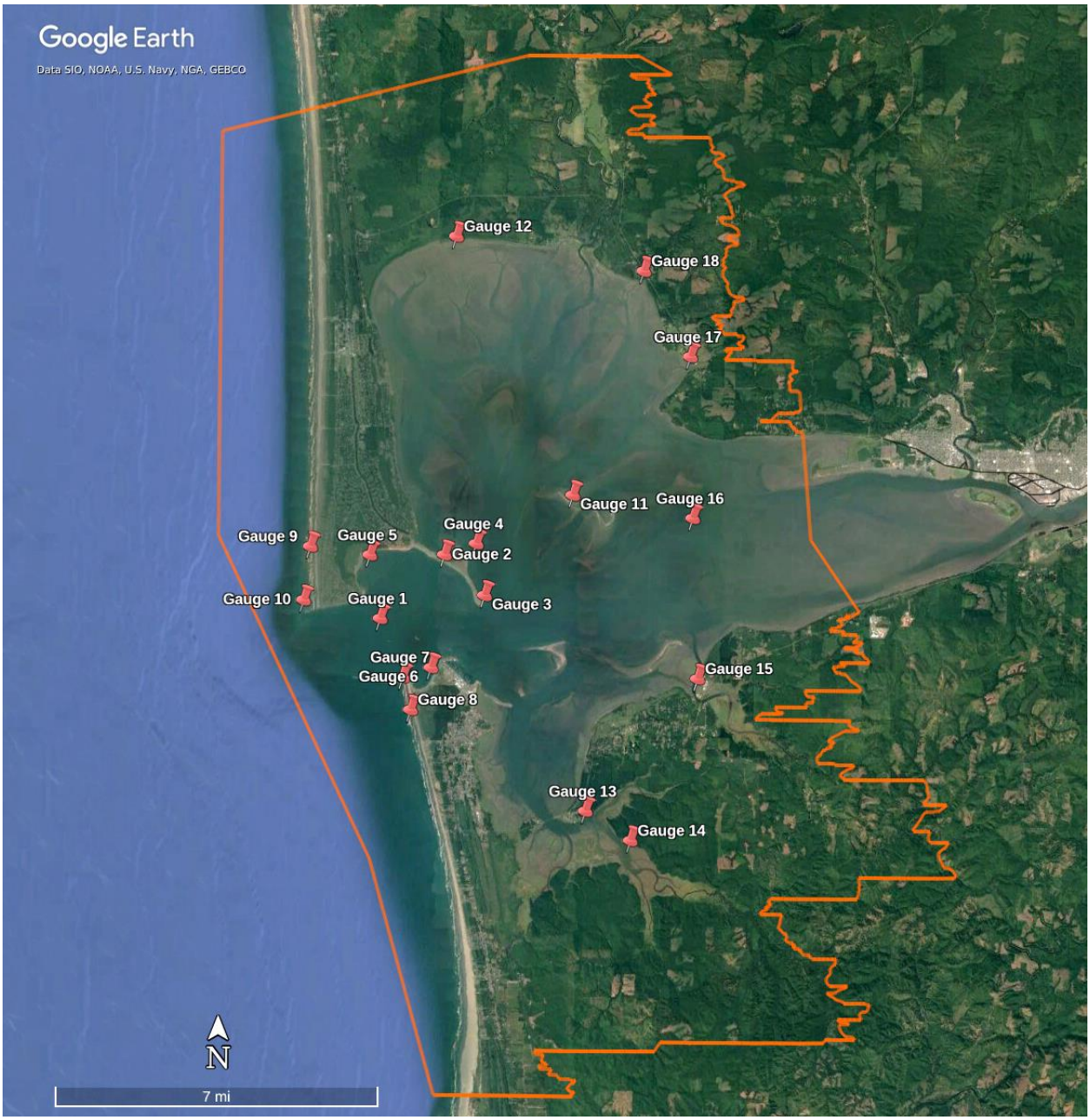

Figure 14. Grays Harbor west synthetic tide gauge location (gauges 1-18).

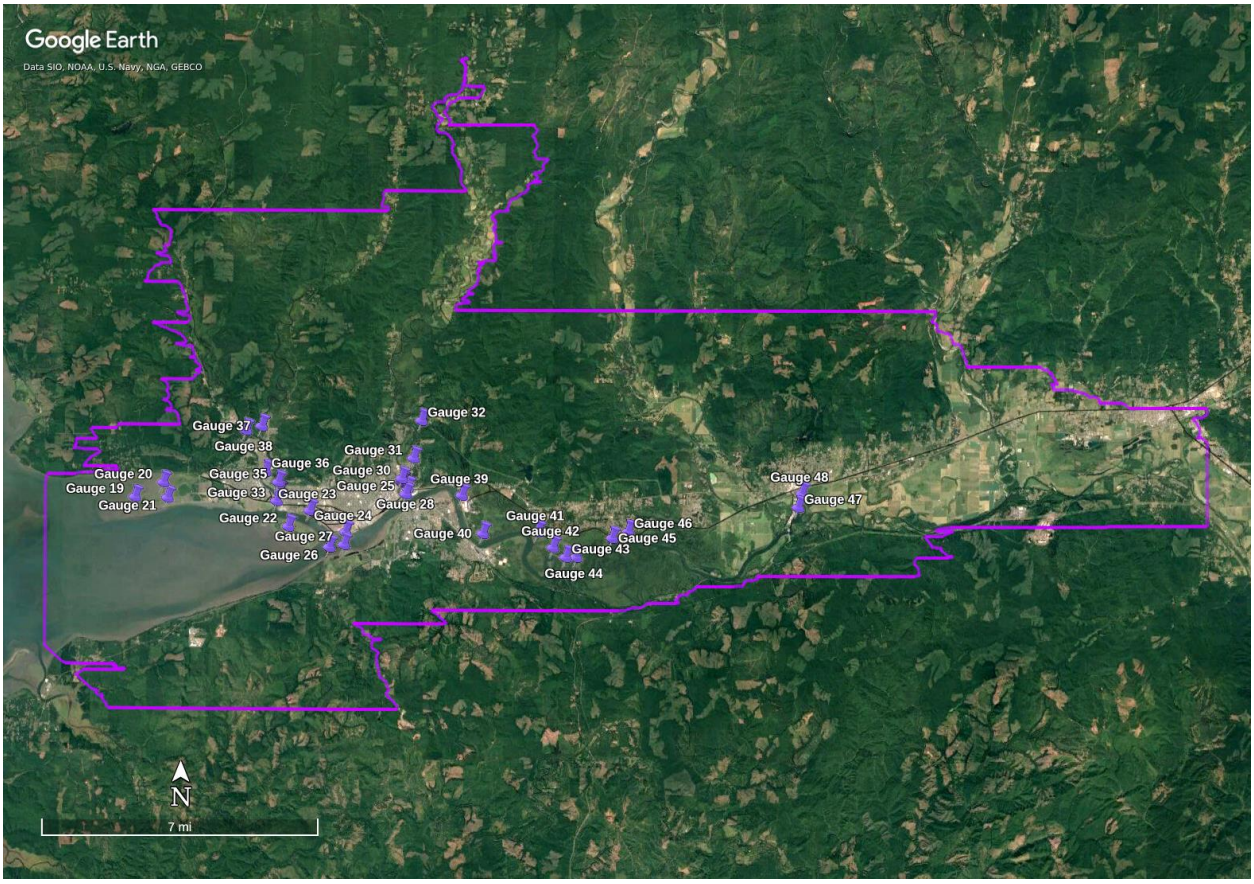

Figure 15. Grays Harbor east synthetic tide gauge locations (gauges 19-48).

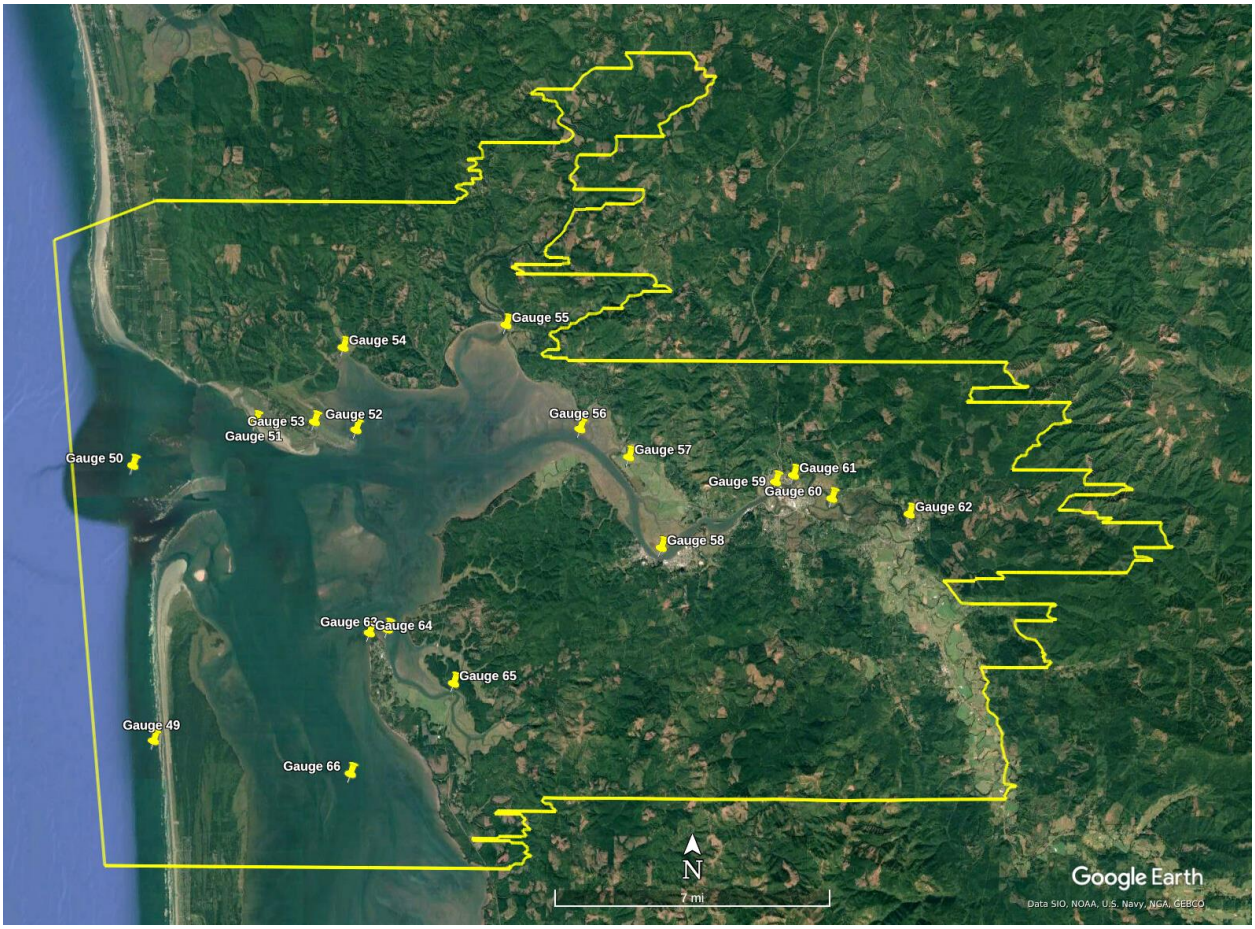

Figure 16. Pacific County north synthetic tide gauge locations (gauges 49-66)

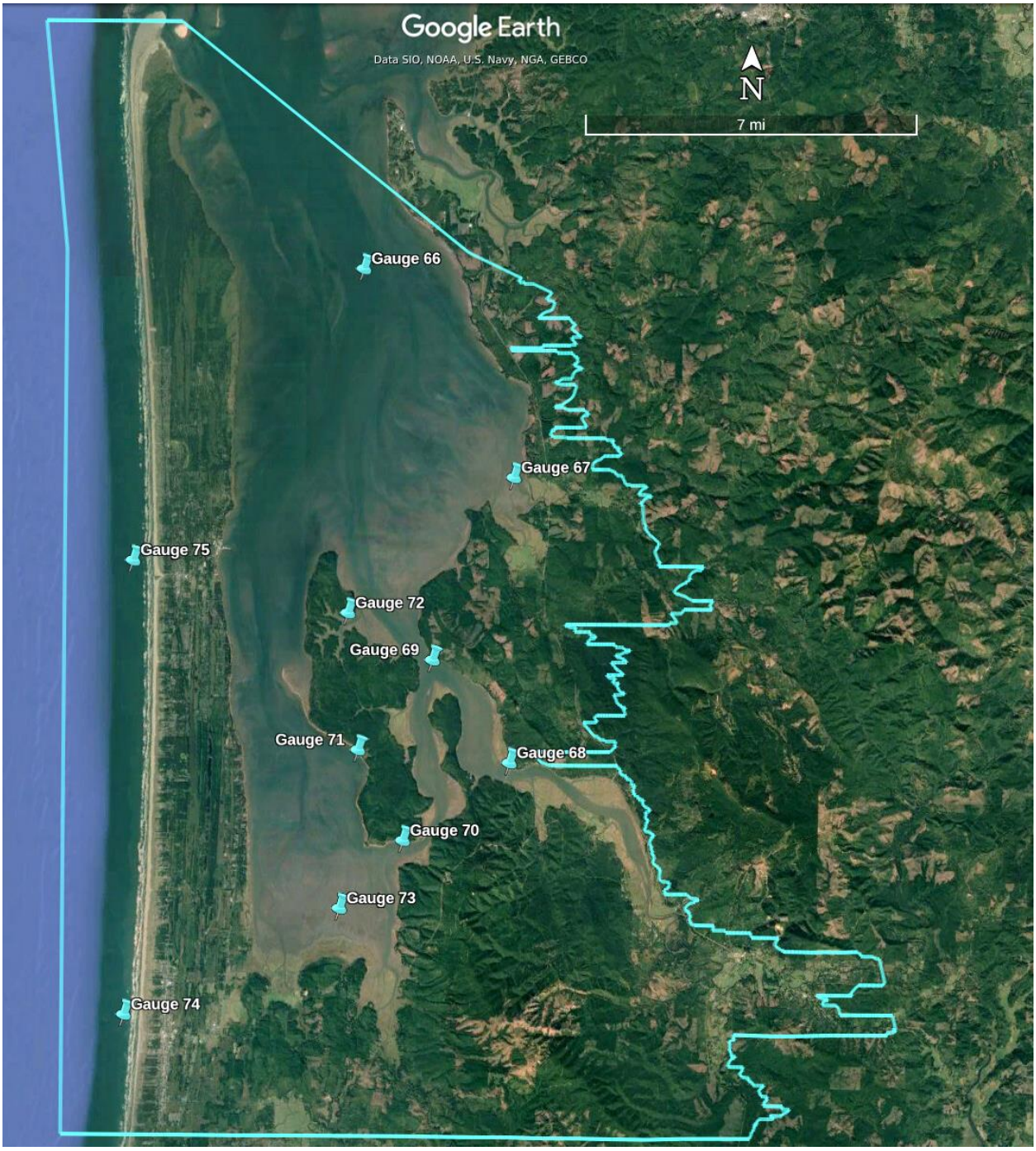

Figure 17. Pacific County south synthetic tide gauge locations (gauges 66-75).

Table 3. Locations of the synthetic gauges used in this study. These gauges are also shown in map view in Figures 13-17. Each gauge records time series results from a tsunami generated by the Cascadia L1 scenario (Section 7.1).

Gauge	Latitude	Longitude	Description	Fgmax region
1	46.92077	-124.148	Grays Harbor entrance	GHw
2	46.94072	-124.119	W of Damon Point State Park	GHw
3	46.92819	-124.1	Damon Point	GHw
4	46.94425	-124.104	E of Damon Point State Park	GHw
5	46.94049	-124.153	Mouth of Oyhut Wildlife Recreation Area	GHw
6	46.9056	-124.124	Halfmoon Bay	GHw
7	46.9026	-124.137	Offshore Westhaven State Park	GHw
8	46.89245	-124.133	Offshore Westport Light State Park	GHw
9	46.94297	-124.18	Offshore Ocean Shores	GHw
10	46.92631	-124.183	Offshore North Jetty Ocean Shores	GHw
11	46.95956	-124.06	W of Sand Island	GHw
12	47.03972	-124.114	Grays Harbor N	GHw
13	46.86141	-124.053	Beardslee Slough	GHw
14	46.85236	-124.033	Sopun Inlet	GHw
15	46.90276	-124.003	John River mouth	GHw
16	46.95263	-124.006	Grays Harbor middle	GHw
17	47.00282	-124.007	Grass Creek mouth	GHw
18	47.02933	-124.029	Chenoius Creek mouth	GHw
19	46.97016	-123.954	West of Bowerman Airport	Ghe
20	46.9755	-123.939	North of Bowerman Airport	Ghe
21	46.96993	-123.937	South of Bowerman Airport	Ghe
22	46.9597	-123.872	Rennie Island SW	Ghe
23	46.96548	-123.861	Rennie Island NE	Ghe
24	46.95774	123.8416	Chehalis River mouth	Ghe
25	46.97162	123.8095	Aberdeen S Aberdeen Bridge	Ghe
26	46.95225	123.8502	Newskah Creek mouth	Ghe
27	46.95317	123.8423	Charley Creek mouth	Ghe
28	46.97385	-123.809	Wishkah River mouth	Ghe
29	46.97589	-123.812	E Heron St S	Ghe
30	46.97727	-123.812	E Wishkah St N	Ghe
31	46.98468	-123.805	Young St W	Ghe
32	46.99838	-123.801	Bear Creek mouth	Ghe
33	46.96897	-123.878	Hoquiam River mouth	Ghe
34	46.97224	-123.877	Burlington Northern Santa Fe N	Ghe
35	46.97576	-123.878	Simpson Ave N	Ghe
36	46.97962	-123.884	Riverside Ave N	Ghe
37	46.99612	-123.886	East Fork Hoquiam River confluence	Ghe
38	46.99457	-123.895	Little Hoqiuam River mouth	Ghe

Gauge	Latitude	Longitude	Description	Fgmax region
39	46.9712	123.7796	Chehalis River W of Junction City	Ghe
40	46.9574	-123.768	Chehalis river N of Cosmopolis	Ghe
41	46.95799	-123.739	Mox Chuck Slough mouth	Ghe
42	46.95246	-123.731	North of Sand Island	Ghe
43	46.94894	-123.724	Chehalis River Blue Slough mouth	Ghe
44	46.94895	-123.718	Chehalis River Preachers Slough mouth	Ghe
45	46.95591	-123.699	South of Higgins Island	Ghe
46	46.95833	-123.691	Chehalis River S of Central Park	Ghe
47	46.96722	-123.6	Chehalis River W of Fox Lumber Mill	Ghe
48	46.97226	-123.598	Chehalis River S of Montesano	Ghe
49	46.59258	-124.076	Offshore Leadbetter Point State Park	PCn
50	46.69373	-124.088	Willapa Bay entrance	PCn
51	46.71024	-124.022	Tokeland Peninsula W	PCn
52	46.70751	-123.968	Tokeland Marina	PCn
53	46.71032	-123.991	Tokeland VES	PCn
54	46.73771	-123.976	Willapa Bay N	PCn
55	46.7464	-123.888	North River mouth	PCn
56	46.7083	-123.848	Willapa River mouth	PCn
57	46.69806	-123.822	Willapa Harbor Airport	PCn
58	46.6648	-123.804	Willapa River South Bend	PCn
59	46.68914	-123.743	South Fork Willapa River confluence	PCn
60	46.68309	-123.713	Willapa River Ellis Slough confluence	PCn
61	46.6916	-123.734	Willapa River US101 Hwy Raymond	PCn
62	46.67744	-123.671	Wilson Creek Willapa River Boat Ramp confluence	PCn
63	46.63422	-123.951	Bay Center E	PCn
64	46.63285	-123.961	Bay Center W	PCn
65	46.61453	-123.915	Palix River US101	PCn
66	46.58104	-123.97	Willapa Bay	PCn/PCs
67	46.51774	-123.903	Nemah mouth	PCs
68	46.43096	-123.905	Naselle River Willapa Bay bridge	PCs
69	46.46213	-123.939	Long Island E	PCs
70	46.40716	-123.952	Long Island S	PCs
71	46.43466	-123.972	Long Island W	PCs
72	46.4763	-123.976	Long Island Archeological Site	PCs
73	46.38641	-123.979	Willapa Bay S	PCs
74	46.35362	-124.074	Offshore Long Beach	PCs
75	46.49189	-124.072	Offshore Ocean Park	PCs

7.1 Gauge output results

The 75 individual synthetic tide gauges are represented by four plots in each respective subsection below. Two of these plots show time series outputs of the flow (water) depth fluctuation (h; left side), and the other two relate to speed (s) and velocity (u and v; right side) for the CSZ L1 scenario at MHW.

The values at h0 indicate the water depth at each gauge prior to earthquake initiation (h0 = 0 for any gauges placed onshore). The subplots beneath each water depth plots represent the change in water heights (h-h0; Δh) over simulation time. Since coseismic subsidence causes the land and sea surface elevations to drop simultaneously, there is no change in water height right after the earthquake (Δh = 0). Thus, following the earthquake, any change in 'h' represents the tsunami wave height relative to the pre-earthquake, water depth conditions initialized at each gauge location.

The speed is shown as a time series of speed vs time ((√ (u2 + v2)); top right), in addition to the individual E—W (u) and N—S (v) velocity components (available upon request by the WGS). The u—v plane located in the lower right plot for each event also allows one to see how the E—W component, u, of the speed compares to the N—S component, v, which can help discern the dominant direction of the tsunami current if one exists. On the other hand, the speed vs time plots simply show one-dimensional current speeds over the course of the simulation. Note that the vertical axes on the gauge plots vary by parameter; the vertical scale is set by the maximum values in each plot to better show the results.

Gauge 1: Grays Harbor entrance

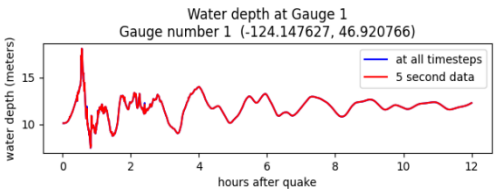

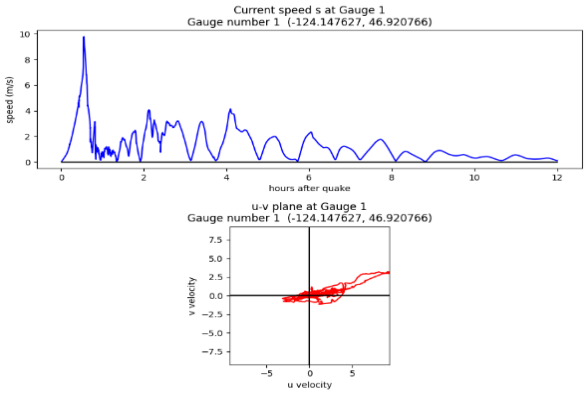

Gauge 2: W of Damon Point State Park

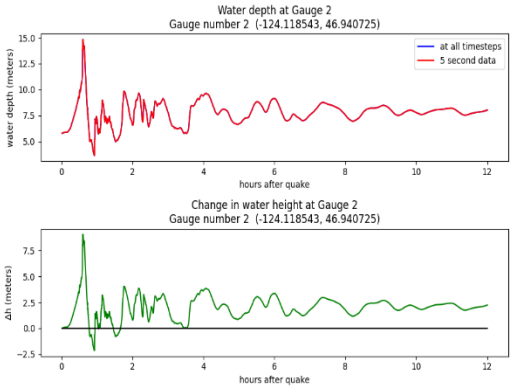

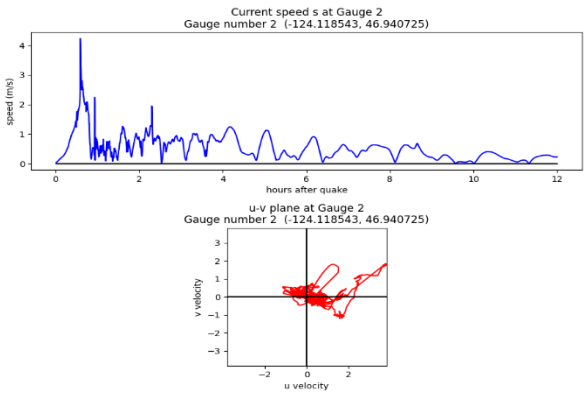

Gauge 3: Damon Point

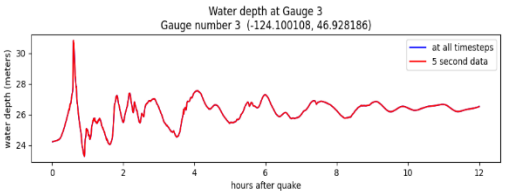

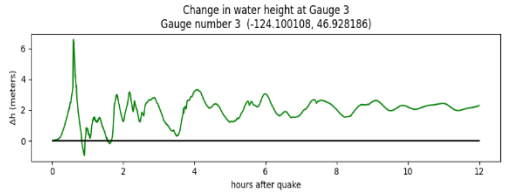

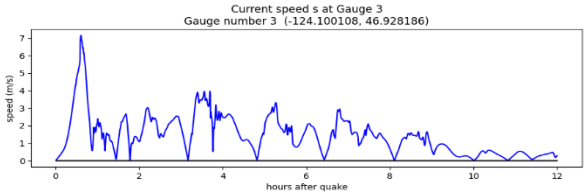

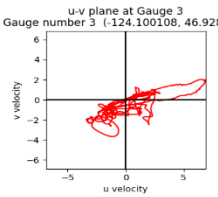

Gauge 4: E of Damon Point State Park

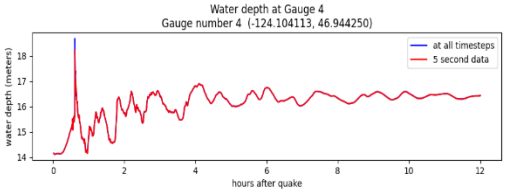

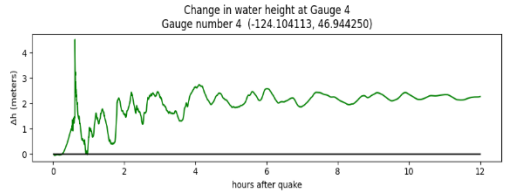

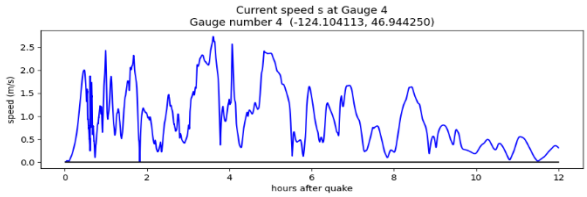

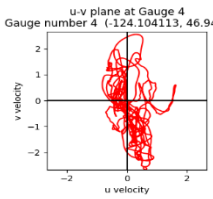

Gauge 5: Mouth of Oyhut Wildlife Recreation Area

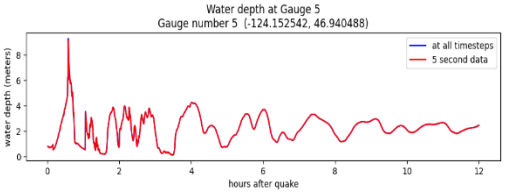

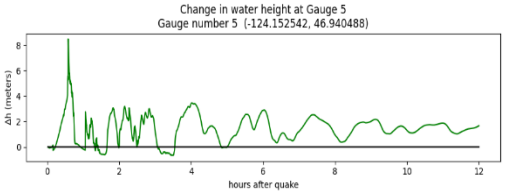

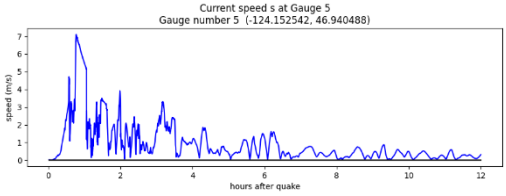

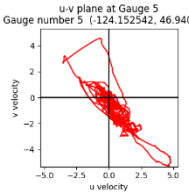

Gauge 6: Halfmoon Bay

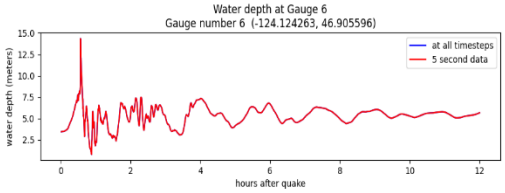

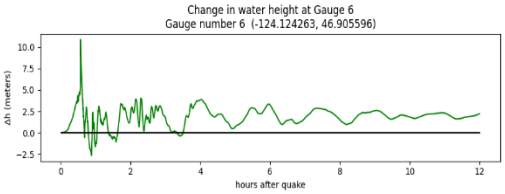

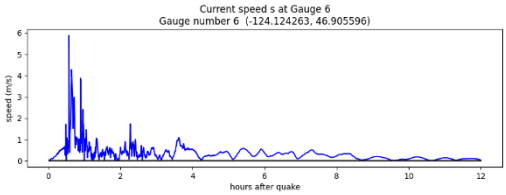

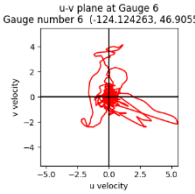

Gauge 7: Offshore Westhaven State Park

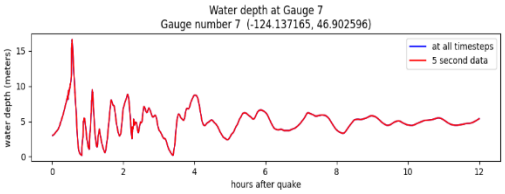

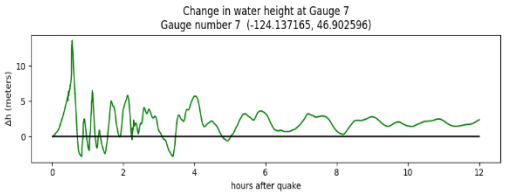

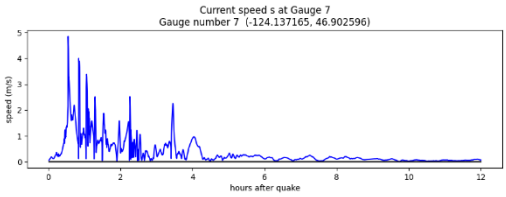

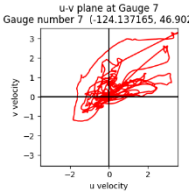

Gauge 8: Offshore Westport Light State Park

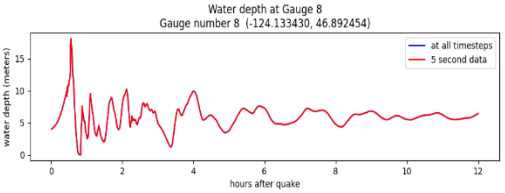

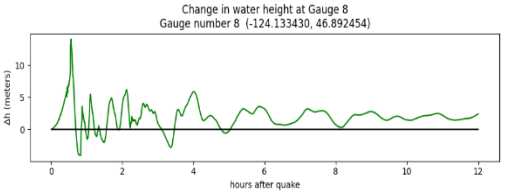

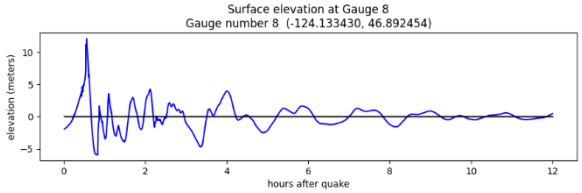

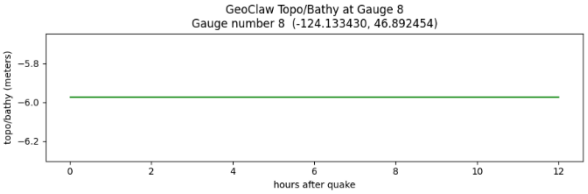

Gauge 9: Offshore Ocean Shores,

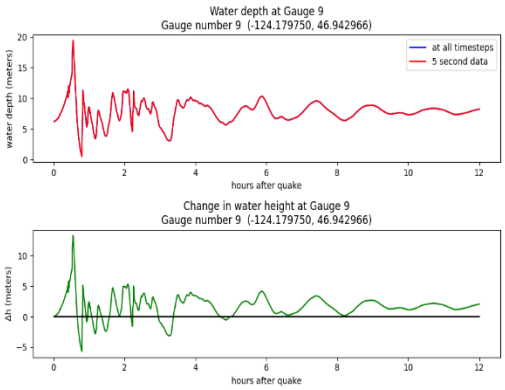

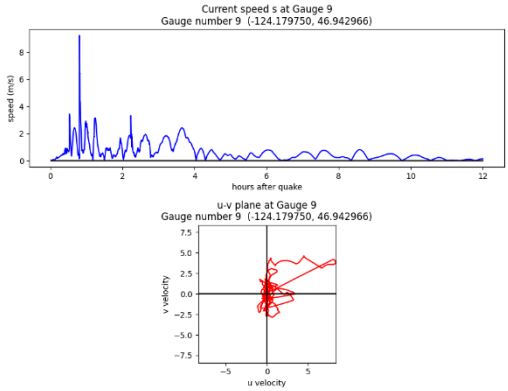

Gauge 10: Offshore North Jetty Ocean Shores

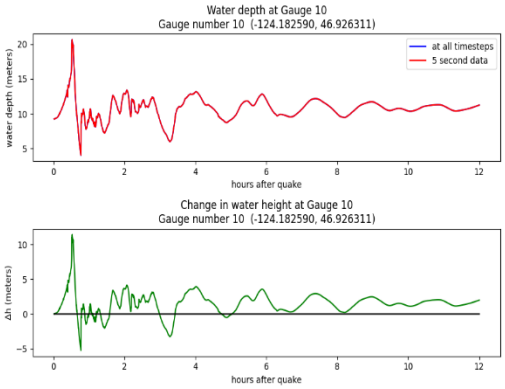

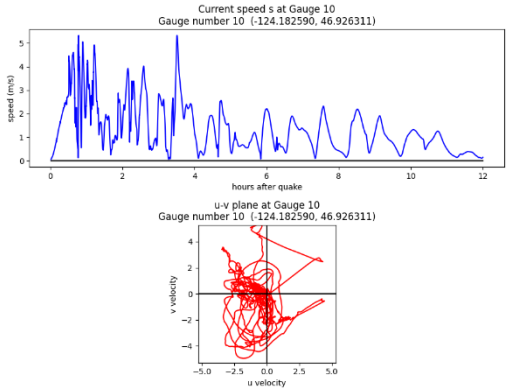

Gauge 11: W of Sand Island

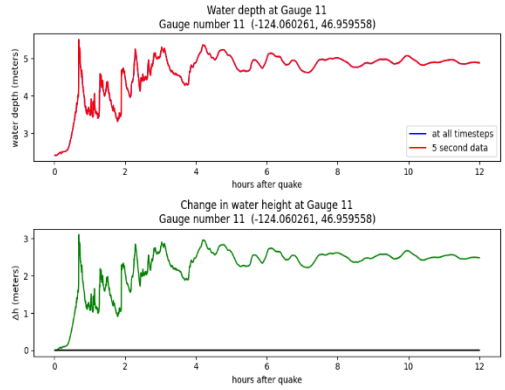

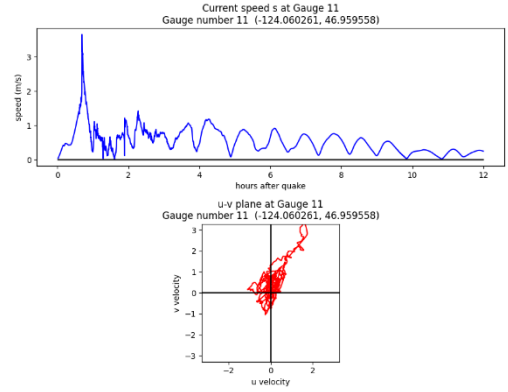

Gauge 12: Grays Harbor N

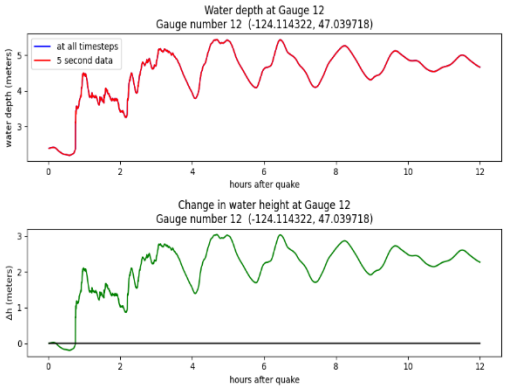

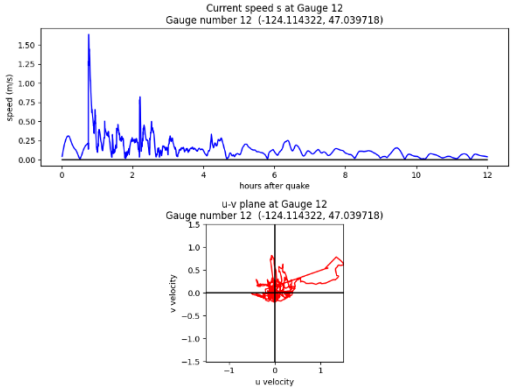

Gauge 13: Beardslee Slough

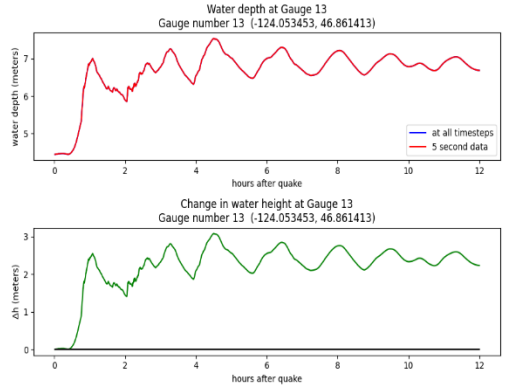

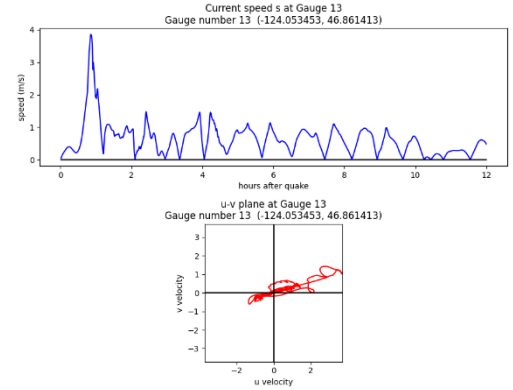

Gauge 14: Sopun Inlet

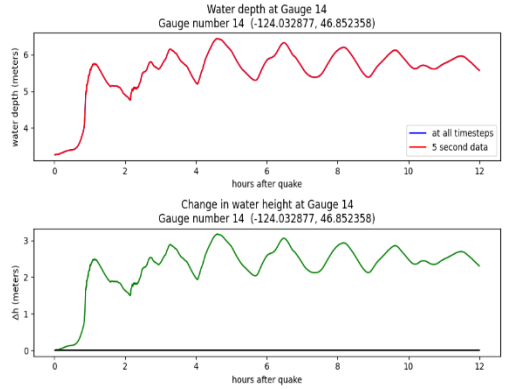

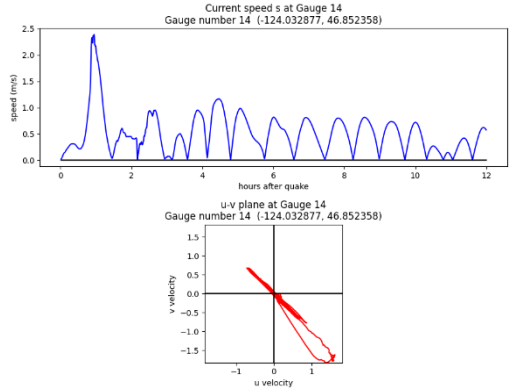

Gauge 15: John River mouth

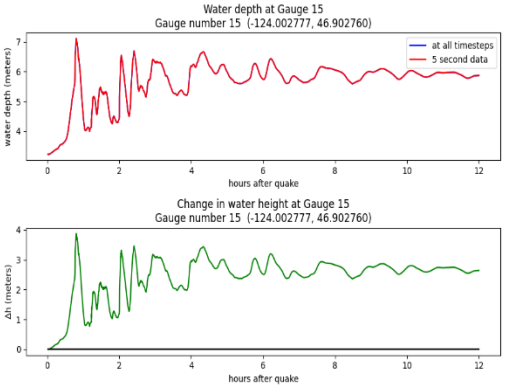

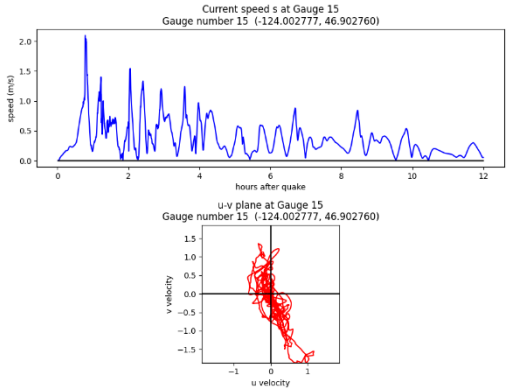

Gauge 16: Grays Harbor middle

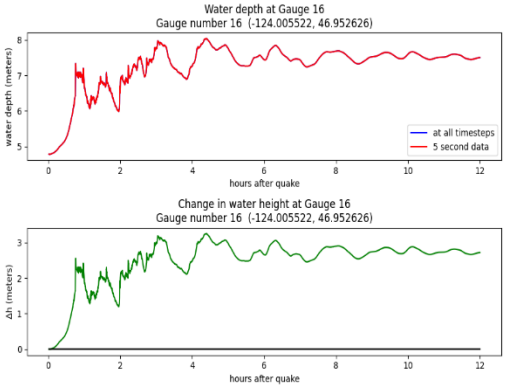

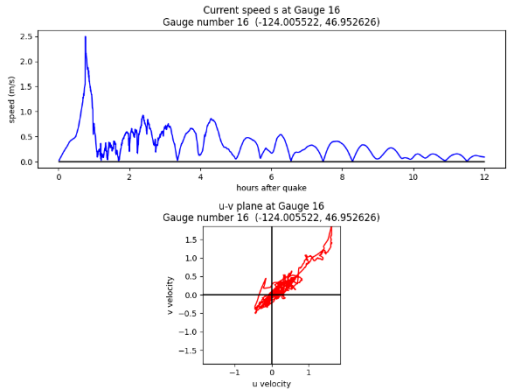

Gauge 17: Grass Creek mouth

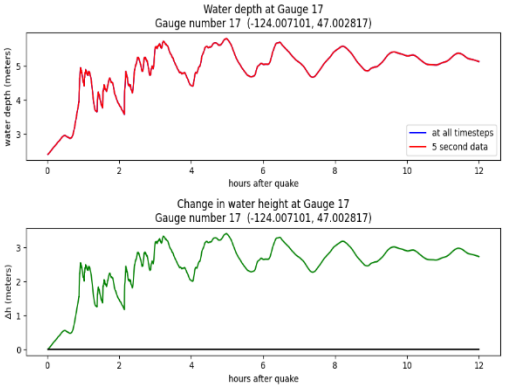

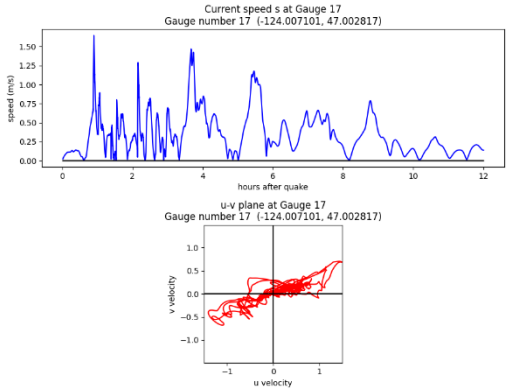

Gauge 18: Chenoius Creek mouth

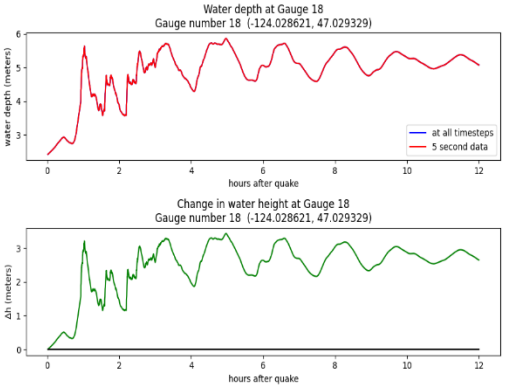

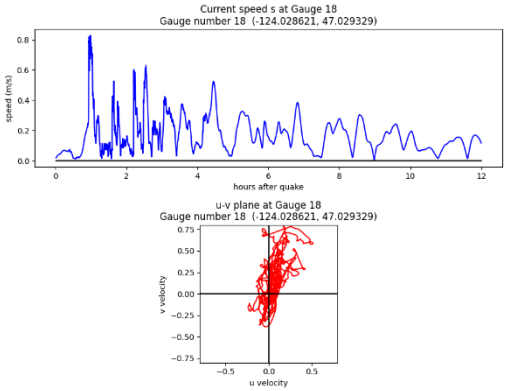

Gauge 19: West of Bowerman Airport

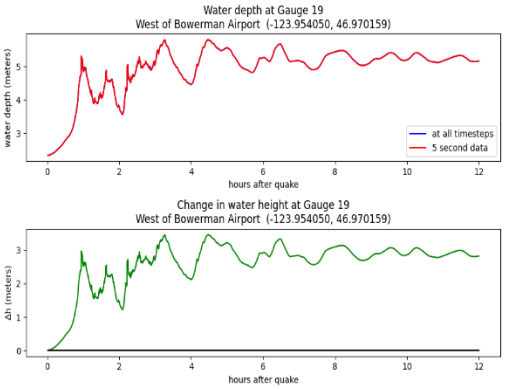

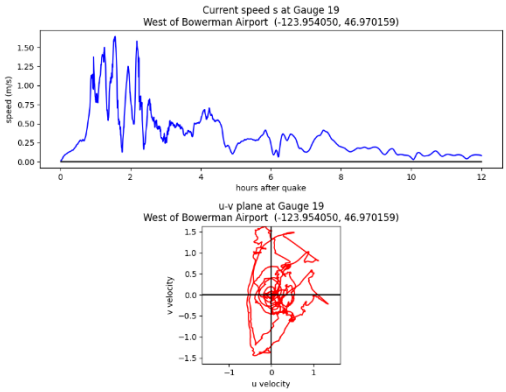

Gauge 20: North of Bowerman Airport

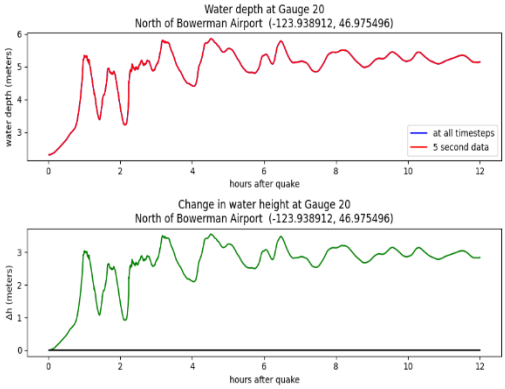

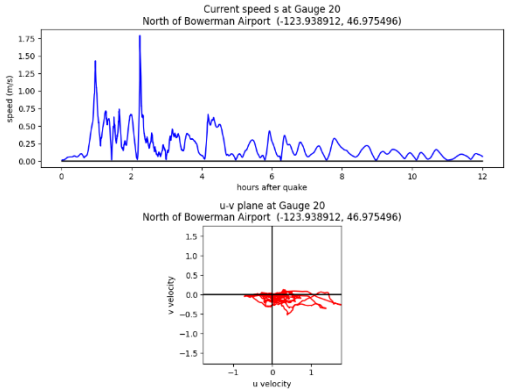

Gauge 21: South of Bowerman Airport

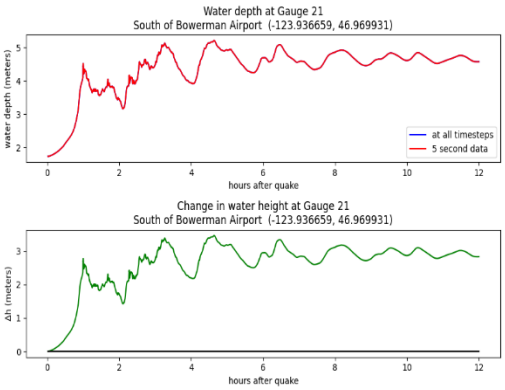

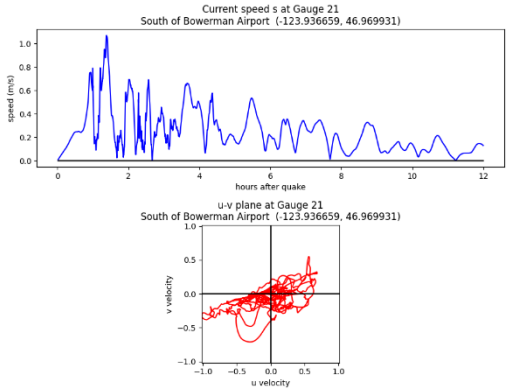

Gauge 22: Rennie Island SW

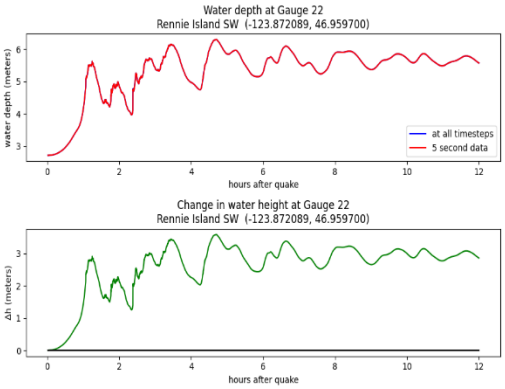

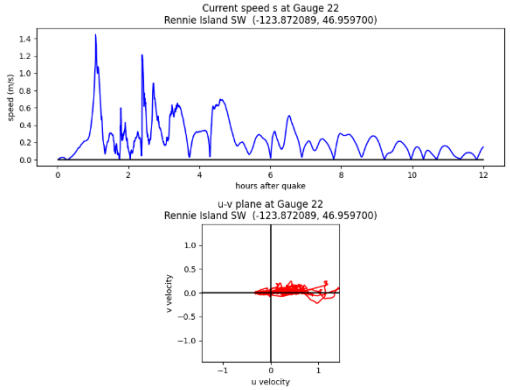

Gauge 23: Rennie Island NE

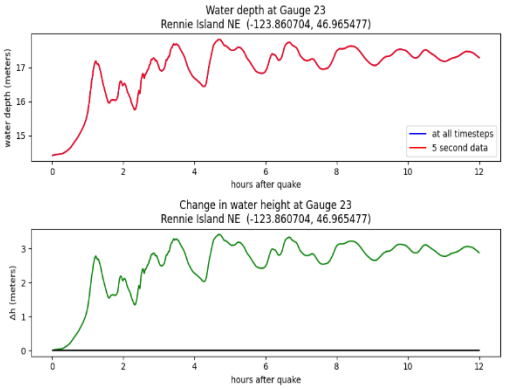

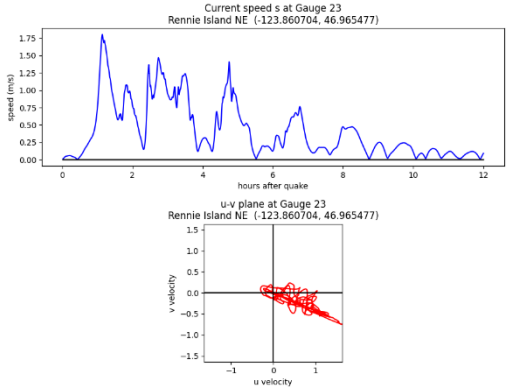

Gauge 24: E of Chehalis River mouth

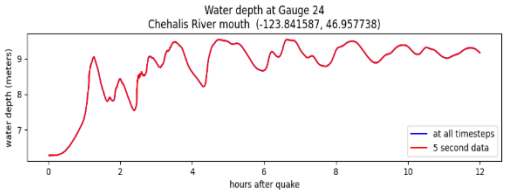

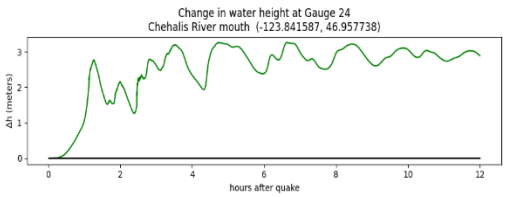

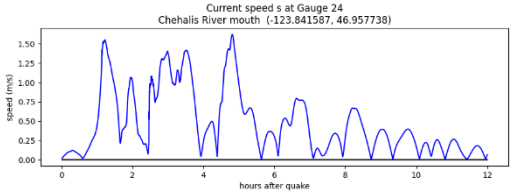

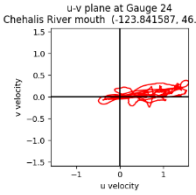

Gauge 25: Aberdeen S Aberdeen Bridge

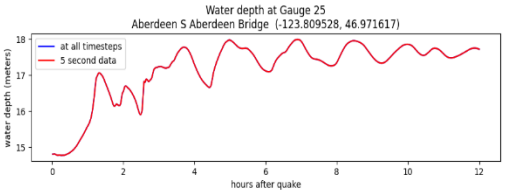

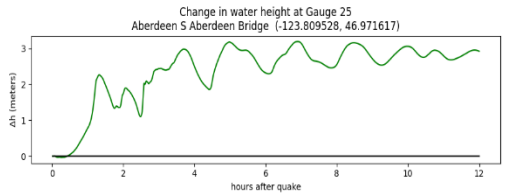

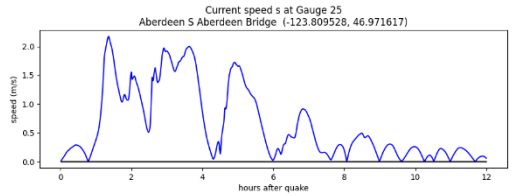

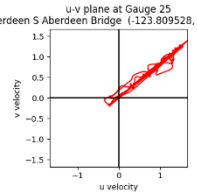

Gauge 26: Newskah Creek mouth

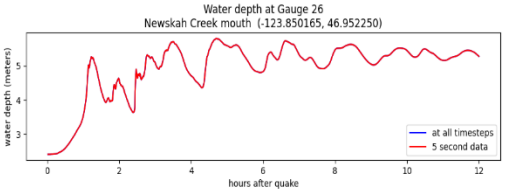

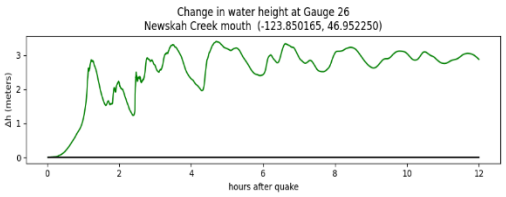

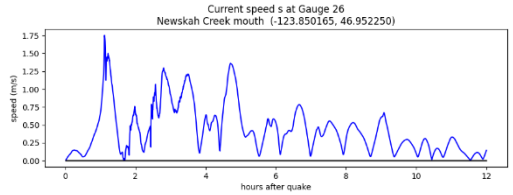

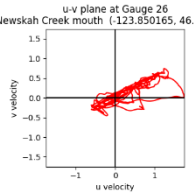

Gauge 27: Charley Creek mouth

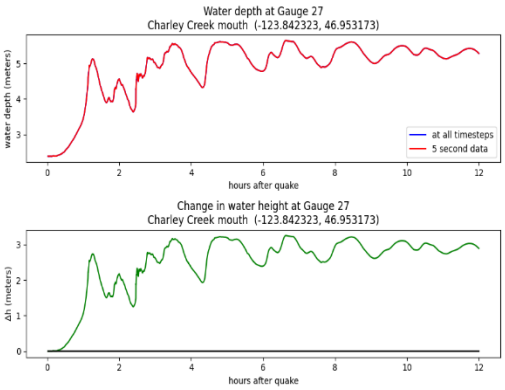

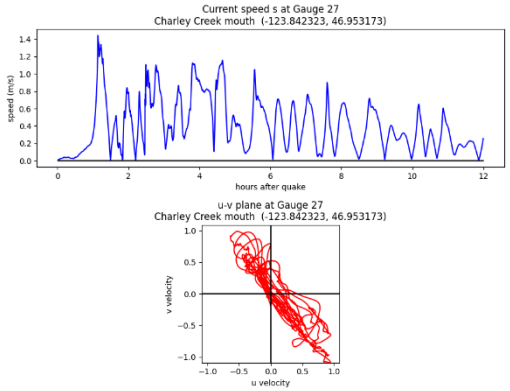

Gauge 28: Wishkah River mouth

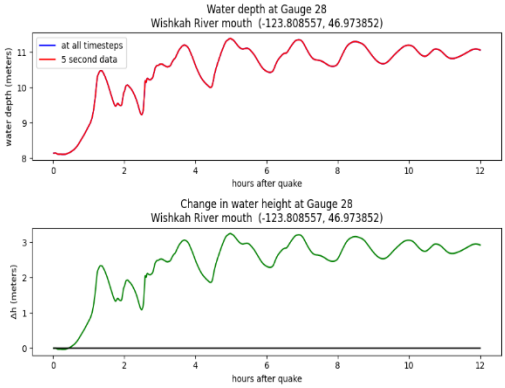

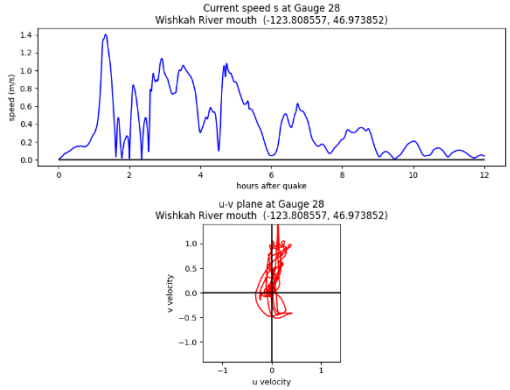

Gauge 29: E Heron St S

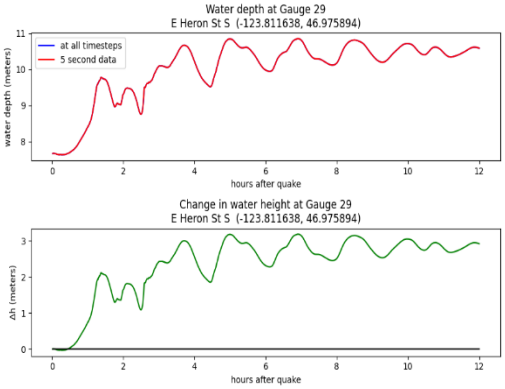

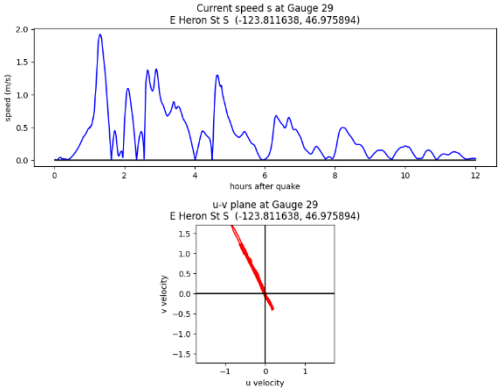

Gauge 30: E Wishkah St N

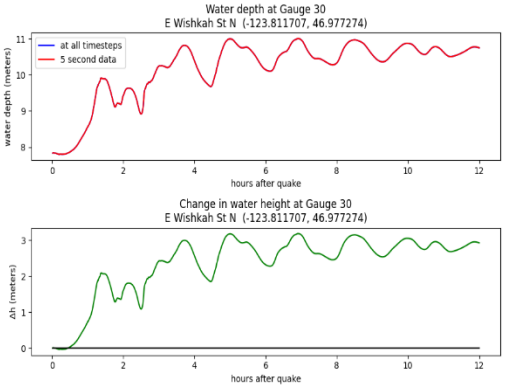

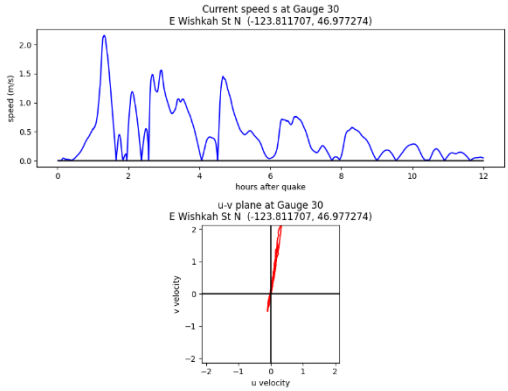

Gauge 31: Young St W

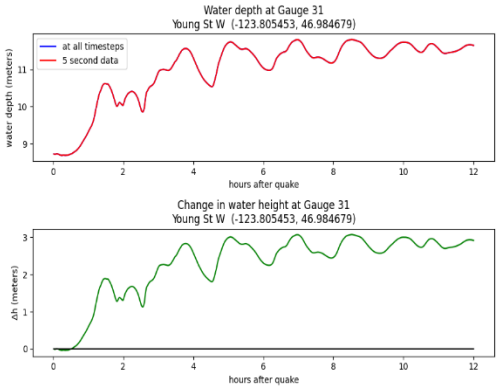

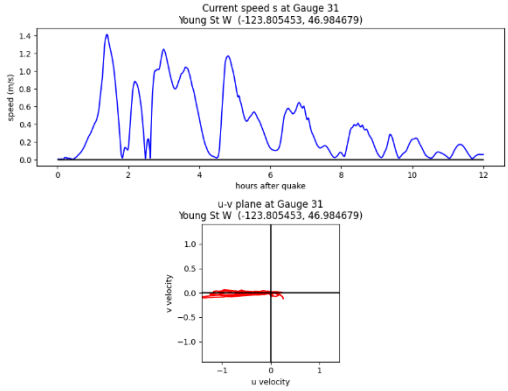

Gauge 32: Bear Creek mouth

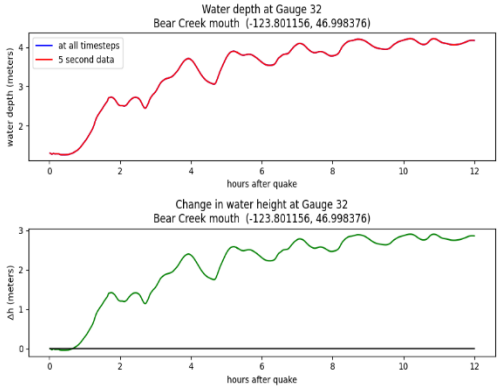

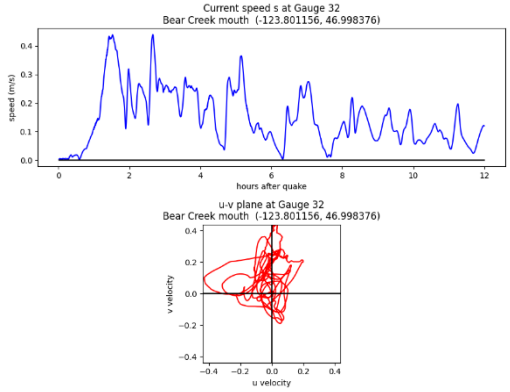

Gauge 33: Hoquiam River mouth

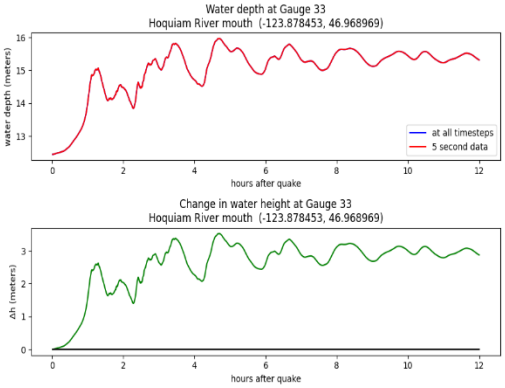

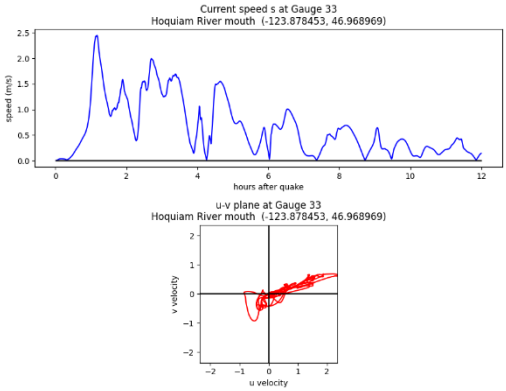

Gauge 34: Burlington Northern Santa Fe N

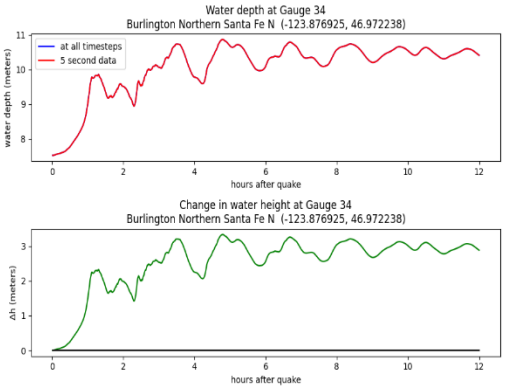

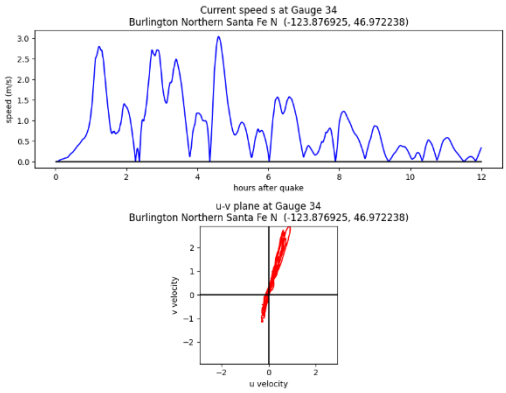

Gauge 35: Simpson Ave N

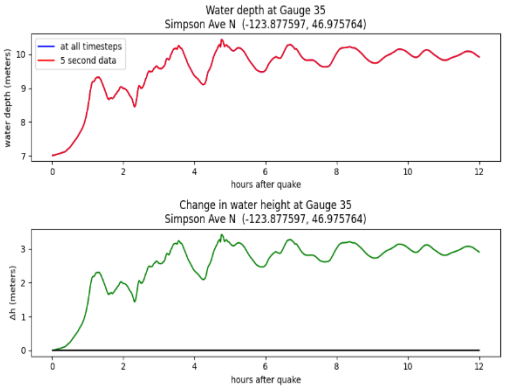

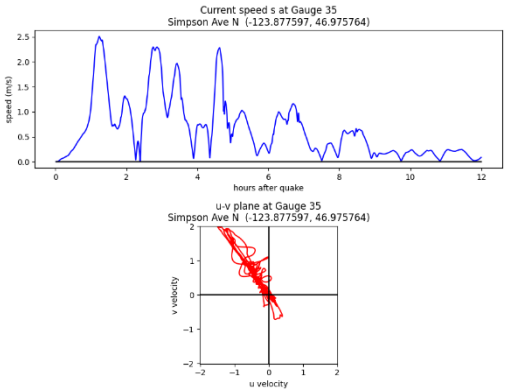

Gauge 36: Riverside Ave N

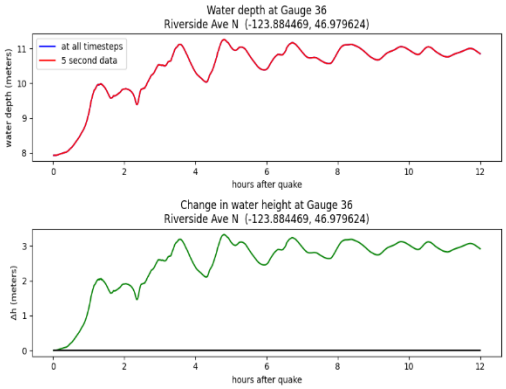

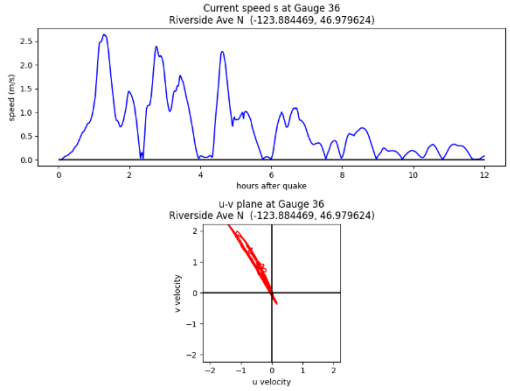

Gauge 37: East Fork Hoquiam River confluence

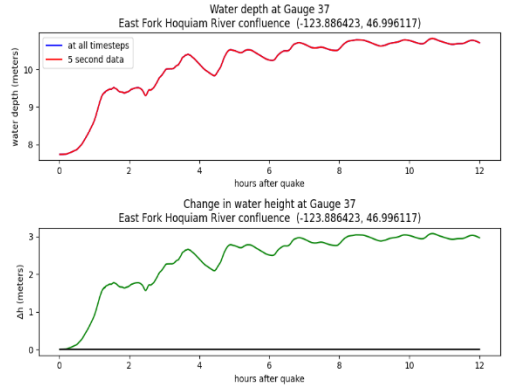

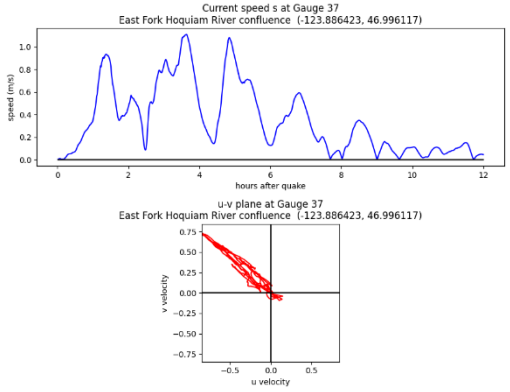

Gauge 38: Little Hoquiam River mouth

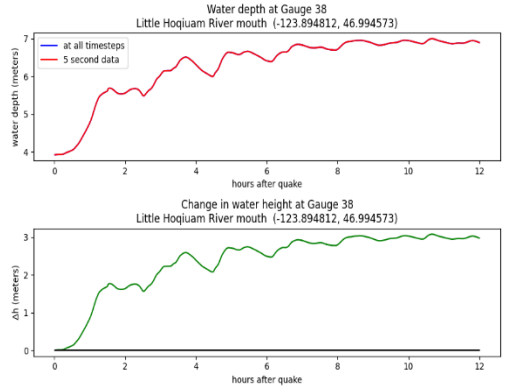

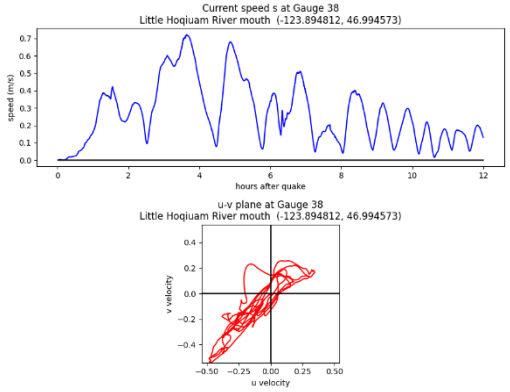

Gauge 39: Chehalis River W of Junction City

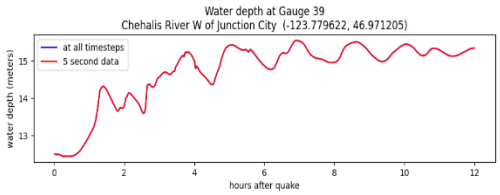

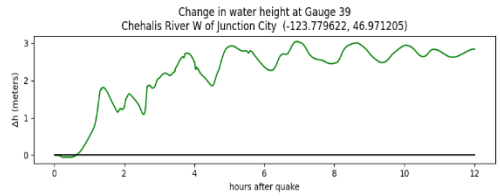

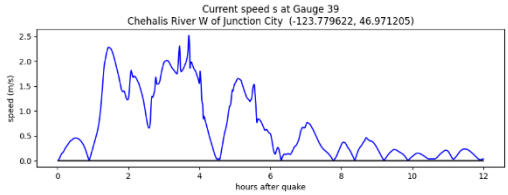

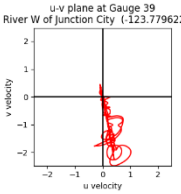

Gauge 40: Chehalis River N of Cosmopolis

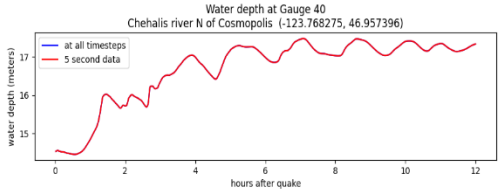

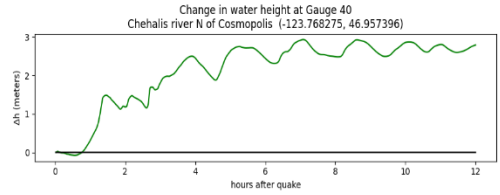

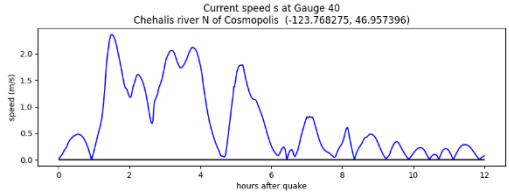

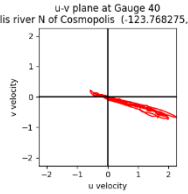

Gauge 41: Mox Chuck Slough mouth

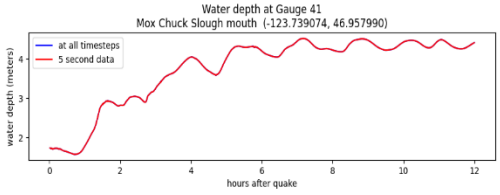

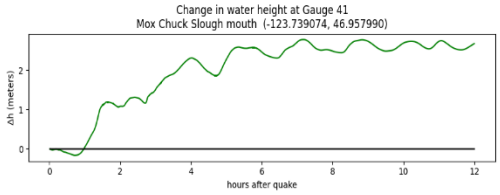

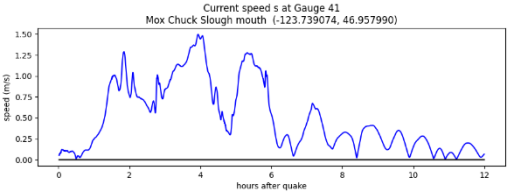

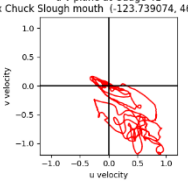

Gauge 42: North of Sand Island

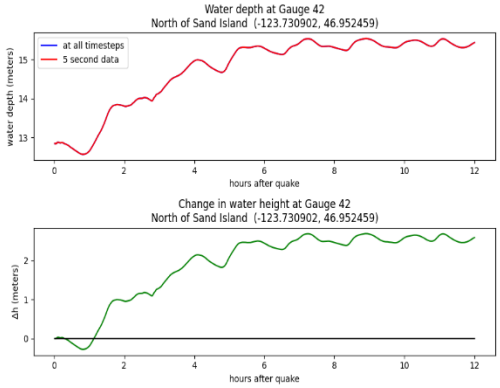

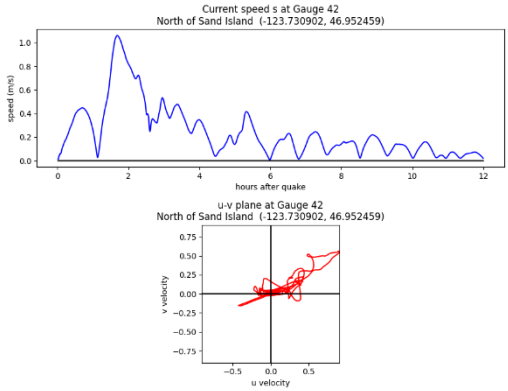

Gauge 43: Chehalis River Blue Slough mouth

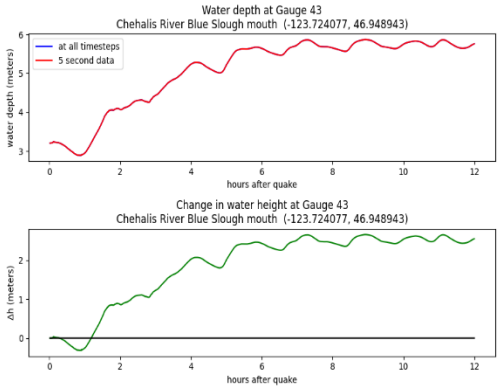

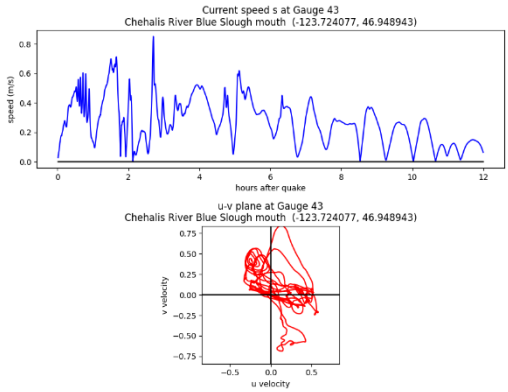

Gauge 44: Chehalis River Preachers Slough mouth

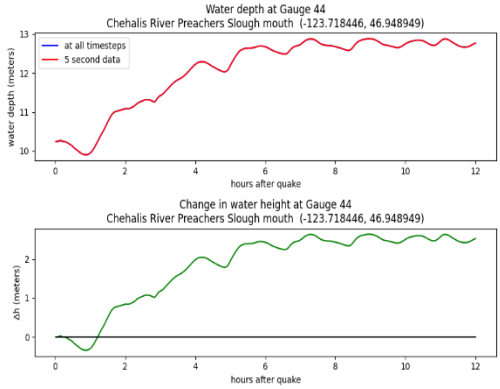

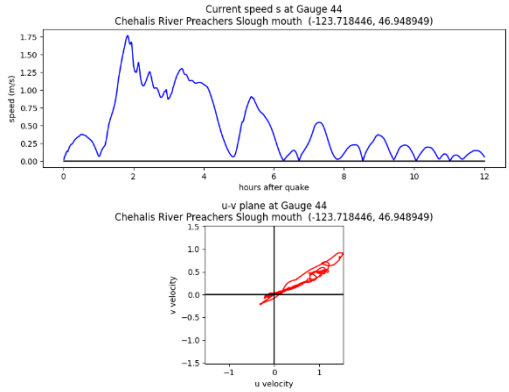

Gauge 45: South of Higgins Island

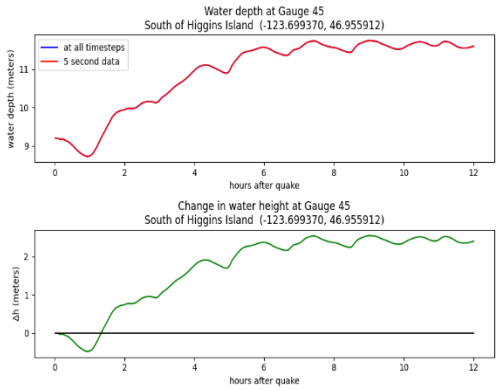

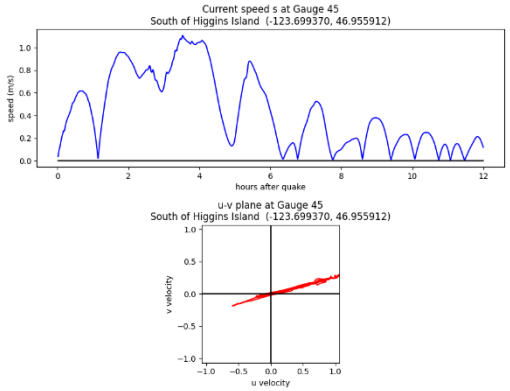

Gauge 46: Chehalis River S of Central Park

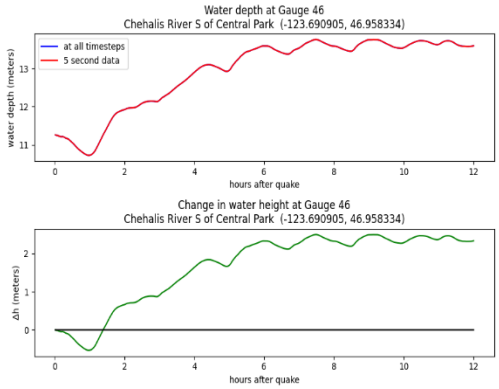

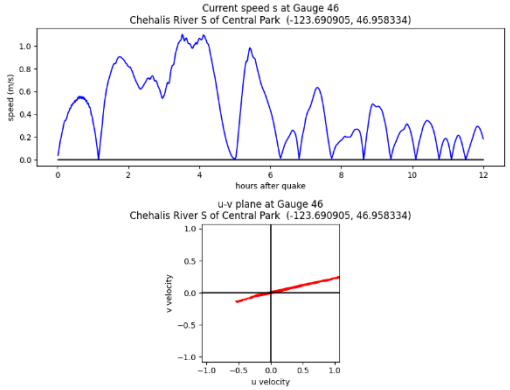

Gauge 47: Chehalis River W of Fox Lumber Mill

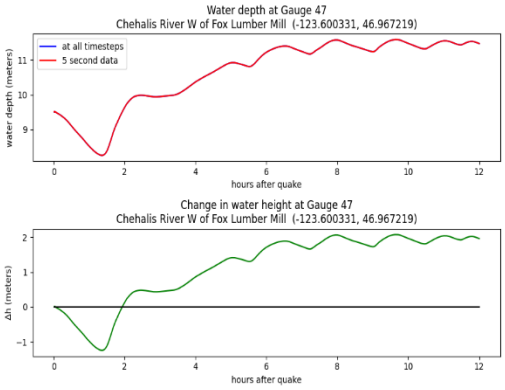

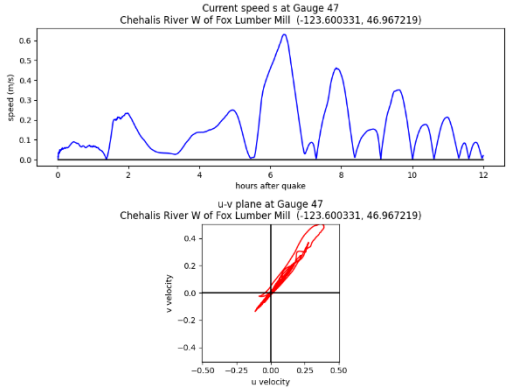

Gauge 48: Chehalis River S of Montesano

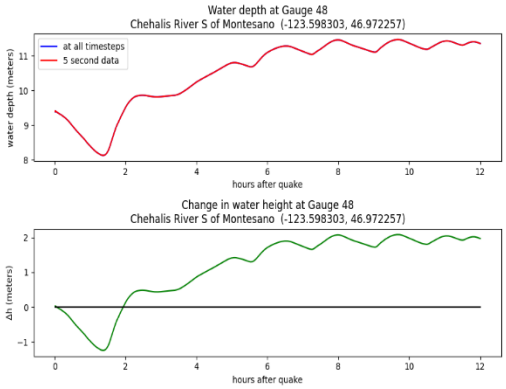

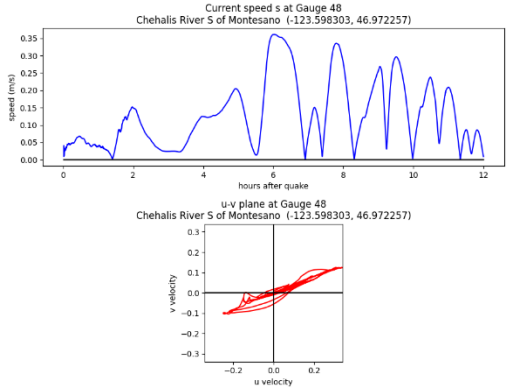

Gauge 49: Offshore Leadbetter Point State Park

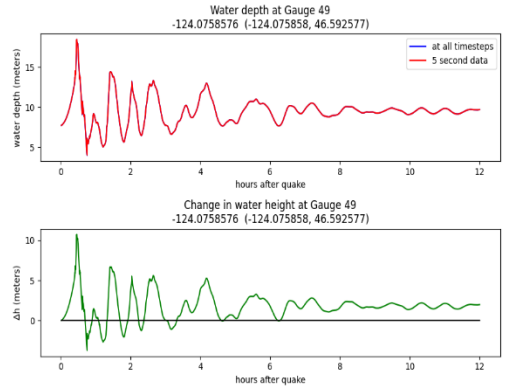

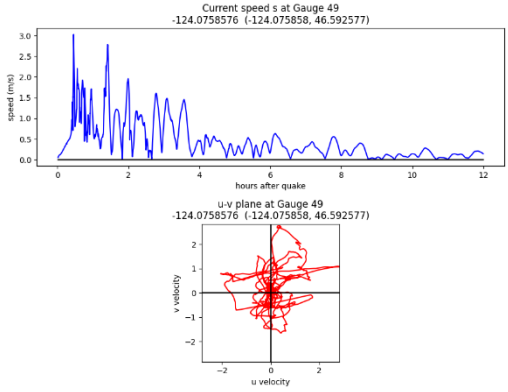

Gauge 50: Willapa Bay entrance

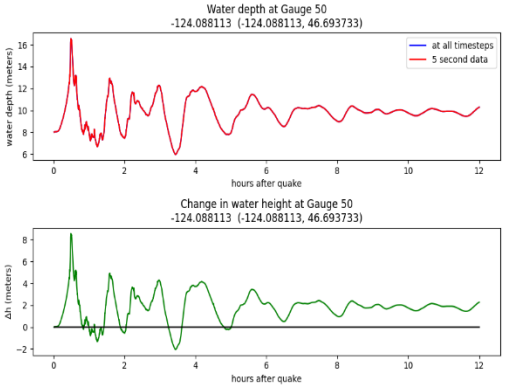

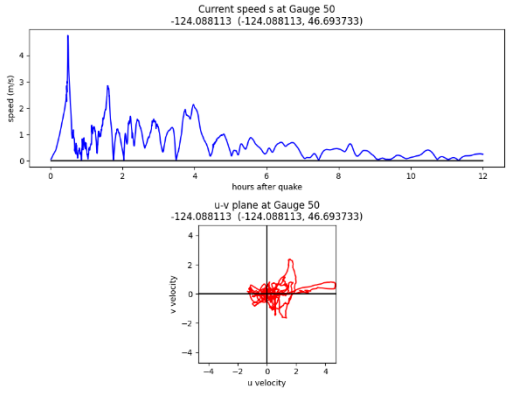

Gauge 51: Tokeland Peninsula W

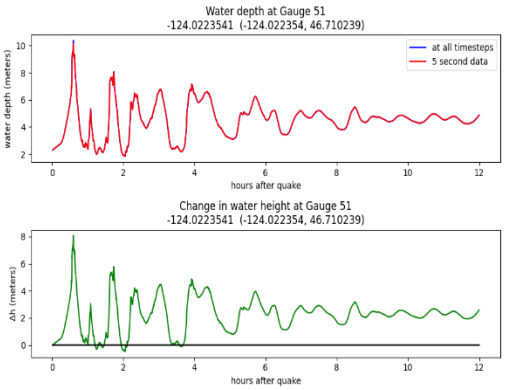

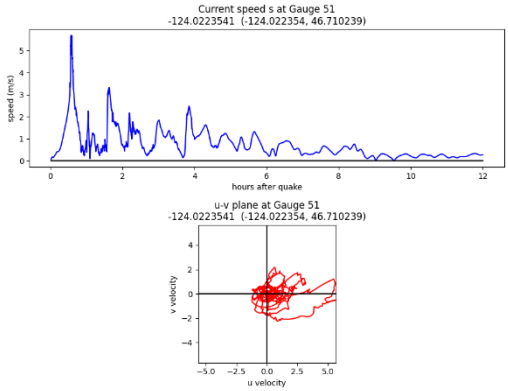

Gauge 52: Tokeland Marina

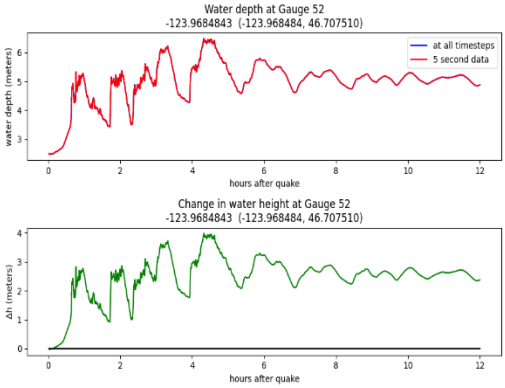

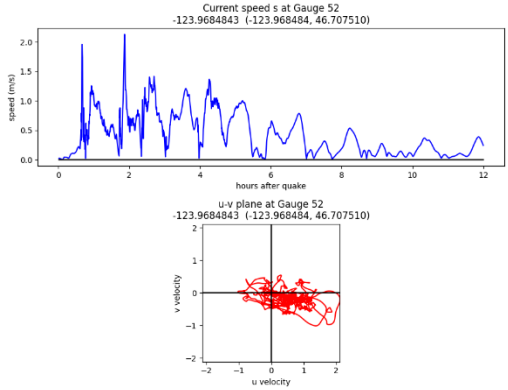

Gauge 53: Tokeland VES

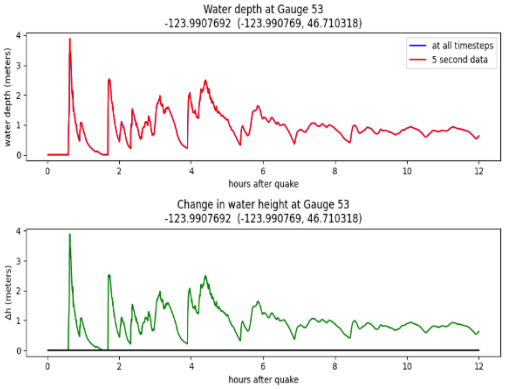

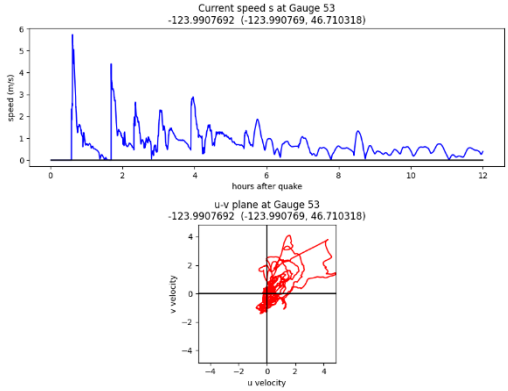

Gauge 54: Willapa Bay N

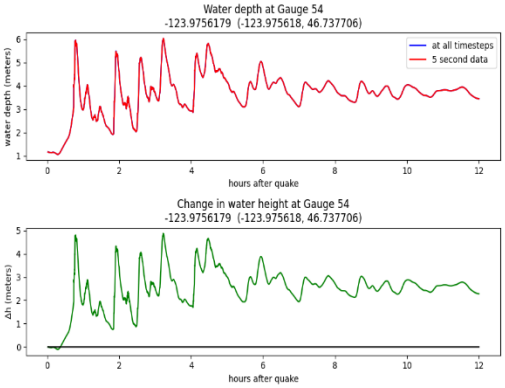

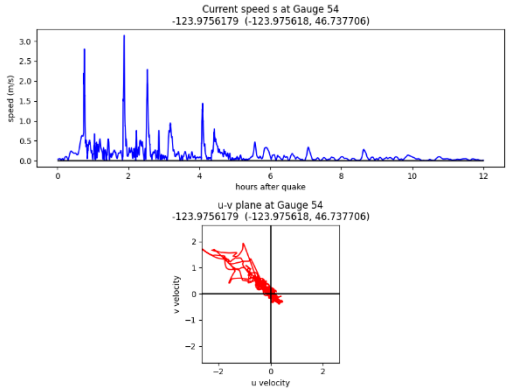

Gauge 55: North River mouth

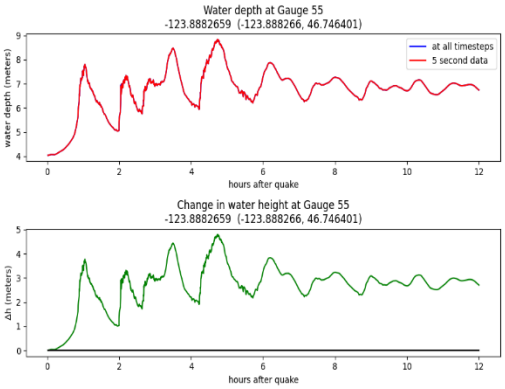

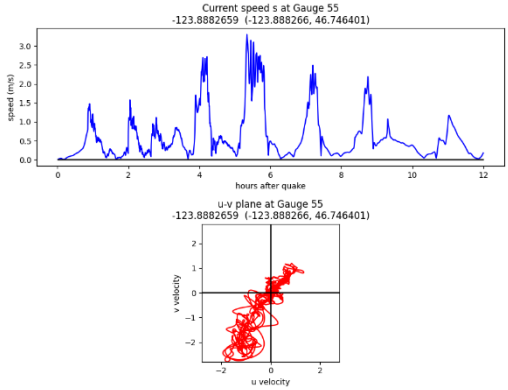

Gauge 56: Willapa River mouth

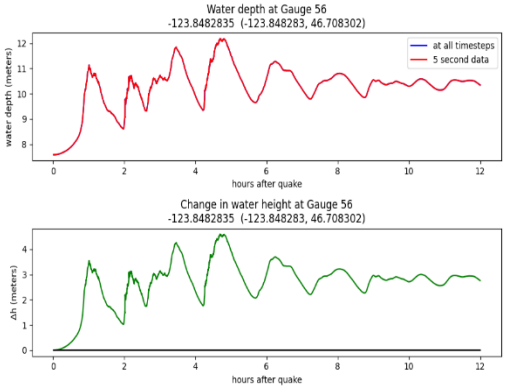

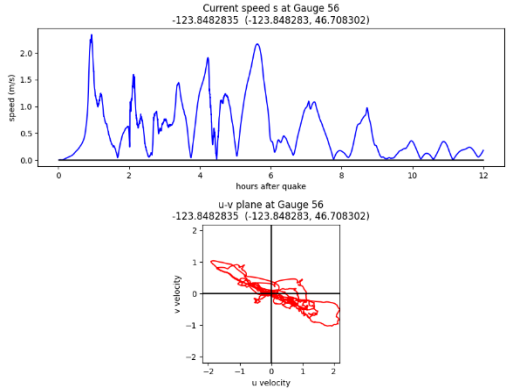

Gauge 57: Willapa Harbor Airport

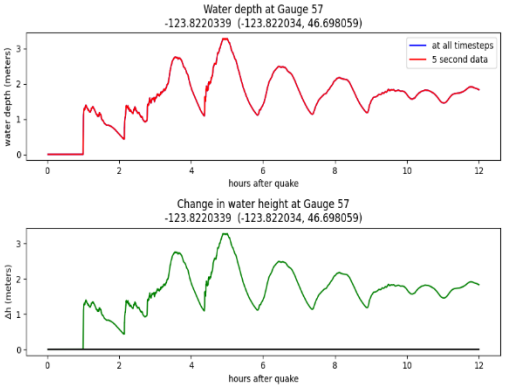

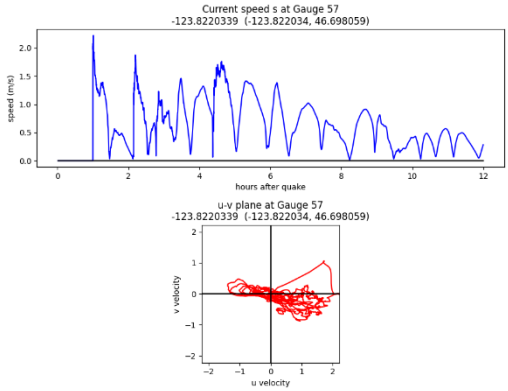

Gauge 58: Willapa River South Bend

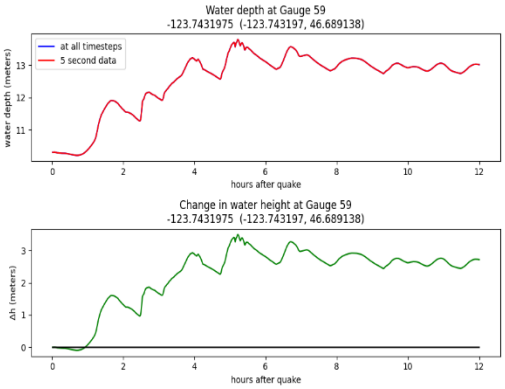

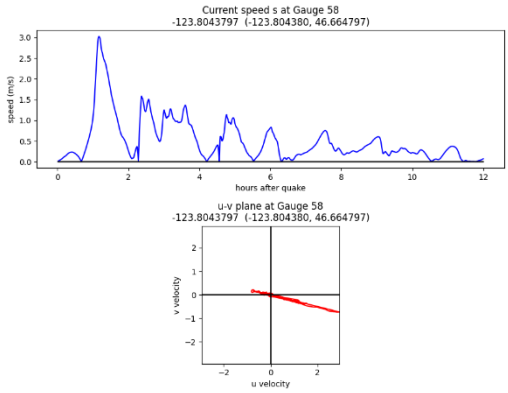

Gauge 59: South Fork Willapa River confluence

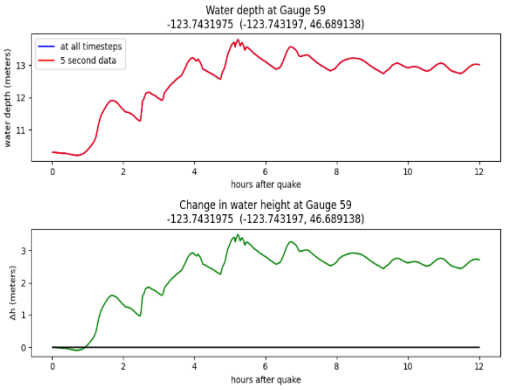

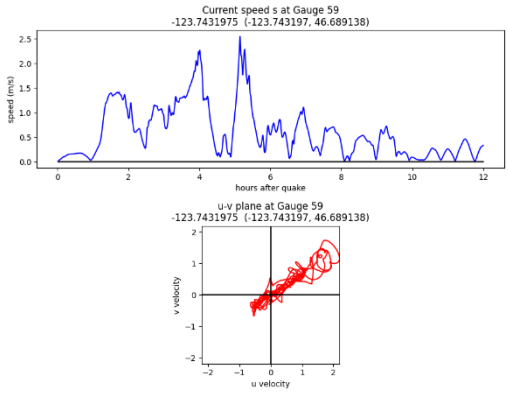

Gauge 60: Willapa River Ellis Slough confluence

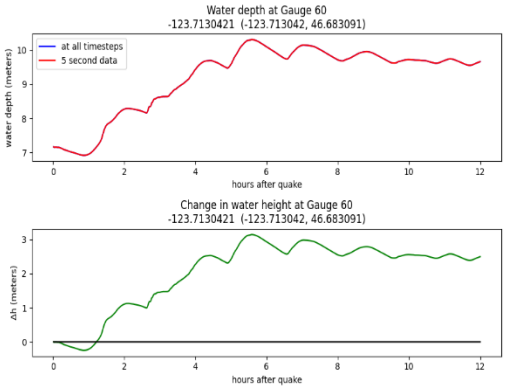

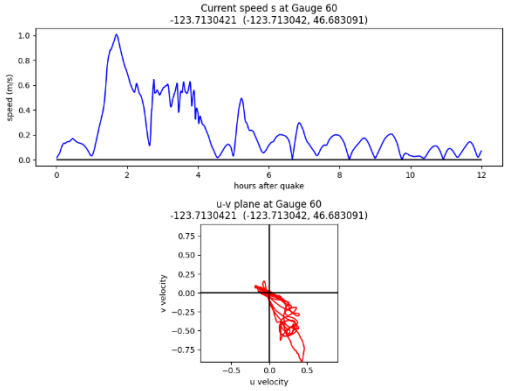

Gauge 61: Willapa River US101 Hwy Raymond

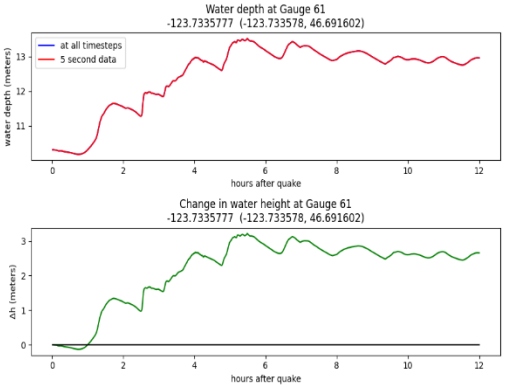

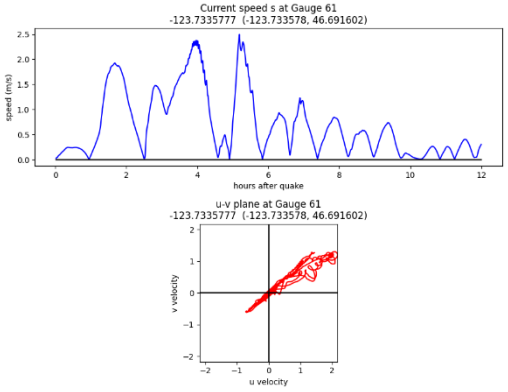

Gauge 62: Wilson Creek Willapa River Boat Ramp confluence

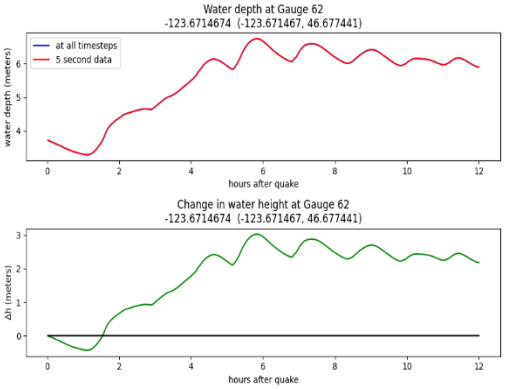

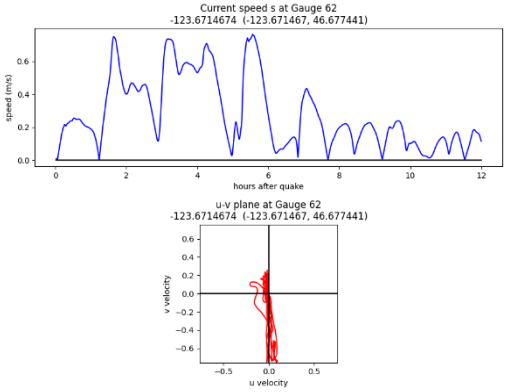

Gauge 63: Bay Center E

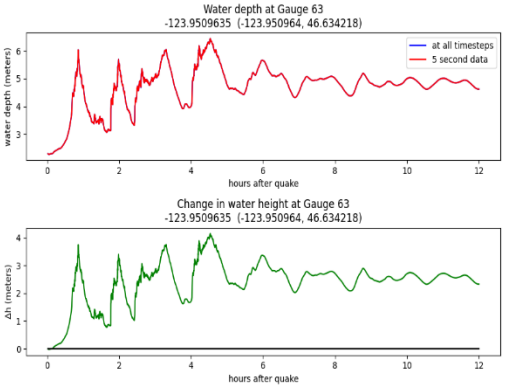

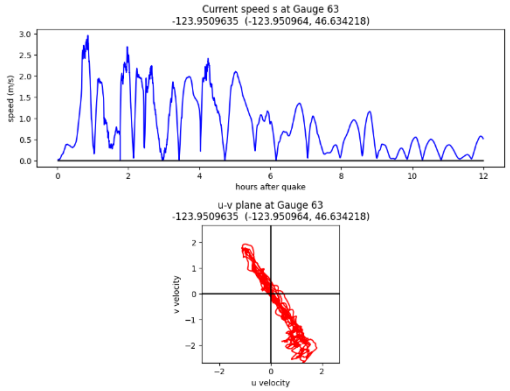

Gauge 64: Bay Center W

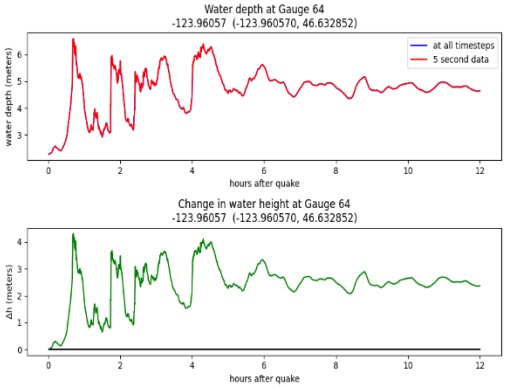

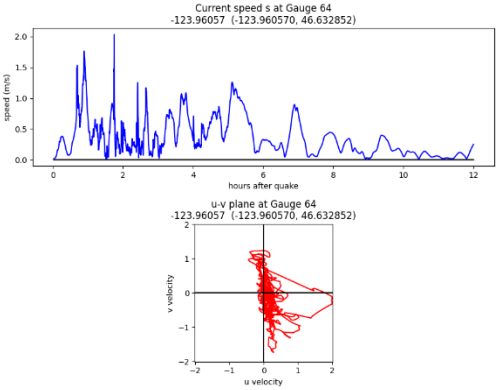

Gauge 65: Palix River US101

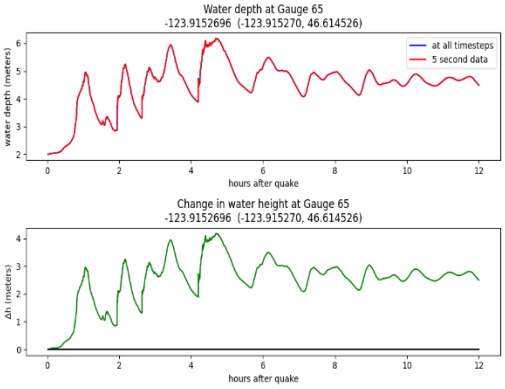

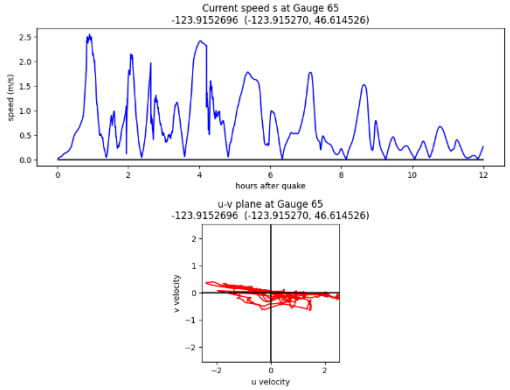

Gauge 66: Willapa Bay

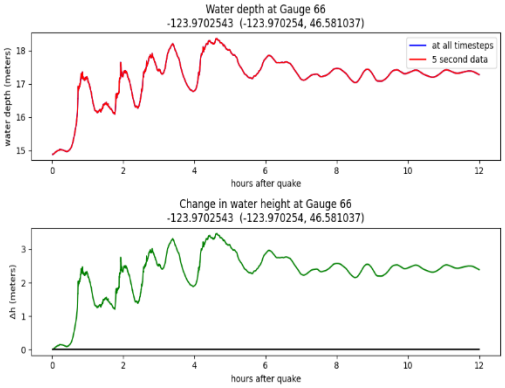

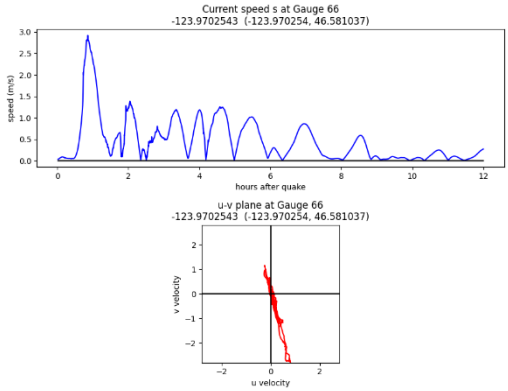

Gauge 67: Nemah mouth

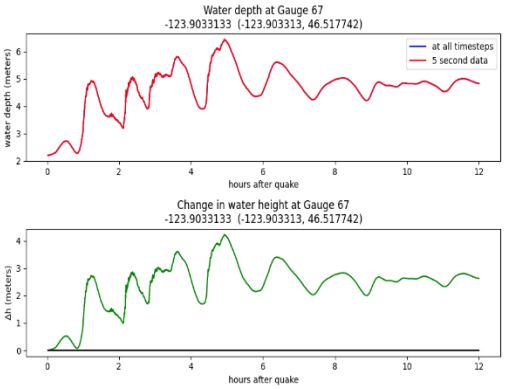

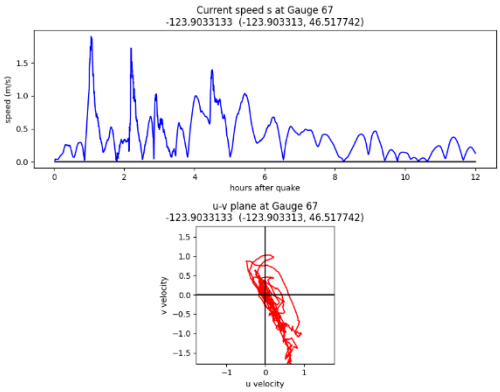

Gauge 68: Naselle River Willapa Bay bridge

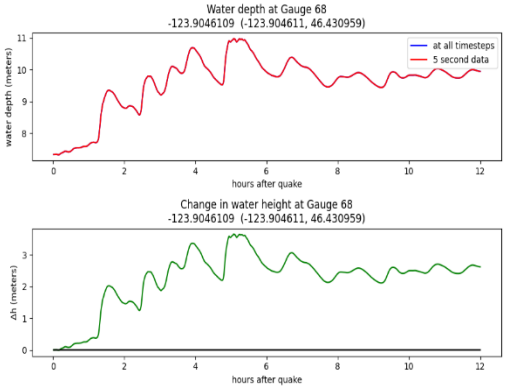

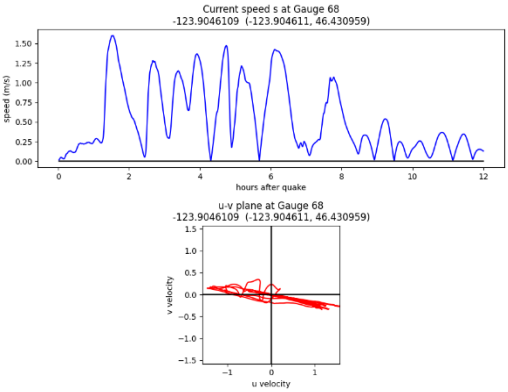

Gauge 69: Long Island E

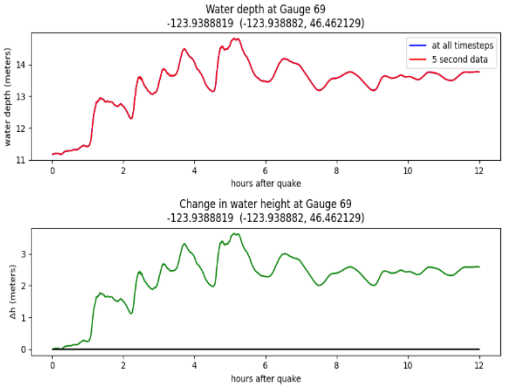

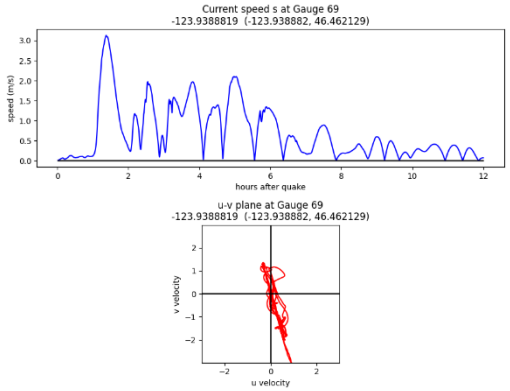

Gauge 70: Long Island S

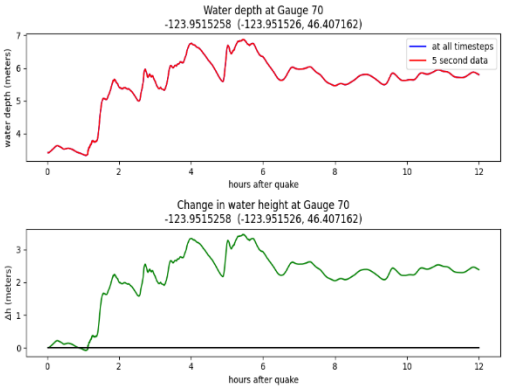

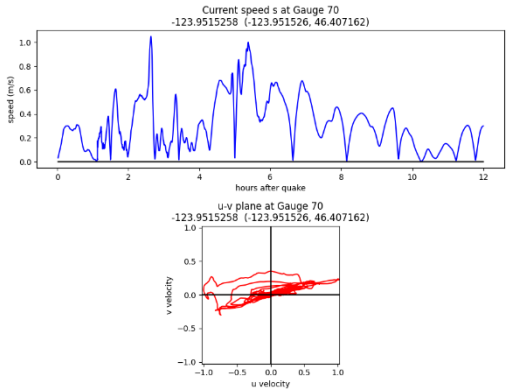

Gauge 71: Long Island W

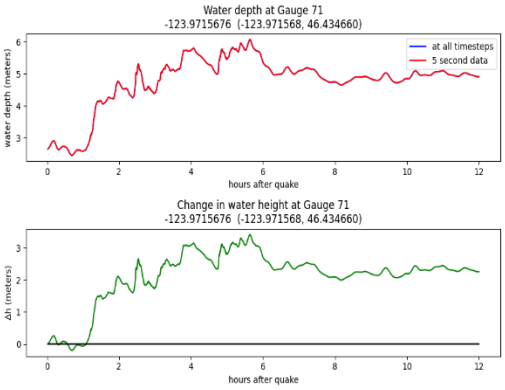

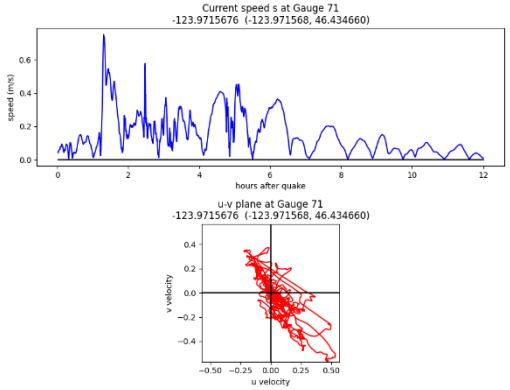

Gauge 72: Long Island Archeological Site

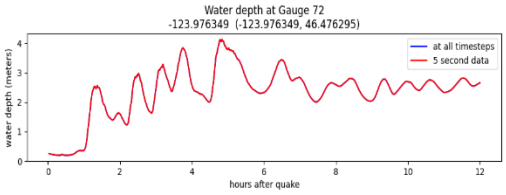

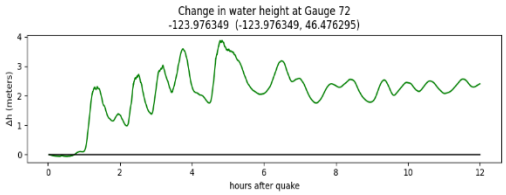

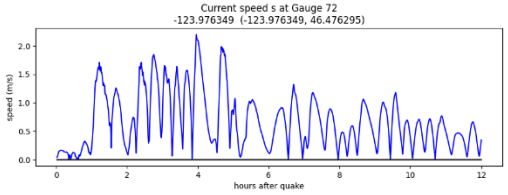

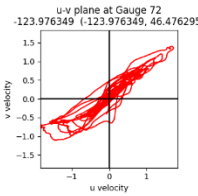

Gauge 73: Willapa Bay S

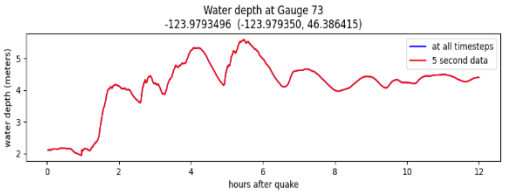

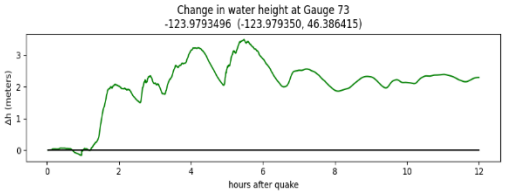

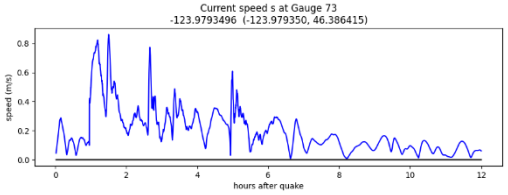

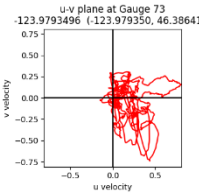

Gauge 74: Offshore Long Beach

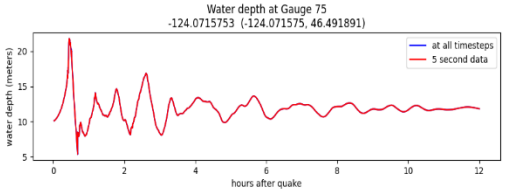

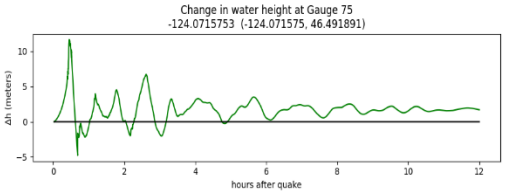

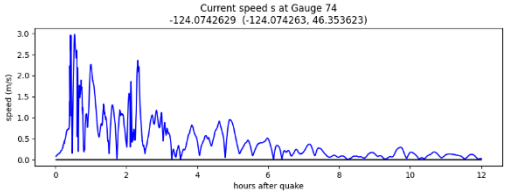

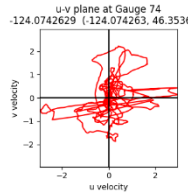

Gauge 75: Offshore Ocean Park

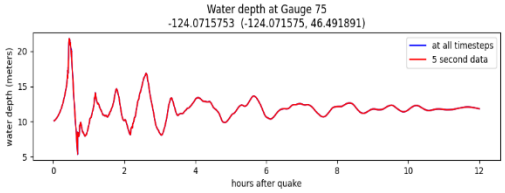

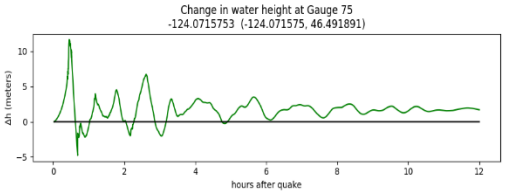

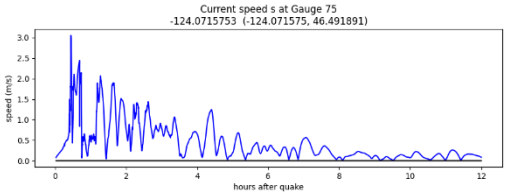

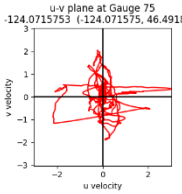

Acknowledgments

We acknowledge the NOAA National Centers of Environmental Information for providing the 1/3 arc-second Astoria (2012) DEM reference to Mean High Water and Guy McWethy (Washington Geological Survey) for his work in modifying it with newer lidar data and incorporating updated water depths along the Chehalis, Hoquiam, Willapa, and Wishkah Rivers. We also acknowledge Witter and others (2011) for developing and providing the Cascadia Subduction Zone L1 earthquake fault model. This work was supported by the Washington Geological Survey.

Data Availability

The computer code and input data used in this study has been archived and is available on request from the Washington Geological Survey. The modified Astoria MHW DEM used in this study is also available upon request from the Washington Geological Survey and the original is available from the National Centers for Environmental Information (NCEI) thredds catalogue at https://www.ngdc.noaa.gov/thredds/catalog/regional/catalog.html. NCEI provides this 2012 Astoria DEM in reference to the MHW datum. MHW can be converted to any other datum with NOAA's VDatum tool: https://vdatum.noaa.gov/vdatumweb/.

References

Adams, L., González, F., and LeVeque, R., 2019, Tsunami Hazard Assessment of Whatcom County, Washington, Project Report – Version 2, http://staff.washington.edu/rjl/pubs/THA_Whatcom.

Amante, Christopher; B. W. Eakins, 2009, ETOPO1 1 Arc-Minute Global Relief Model: Procedures, Data Sources and Analysis: NOAA Technical Memorandum NESDIS NGDC-24, 19 p. [https://www.ngdc.noaa.gov/mgg/global/relief/ETOPO1/docs/ETOPO1.pdf]

Atwater, B. F.; Hemphill-Haley, Eileen, 1997, Recurrence intervals for great earthquakes of the past 3,500 years at northeastern Willapa Bay, Washington: U.S. Geological Survey Professional Paper 1576, 108 p. [https://doi.org/10.3133/pp1576]

Atwater, B. F.; Satoko, Musumi-Rokkaku; Kenji, Satake; Yoshinobu, Tsuji; Kazue, Ueda; Yamaguchi, D. K., 2005, The orphan tsunami of 1700—Japanese clues to a parent earthquake in North America: U.S. Geological Survey in association with University of Washington Press, U.S. Geological Survey Professional Paper 1707, 135 p. [https://doi.org/10.3133/pp1707]

Atwater, B. F.; Tuttle, M. P.; Schweig, E. S.; Rubin, C. M.; Yamaguchi, D. K.; Hemphill-Haley, Eileen, 2004, Earthquake recurrence inferred from paleoseismology. IN Gillespie, A. R.; Porter, S. C.; Atwater, B. F., editors, The Quaternary period in the United States: Developments in Quaternary Science, v. 1, p. 331-350.

Berger, M. J.; George, D. L.; LeVeque, R. J.; Mandli, K. T., 2011, The GeoClaw software for depth-averaged flows with adaptive refinement: Advances in Water Resources, v. 34, no. 9, p. 1195–1206. [https://doi.org/10.1016/j.advwatres.2011.02.016]

Burgette, R. J.; Weldon, R. J.; Schmidt, D. A., 2009, Interseismic uplift rates for western Oregon and along-strike variation in locking on the Cascadia subduction zone: Journal of Geophysical Research Solid Earth, v. 114, no. B1, 24 p. [https://doi.org/10.1029/2008JB005679]

Clawpack Development Team, Clawpack software, 2023, Version 5.9.0, http://www.clawpack.org, DOI 10.17605/osf.io/kmw6h.

Dolcimascolo, Alexander; Eungard D. W.; Allen, Corina, 2023, Tsunami hazard maps of the Chehalis, Hoquiam, Willapa, and Wishkah Rivers—Model results from an L1 Mw 9.0 Cascadia subduction zone megathrust earthquake scenario: Washington Geological Survey Map Series 2023-02, 1 sheet, scale 1:48,000 and 1:166,000. [https://fortress.wa.gov/dnr/geologydata/tsunami_hazard_maps/ger_ms2023-02_tsunami_hazard_sw_wa_rivers.pdf]

Eungard, D. W.; Forson, Corina; Walsh, T. J.; Gica, Edison; Arcas, Diego, 2018c, Tsunami hazard maps of southwest Washington—Model results from a ~2,500-year Cascadia subduction zone earthquake scenario: Washington Geological Survey Map Series 2018-01, originally published March 2018, 6 sheets, scale 1:48,000, 11 p. text. [http://www.dnr.wa.gov/publications/ger_ms201801_tsunami_hazard_southwest_washington.zip]

Gica, Edison; Diego, Arcas; Titov, Vasily, 2014, Tsunami Inundation Modeling of Ocean Shores and Long Beach, Washington due to a Cascadia Subduction Zone Earthquake, p. 1-33.

Goldfinger, Chris; Galer, Steve; Beeson, Jeffrey; Hamilton, Tark; Black, Bran; Romsos, Chris; Patton, Jason; Nelson, C. H.; Hausmann, Rachel; Morey, Ann, 2017, The importance of site selection, sediment supply, and hydrodynamics: A case study of submarine paleoseismology on the northern Cascadia margin, Washington, USA: Marine Geology, v. 384, no. 17, p. 25–46. [https://doi.org/10.1016/j.margeo.2016.06.008]

Goldfinger, Chris; Nelson, C. H.; Morey, A. E.; Johnson, J. E.; Patton, J. R.; Karabanov, E. B.; Gutierrez-Pastor, Julia; Eriksson, A. T.; Gracia, Eulalia; Dunhill, Gita; Enkin, R. J.; Dallimore, Audrey; Vallier, Tracy, 2012, Turbidite event history—Methods and implications for Holocene paleoseismicity of the Cascadia Subduction Zone: U.S. Geological Survey Professional Paper 1661-F, 170 p. [https://doi.org/10.3133/pp1661F]

González, F. I.; LeVeque, R. J.; Chamberlain, Paul; Hirai, Bryant; Varkovitsky, Jonathan; George, D. L., 2011, Validation of the GeoClaw model—NTHMP MMS tsunami inundation model validation workshop: University of Washington, 84 p. [https://depts.washington.edu/clawpack/links/nthmp-benchmarks/geoclaw-results.pdf] NTHMP Model Benchmarking Workshop, http://depts.washington.edu/clawpack/links/nthmp-benchmarks/geoclaw-results.pdf.

International Code Council, 2015, 2015 International Building Code, 690 p. [https://codes.iccsafe.org/content/IBC2015]

Jacoby, G. C.; Bunker, D. E.; Benson, B. E., 1997, Tree-ring evidence for an A.D. 1700 Cascadia earthquake in Washington and northern Oregon: Geology, v. 25, no. 11, p. 999–1002. [https://doi.org/10.1130/0091-7613(1997)025<0999:TREFAA>2.3.CO;2]

LeVeque R. J.; Adams, L. M.; González, F. I., 2019, Tsunami Hazard Assessment of Portions of Island and Skagit Counties, Washington [webpage]: University of Washington. [accessed Apr. 28, 2011, at http://depts.washington.edu/ptha/IslandSkagitTHA_2019/]

LeVeque, R. J.; George, D. L.; Berger, M. J, 2011, Tsunami modelling with adaptively refined finite volume methods: Acta Numerica, v. 20, p. 211–289. [https://doi.org/10.1017/S0962492911000043]

NOAA National Geophysical Data Center (NGDC), 2012, Astoria, Oregon 1/3 Arc-second MHW Coastal Digital Elevation Model: NOAA National Centers for Environmental Information, [accessed Jul. 17, 2023 at https://www.ncei.noaa.gov/metadata/geoportal/rest/metadata/item/gov.noaa.ngdc.mgg.dem:5490/html].

Office of Coast Survey, 2023: NOAA Electronic Navigational Charts (ENC), [https://www.fisheries.noaa.gov/inport/item/39976]

Petersen, M. D.; Cramer, C. H.; Frankel, A. D., 2002, Simulations of seismic hazard for the Pacific Northwest of the United States from earthquakes associated with the Cascadia subduction zone: Pure and Applied Geophysics, v. 159, no. 9, p. 2147-2168.

Satake, Kenji; Wang, Kelin; Atwater, B. F., 2003, Fault slip and seismic moment of the 1700 Cascadia earthquake inferred from Japanese tsunami descriptions: Journal of Geophysical Research, v. 108, no. B11, 17 p. [https://doi.org/10.1029/2003JB002521]

USGS, 2019, Olympic Peninsula Area 2 LiDAR Project, collected between Feb. 19, 2018 and Apr. 25, 2019 by Quantum Spatial Inc., 3-ft resolution, accessed Apr. 12, 2023 [http://lidarportal.dnr.wa.gov/], metadata available on portal [ger_southwest_wa_opsw_2019_lidar_report.pdf]

Witter, R. C.; Zhang, Y. J.; Wang, Kelin; Priest, G. R.; Goldfinger, Chris; Stimely, L. L.; English, J. T.; Ferro, P. A., 2011, Simulating tsunami inundation at Bandon, Coos County, Oregon, using hypothetical Cascadia and Alaska earthquake scenarios: Oregon Department of Geology and Mineral Industries Special Paper 43, 57 p. [http://www.oregongeology.org/pubs/sp/p-SP-43.htm]

Witter, R. C.; Zhang, Y. J.; Wang, Kelin; Priest, G. R.; Goldfinger, Chris; Stimely, Laura; English, J. T.; Ferro, P. A., 2013, Simulated tsunami inundation for a range of Cascadia megathrust earthquake scenarios at Bandon, Oregon, USA: Geosphere, v. 9, no. 6, p. 1783–1803. [https://doi.org/10.1130/GES00899.1]

Yamaguchi, D. K.; Atwater, B. F.; Bunker, D. E.; Benson, B. E.; Reid, M. S., 1997, Tree-ring dating the 1700 Cascadia earthquake: Nature, v. 389, p. 922–923. [https://doi.org/10.1038/40048]

Yousefi, Maryam; Milne, Glenn; Li, Shaoyang; Wang, Kelin; Bartholet, Alan, 2020, Constraining interseismic deformation of the Cascadia subduction zone: new insights from estimates of vertical land motion over different timescales: Journal of Geophysical Research: Solid Earth, v. 125, no. 3, article e2019JB018248. [https://doi.org/10.1029/2019JB018248]

Appendix A. GeoClaw Output and Version Information

Output was delivered as NetCDF for each fgmax region and modeled earthquake source (Cascadia Subduction Zone) at high tide (MHW).

The netCDF files contain multiple field variables. A pre-processing script generates a few variables before the initiation of the GeoClaw run based on the fgmax region as part of the input. Following the GeoClaw run, the fgmax output generates other variables. Note that all variables are stored on two-dimensional uniform grids as defined by the lon and lat arrays. Only the points on this grid where fgmax point == 1 are used as fgmax points and only at these points is fgmax output available.

Values created as part of the GeoClaw input:

- lon: longitude, x (degrees),
- lat: latitude, y (degrees),
- Z: topography value Z from the DEM, relative to MHW (m),
- fgmax point: 1 if this point is used as an fgmax point, 0 otherwise,
- force_dry_init: 1 if this point is initialized as usual, 0 if this point is forced to be dry, regardless of initial topography value.

Values created based on the GeoClaw output:

- dz: Co-seismic surface deformation interpolated to each point (m),
- B: post-seismic topography value B from GeoClaw at gauge location (m),
- h: maximum depth of water over simulation (m),
- s: maximum speed over simulation (m/s),
- hss: maximum momentum hs^2 over simulation (m^3/s^2),
- hmin: minimum depth of water over simulation (m),
- arrival time: apparent arrival time (rising wave > 0.05 m) of tsunami (s),

In addition, the netCDF files contain the following metadata values:

- tfinal: final time of GeoClaw simulation (seconds),
- history: record of times data was added to file,
- outdir: location of output directory where data was found,
- run_finished: date and time run finished,

The fgmax points align exactly with the 1/3" DEM points. The finest level computational finite volume grid also aligns so that cell centers are exactly at the fgmax points, and Z in the netCDF file is the value from the DEM at this point. However, by integrating a piecewise bilinear function that interpolates the 1/3" DEM obtains the topography value B used in a grid cell in GeoClaw, which is not exactly equal to Z initially. Moreover, B is the value after any co-seismic deformation associated with the event.

GeoClaw Version 5.9.0

The modeling for this project used GeoClaw Version 5.9.0. GeoClaw is open source, part of the Clawpack software, and available at http://www.clawpack.org. Refer to the official version 5.9.0 release notes to view changes and modifications from previous GeoClaw versions.

Appendix B. Gauge Report Summaries

The following subheadings of this appendix include summary tables of key data for all synthetic tide gauges included in each respective fgmax job run. All data corresponds to a tsunami simulated from the Cascadia Subduction Zone (CSZ) L1 earthquake source modeled at Mean High Water (MHW). The variables within each table are defined as:

- B0: pre-seismic bathymetry/topography elevation (m)
- B: post-seismic bathymetry/topography elevation (m)
- dzi: co-seismic surface deformation (m)
- max h: maximum depth of water over simulation (m)
- min h: : minimum depth of water over simulation (m)
- max zeta: maximum surface elevation (eta) offshore above MHW; or maximum depth (h) onshore (m)
- max Δh: maximum change in water depth/height (h0-h; [max zeta-dzi]) over simulation (m)
- max eta post-earthquake: post-seismic maximum surface elevation (B + h) above MHW (m) over simulation (m)
- max s: maximum speed over simulation (m/s)
- max hs: maximum momentum over simulation (m^2/s)
- max hhs: maximum momentum flux hs^2 over simulation (m^3/s^2)
- tmax: time of maximum zeta over simulation (minutes)
- tmin: time of minimum zeta over simulation (minutes)
- tfirstPOS: time of first rising wave arrival (zeta > 0.025 m) over simulation (minutes)
- tfirstNEG: time of first falling wave arrival (zeta < 0.025 m) over simulation (minutes)
- tfirstDRAW: time of first significant fall wave arrival (h0-h > 0.3048 m) over simulation (minutes)
- tfirstADVIS: time of first "advisory-level" wave arrival (h-h0 > 0.3048 m) over simulation (minutes). This threshold matches the Advisory Alert-level defined by the National Tsunami Hazard Mitigation Program (NTHMP)
- tfirstWARN: time of first "warning-level" wave arrival (h-h0 > 0.9144 m) over simulation (minutes). This threshold matches the Warning Alert-level defined by the NTHMP

*Note: Coseismic subsidence generated by the CSZ L1 scenario causes the land/seafloor and water surface levels to drop simultaneously. Following this drop, the water surface level begins to rebound back to the pre-earthquake conditions over the course of the simulated tsunami and the land/seafloor does not. The rate at which the water surface level recovers is not captured in the tsunami simulation. Thus, determining offshore wave amplitude is challenging because amplitude refers to the height above water surface level, which becomes a dynamic and uncertain variable where there are coseismic elevation changes. Rather, because flow depth (h) does not change during coseismic impacts, we instead report the change in water depth (max Δh) over the simulation to capture the maximum impact of the tsunami water height. This value represents both the tsunami wave amplitude and the amount of sea-level recovery following the earthquake. This value may not represent the largest wave amplitude, which is generally the first wave in this study area.
**Note: tfirstDRAW timings reported as n/a suggest that the change in water depth (Δh) never falls a foot or more (-0.3048 m) below the water depth (h0) at the time of the earthquake. This is due to the water surface level recovery back to MHW following the earthquake deformation, which ultimately masks any trough or apparent negative wave phase of the tsunami.

B.1 Fgmax region: Grays Harbor west

Gauge	B0	B	dzi	max h	min h	max zeta	max Δh	max eta post-quake	max s	max hs	max hss	tmax	tmin	tfirstPOS	tfirstNEG	tfirstDRAW	tfirstADVIS	tfirstWARN
1	-10.12	-12.01	-1.89	18.06	7.48	6.04	7.93	6.04	9.78	168.45	1634.25	33.76	49.12	4.4	43.7	44.3	10.2	15.1
2	-5.77	-7.91	-2.14	14.82	3.66	6.91	9.05	6.91	4.23	58.46	247.28	36.25	55.88	1.2	46.8	47.1	12.8	17.2
3	-24.22	-26.46	-2.23	30.81	23.28	4.36	6.59	4.36	7.15	218.48	1559.75	36.16	54.62	2	50.3	51	14.9	20.6
4	-14.19	-16.43	-2.24	18.68	14.12	2.25	4.49	2.25	2.73	43.26	115.46	36.87	2.81	17	1	n/a	22.1	30.1
5	-0.82	-2.72	-1.9	9.27	0.15	6.97	8.87	6.55	7.1	42.51	195.65	34.97	208.69	8.5	1.4	80.3	15.5	19.1
6	-3.44	-5.47	-2.03	14.35	0.82	8.88	10.91	8.88	5.89	84.36	496.64	34.15	53.39	1.4	40.6	40.8	11.4	15.3
7	-2.99	-4.92	-1.92	16.61	0.18	11.69	13.61	11.69	4.84	74.33	360	34	50.29	1.5	42.8	43	4.9	10.5
8	-4.04	-5.97	-1.93	18.11	0.04	12.14	14.07	12.14	5.26	77.85	354.81	33.86	50.12	1.3	41.8	42	4.8	10.1
9	-6.15	-7.85	-1.7	19.42	0.51	11.57	13.27	11.57	9.23	61	299.31	32.92	48.2	1.1	40.2	40.4	4.9	9.9
10	-9.23	-10.86	-1.64	20.65	4.01	9.79	11.42	9.79	5.32	89.08	397.19	31.62	46.37	1.6	40.1	40.5	7.2	11
11	-2.4	-4.92	-2.52	5.51	2.4	0.59	3.11	0.59	3.66	20.15	73.64	41.38	1.55	6.2	n/a	n/a	25.9	33.5
12	-2.39	-4.76	-2.37	5.44	2.2	0.68	3.05	0.68	1.63	5.61	9.18	281.29	35.36	6.7	14.5	n/a	45.3	45.7
13	-4.45	-6.84	-2.39	7.53	4.45	0.69	3.08	0.69	3.85	24.29	93.25	269.92	1.02	27.1	n/a	n/a	36.6	45.7
14	-3.27	-5.75	-2.48	6.44	3.27	0.69	3.17	0.69	2.39	12.64	30.19	275.85	0	8.6	n/a	n/a	42	51.1
15	-3.22	-5.92	-2.7	7.11	3.22	1.19	3.88	1.19	2.1	14.42	29.38	48.28	2.4	5.2	n/a	n/a	21.3	35.8
16	-4.78	-7.53	-2.75	8.04	4.77	0.5	3.25	0.5	2.49	18.28	45.59	264.25	2.2	8.1	n/a	n/a	24.4	37.5
17	-2.4	-5.21	-2.81	5.82	2.4	0.61	3.42	0.61	1.64	7.65	12.59	298.78	0	2.3	n/a	n/a	15.3	46.7
18	-2.42	-5.18	-2.76	5.86	2.42	0.68	3.44	0.68	0.83	4.34	3.59	298.21	0	2.1	n/a	n/a	16.1	50.5

B.2 Fgmax region: Grays Harbor east

Gauge	B0	B	dzi	max h	min h	max zeta	max Δh	max eta post-quake	max s	max hs	max hss	tmax	tmin	tfirstPOS	tfirstNEG	tfirstDRAW	tfirstADVIS	tfirstWARN
19	-2.34	-5.24	-2.9	5.81	2.34	0.57	3.47	0.57	1.64	7.3	11.44	268.33	0	5.9	n/a	n/a	24.2	44
20	-2.31	-5.24	-2.93	5.86	2.31	0.62	3.55	0.62	1.79	8.14	14.58	271.04	1.76	6.1	n/a	n/a	22.8	46.6
21	-1.74	-4.66	-2.93	5.21	1.74	0.54	3.47	0.54	1.07	3.96	4.23	278.1	0	6.2	n/a	n/a	26.8	46.2
22	-2.72	-5.66	-2.94	6.3	2.72	0.64	3.58	0.64	1.45	7.36	10.65	282.16	0	11.5	n/a	n/a	32.8	53.7
23	-14.41	-17.35	-2.93	17.83	14.41	0.48	3.42	0.48	1.8	30.22	54.45	280.85	0	7.6	n/a	n/a	34.1	54.4
24	-6.28	-9.18	-2.9	9.54	6.28	0.36	3.26	0.36	1.62	15.44	25.04	398.17	5.37	18.6	n/a	n/a	37.1	57.3
25	-14.8	-17.62	-2.82	17.99	14.77	0.37	3.19	0.37	2.17	37.05	80.5	412.98	15.45	28.4	7.9	n/a	44	63.8
26	-2.41	-5.32	-2.92	5.8	2.41	0.48	3.39	0.48	1.75	8.23	14.37	281.93	0	16.9	n/a	n/a	35.7	56.5
27	-2.39	-5.29	-2.9	5.64	2.39	0.35	3.25	0.35	1.44	6.75	9.6	398.42	6.86	18	n/a	n/a	37	57.2
28	-8.14	-10.95	-2.82	11.38	8.1	0.43	3.25	0.43	1.4	14.7	20.64	298.8	15.83	28.6	9.1	n/a	44.5	64.1
29	-7.65	-10.48	-2.83	10.85	7.63	0.37	3.2	0.37	1.92	18.49	35.46	414.61	11.73	28.3	n/a	n/a	45	64.9
30	-7.82	-10.65	-2.83	11.01	7.8	0.36	3.19	0.36	2.16	21.1	45.49	414.81	12.05	28.6	n/a	n/a	45.2	65.3
31	-8.73	-11.54	-2.81	11.8	8.69	0.26	3.07	0.26	1.42	14.92	21.12	510.92	15.07	34	10.7	n/a	49.9	69.3
32	-1.32	-4.11	-2.79	4.22	1.27	0.11	2.9	0.11	0.44	1.42	0.52	611.93	25.17	43.1	3	n/a	61	80.7
33	-12.44	-15.39	-2.95	15.96	12.44	0.57	3.52	0.57	2.45	36.39	89	282.08	0	5.9	n/a	n/a	32.1	52.6
34	-7.52	-10.47	-2.95	10.86	7.52	0.39	3.34	0.39	3.05	32.09	97.74	287.21	1.48	6.6	n/a	n/a	32.7	53.2
35	-7.02	-9.97	-2.95	10.44	7.01	0.47	3.42	0.47	2.51	23.3	58.4	285.95	2.16	7.5	n/a	n/a	33.2	53.8
36	-7.93	-10.88	-2.95	11.26	7.93	0.37	3.33	0.37	2.64	26.29	69.37	288.41	0	9.3	n/a	n/a	34.9	55.5
37	-7.74	-10.7	-2.96	10.82	7.74	0.12	3.08	0.12	1.11	11.51	12.77	639.4	0	15.5	n/a	n/a	40.2	60.6
38	-3.92	-6.88	-2.96	7	3.92	0.11	3.08	0.11	0.72	4.69	3.39	640.18	0	16.5	n/a	n/a	41.3	61.8
39	-12.5	-15.23	-2.73	15.55	12.44	0.32	3.05	0.32	2.52	38.04	95.74	414.76	16.61	40.4	9.8	n/a	53.5	71.2
40	-14.53	-17.23	-2.69	17.47	14.46	0.25	2.94	0.25	2.36	37.83	89.39	424.7	33.97	3.1	17.8	n/a	59.6	75.7

Gauge	B0	B	dzi	max h	min h	max zeta	max Δh	max eta post-quake	max s	max hs	max hss	tmax	tmin	tfirstPOS	tfirstNEG	tfirstDRAW	tfirstADVIS	tfirstWARN
41	-1.76	-4.33	-2.58	4.51	1.58	0.18	2.75	0.18	1.5	6.01	8.99	431.52	42.94	60	1.7	n/a	70.1	84.3
42	-12.84	-15.38	-2.54	15.53	12.57	0.16	2.7	0.16	1.06	14.66	15.56	534.65	48.59	4.6	22.6	n/a	78.9	96.8
43	-3.2	-5.72	-2.52	5.87	2.89	0.15	2.67	0.15	0.85	3.64	3.1	535.36	52.08	6.1	21.3	47.5	81.8	128
44	-10.24	-12.74	-2.49	12.88	9.9	0.14	2.64	0.14	1.77	19.52	34.53	537.64	52.23	7.4	20.1	44.7	83.6	135.7
45	-9.2	-11.6	-2.4	11.74	8.72	0.14	2.54	0.14	1.11	11.73	12.97	540.6	57.31	80.7	8.2	37.7	90.5	150.9
46	-11.26	-13.62	-2.36	13.76	10.73	0.14	2.5	0.14	1.1	14.25	15.62	448.38	59.01	84.1	6.5	36.6	93.9	180.7
47	-9.51	-11.42	-1.91	11.58	8.26	0.16	2.07	0.16	0.63	7.17	4.52	579.36	82	116.9	5	25.5	127.4	245.5
48	-9.4	-11.3	-1.9	11.46	8.13	0.17	2.07	0.17	0.36	4.01	1.45	580.75	81.76	117.4	4.3	24.9	127.9	247.1
19	-2.34	-5.24	-2.9	5.81	2.34	0.57	3.47	0.57	1.64	7.3	11.44	268.33	0	5.9	n/a	n/a	24.2	44
20	-2.31	-5.24	-2.93	5.86	2.31	0.62	3.55	0.62	1.79	8.14	14.58	271.04	1.76	6.1	n/a	n/a	22.8	46.6
21	-1.74	-4.66	-2.93	5.21	1.74	0.54	3.47	0.54	1.07	3.96	4.23	278.1	0	6.2	n/a	n/a	26.8	46.2
22	-2.72	-5.66	-2.94	6.3	2.72	0.64	3.58	0.64	1.45	7.36	10.65	282.16	0	11.5	n/a	n/a	32.8	53.7

B.3 Fgmax region: Pacific County north

Gauge	B0	B	dzi	max h	min h	max zeta	max Δh	max eta post-quake	max s	max hs	max hss	tmax	tmin	tfirstPOS	tfirstNEG	tfirstDRAW	tfirstADVIS	tfirstWARN
49	-7.7	-9.5	-1.8	18.43	3.98	8.93	10.73	8.93	3.03	55.52	168.07	27.67	45.57	1.3	42.2	42.4	5.1	9.6
50	-8.01	-9.88	-1.86	16.57	5.98	6.69	8.55	6.69	4.76	78.12	371.53	29.46	206.61	1.8	50.3	60.6	10.4	14.2
51	-2.3	-4.62	-2.32	10.38	1.83	5.76	8.08	5.76	5.68	58.89	334.27	36.12	123.46	1.9	72.9	75.1	9.4	19
52	-2.51	-5.1	-2.59	6.48	2.48	1.38	3.97	1.38	2.13	10.81	23	259.67	2.68	10.5	1.9	n/a	26.2	36.7
53	1.51	-0.97	-2.49	3.89	0	3.89	6.38	2.92	5.74	18.67	106.99	37.68	0	35.2	n/a	n/a	35.3	35.8
54	-1.16	-3.75	-2.59	6.03	1.06	2.27	4.87	2.27	3.14	12.6	35.3	193.35	17.69	22.5	4	n/a	28.3	38.6
55	-4.03	-6.86	-2.83	8.83	4.03	1.97	4.8	1.97	3.3	21.85	72.21	283.6	0	4.7	n/a	n/a	29.9	46
56	-7.58	-10.4	-2.82	12.18	7.58	1.78	4.6	1.78	2.34	24.49	57.37	281.28	2.84	9.9	n/a	n/a	30.1	46
57	1.09	-1.71	-2.8	3.28	0	3.28	6.08	1.57	2.22	4.42	7.77	300.19	0	60	n/a	n/a	60.1	60.5
58	-8.47	-11.23	-2.75	13.21	8.47	1.98	4.74	1.98	3.02	29.78	90.02	303.75	2.91	20.6	n/a	n/a	48.4	62.7
59	-10.3	-12.92	-2.62	13.79	10.21	0.87	3.49	0.87	2.55	34.56	88.06	313.22	42.31	57.3	14.6	n/a	69.9	79.1
60	-7.16	-9.68	-2.52	10.31	6.92	0.63	3.15	0.63	1.01	8.03	8.09	335.02	52.3	74.5	12.6	n/a	83.2	107.2
61	-10.3	-12.9	-2.6	13.52	10.17	0.62	3.22	0.62	2.49	33.43	83.37	329.29	44.42	61.4	10	n/a	73.6	82.8
62	-3.73	-6.08	-2.35	6.75	3.29	0.67	3.02	0.67	0.76	5	3.8	350.66	66.68	93.5	2.8	37.1	100.2	158.8
63	-2.3	-4.86	-2.56	6.44	2.27	1.58	4.14	1.58	2.96	17.21	50.41	272.14	3.2	10.3	2.5	n/a	26.8	37.2
64	-2.27	-4.79	-2.53	6.59	2.27	1.8	4.32	1.8	2.03	10.05	19.47	42.28	0	2.2	n/a	n/a	11.6	32.5
65	-1.99	-4.65	-2.66	6.17	1.99	1.52	4.18	1.52	2.55	10.89	27.44	281.09	0	5.4	n/a	n/a	32	46.4

B.4 Fgmax region: Pacific County south

Gauge	B0	B	dzi	max h	min h	max zeta	max Δh	max eta post-quake	max s	max hs	max hss	tmax	tmin	tfirstPOS	tfirstNEG	tfirstDRAW	tfirstADVIS	tfirstWARN
66	-14.89	-17.32	-2.43	18.34	14.88	1.03	3.46	1.03	2.91	50.39	146.46	276.39	1.56	4	n/a	n/a	34.6	41.1
67	-2.2	-4.79	-2.58	6.44	2.2	1.65	4.23	1.65	1.9	8.17	15.31	295.65	2.21	6.6	n/a	n/a	20.7	60
68	-7.33	-9.83	-2.5	10.98	7.32	1.15	3.65	1.15	1.6	14.95	23.91	304.57	9.62	12.8	n/a	n/a	60.3	79.3
69	-11.18	-13.62	-2.44	14.82	11.18	1.2	3.63	1.2	3.13	40.46	126.52	307.52	15.24	18.2	n/a	n/a	63.8	68.4
70	-3.41	-5.76	-2.35	6.87	3.33	1.11	3.46	1.11	1.05	6.84	6.85	326.89	64.65	4.7	56.4	n/a	74.2	87.2
71	-2.65	-4.94	-2.29	6.07	2.46	1.13	3.42	1.13	0.75	2.9	2.05	338.26	41.55	2.3	35.2	n/a	71.6	77.8
72	-0.26	-2.55	-2.3	4.13	0.2	1.57	3.87	1.57	2.2	7.53	14.43	290.07	31.53	45.8	6	n/a	63.5	67.2
73	-2.11	-4.35	-2.24	5.6	1.94	1.25	3.49	1.25	0.86	3.17	2.45	328.42	56.86	8.8	43.5	n/a	84.1	90.4
74	-7.77	-9.47	-1.69	20.1	3.33	10.64	12.33	10.64	2.98	58.71	173.57	27.25	36.6	1.4	34	34.1	4.6	9.3
75	-10.1	-11.84	-1.74	21.8	5.35	9.96	11.69	9.96	3.05	64.83	197.62	27.03	41.28	1.5	37.5	37.7	4.9	9.4